ISTANBUL TECHNICAL UNIVERSITY ★ GRADUATE SCHOOL OF SCIENCE ENGINEERING AND TECHNOLOGY

FRICTION INDUCED VIBRATION BASED PATTERN DETECTION ON AN ARTIFICIAL SKIN BY PRELOAD CONTROL

M.Sc. THESIS

Ayşegül GÜVENÇ

Department of Mechanical Engineering

System Dynamics and Control Programme

FEBRUARY 2012

ISTANBUL TECHNICAL UNIVERSITY ★ GRADUATE SCHOOL OF SCIENCE ENGINEERING AND TECHNOLOGY

FRICTION INDUCED VIBRATION BASED PATTERN DETECTION ON AN ARTIFICIAL SKIN BY PRELOAD CONTROL

M.Sc. THESIS

Ayşegül GÜVENÇ
(503081602)

Department of Mechanical Engineering

System Dynamics and Control Programme

Thesis Advisor: Assist. Prof. Dr. İlker Murat KOÇ

FEBRUARY 2012

İSTANBUL TEKNİK ÜNİVERSİTESİ ★ FEN BİLİMLERİ ENSTİTÜSÜ

ÖNYÜKLEME KUVVET KONTROLÜ İLE BİR YAPAY YÜZEY ÜZERİNDE SÜRTÜNMENİN YOL AÇTIĞI TİTREŞİME DAYANAN DESEN ALGILAMA

YÜKSEK LİSANS TEZİ

Ayşegül GÜVENÇ
(503081602)

Makina Mühendisliği Anabilim Dalı

Sistem Dinamiği ve Kontrol Programı

Tez Danışmanı: Yrd. Doç. Dr. İlker Murat KOÇ

ŞUBAT 2012

Ayşegül Güvenç, a **M.Sc.** student of ITU **Graduate School of Science Engineering and Technology** student ID 503081602, successfully defended the **thesis** entitled "**FRICTION INDUCED VIBRATION BASED PATTERN DETECTION ON AN ARTIFICIAL SKIN BY PRELOAD CONTROL**", which she prepared after fulfilling the requirements specified in the associated legislations, before the jury whose signatures are below.

Thesis Advisor :   **Assist. Prof. Dr. İlker Murat KOÇ**   ....
                        İstanbul Technical University

Jury Members :   **Prof. Dr. Ata MUĞAN**   ....
                        İstanbul Technical University

                        Assist. Prof. Dr. İlker Murat KOÇ   ....
                        Istanbul Technical University

                        Assist. Prof. Dr. Gülay ÖKE   ....
                        Istanbul Technical University

Date of Submission : 06 May 2011
Date of Defense :   21 February 2012

To my family,

FOREWORD

February 2012   Ayşegül GÜVENÇ
                                                                          (System Engineer)

x

TABLE OF CONTENTS

ABBREVIATIONS

PDMS   **:** Polydimethylsiloxane
FFT   **:** Fast Fourier Transform
RA   **:** Rapidly Adapting Units
SA   **:** Slowly Adapting Units
JKR   **:** Johnson-Kendall-Roberts
DMT   **:** Derjaguin-Muller-Toporov
PID   **:** Proportional-Integral-Derivative
SMC   **:** Sliding Mode Control

LIST OF TABLES

LIST OF FIGURES

FRICTION INDUCED VIBRATION BASED PATTERN DETECTION ON AN ARTIFICIAL SKIN BY PRELOAD CONTROL

SUMMARY

In recent years, tribological investigations on micro- and nano-scale develop rapidly. The tendency of observing and mimicking the nature take the significant role in this growth. Thus, bio-inspired and human-centered studies become the origin of this scientific area. To comprehend the frictional and adhesional interactions between surfaces moving relative to each other more closely, many experimental structures are designed and studies are realized by the scientists. In addition, to carry out such studies, clear understanding about the perceptual mechanism of animals and/or humans is the crucial subject.

Human beings have an indispensable perceptual mechanism which allows them to communicate with the environment and survive. One of the essential components of this mechanism is the human skin with a critical role in the sense of touch. Especially, on the human body the most touch sensing is at the fingertips which can perceive surface texture approximately on a 1 cm^2 area of contact, and at 10-40 kPa stress levels. The skin undertakes a significant task on human interaction with the surrounding by conveying information from external stimuli to the embedded receptors. Tactile properties of the skin allow humans to process this information and respond to physical sensations such as vibrations, pressure distribution, and temperature with the aid of its feedback system. Such an interesting feature of human texture perception mechanism encourages the researchers in recent years to emulate the sense of touch by producing artificial surfaces. Studies related on the artifacts also allow scientists to comprehend how the process works to acquire tactile sensation, and improve applications in the fields of robotics with an autonomously surface detection task or surgical task, medicine, fabrics, and cosmetics.

To acquire tactile sensation, contact and relative motion are necessary subjects. In a static contact, the surface texture perception mechanism does not have an effective result. When a relative motion between two surfaces contacting to each other occurs which means dynamic contact takes place under relevant preload and sliding velocity, perception of the surface characteristics becomes possible. Tactile sensing takes some forms comprising the detection of texture, shape, force, friction, temperature, and pain. Fundamental dimension of the texture perception is the roughness. The relation between surface roughness and the tactile sensation is investigated by taking into account the frictional properties of the surfaces contacting to each other. Lateral motion of the surface over the other one permits to perceive the roughness.

Therefore, the crucial process, emulating the sense of touch, needs a multidisciplinary study comprising tribology, vibration, and control. Frictional studies related on the surface roughness and tactile sensation have been carried out by many researchers, whereas friction induced vibration based pattern detection is an

ongoing research topic. This promising approach needs to consider not only the frictional studies between the contacting surfaces in a dynamic contact but also data analysis in frequency domain. Consequently, analysis about the friction induced vibration based pattern detection by preload control includes multidisciplinary study containing tribology, vibration, and control.

During the relative motion between the human-inspired micropatterned artificial surface and rigid specimen like glass tip, sliding generates vibrations called friction induced vibrations. Vibrations activate the related mechanoreceptor through which these vibrations are converted into electric impulses and conveyed the information of the object surface to the brain. After these steps, human can perceive the properties of the surface structure including the roughness. To adapt these procedures to the artifacts for detecting their pattern, the artificial micropatterned surfaces have various features in size and spacing such as different groove width, ridge width, ridge height and orientation. The friction induced vibrations occurred during the surface scanning allow to detect the frequency belonging to the pattern of the artificial skin, and carrying the information of the scanned surface like wavelength and height of ridges while the preload applied to the surface is kept constant. It should be paid attention that one of the crucial working conditions which have to be provided is constant preload. For this aim, various methods have been carried out by researchers in literature such as using a dead weight, mounting a drum on a beam, using manual stage, or analogue voltage meter. One of the prevalent methods is using a dead weight. However, such an approach does not provide to guarantee to keep the system parameter, preload, consistent. If this essential working condition is carried out by a force-feedback controller, the preload remains unchanged during sliding after reaching to the predefined value. It should also be noted that using a controller enables to investigate the preload error on every step of experiments which allows to have accurate and sensitive analysis. In addition, to use dead weight causes the system to have a fixed structure on which the preload value cannot be changed if it is necessary. As a result, designing a semi-autonomous system, on which the preload is kept constant by using a force-feedback controller during surface scanning, and can be changed in necessary situations, carries the basic idea of this study.

In this study, an approach of pattern detection on artificially made surface based on friction induced vibrations is exhibited in details. First, custom built semi-autonomous friction-adhesion set-up is designed, and validated using flat soft polymer (PDMS- Polydimethlysiloxane) as a control sample, rubbed against a rigid glass tip. Meanwhile, for constant preload during surface scanning three different force-feedback controllers, PID (Proportional-Integrative-Derivative), Adaptive PID, and SMC (Sliding Mode Controller), are designed and examined. The comparative outcomes indicated that using SMC allowed performing the experiments under constant preload with a minimum percentage of error. Then, to obtain appropriate working conditions such as travel interval, sliding velocity and preload, some tests are realized. Thus, the occurrence circumstances of stick-slip oscillations and steady sliding between soft polymer and rigid surface are analyzed. Effects of different design parameters such as sliding velocity, preload and tip diameter on pattern detection and friction are investigated by producing human-inspired artificial skin with evenly spaced parallel ridges made of PDMS. According to the results of the tests, the preload remains consistent with a minimum percentage of error at low sliding velocity and under high preload value. Furthermore, linear proportionality between the frequency belonging to the pattern, and the sliding velocity is presented

based on the ratio of the sliding velocity and wavelength of the ridges ($f = V/\lambda$). Additionally, tip diameter effect on reducing the preload error, and filtering harmonics of the signal is also observed. In consequence of this study, the information of the scanned surface like wavelength and height of ridges is obtained with the aid of the approach related on the friction induced vibration based pattern detection while the preload applied to the surface is kept constant by the force-feedback controller.

ÖNYÜKLEME KUVVET KONTROLÜ İLE BİR YAPAY YÜZEY ÜZERİNDE SÜRTÜNMENİN YOL AÇTIĞI TİTREŞİME DAYANAN DESEN ALGILAMA

ÖZET

Son yıllarda mikro ve nano ölçekteki tribolojik araştırmalar hızlı bir şekilde gelişmektedir. Doğayı gözlemleme ve taklit etme eğilimi, bu gelişimde önemli rol oynamaktadır. Böylece biyolojiden esinlenilmiş ve insan odaklı çalışmalar, bu bilimsel alanın orijini, çıkış noktası haline gelmiştir. Birbiri üzerinde hareket eden yüzeyler arasındaki sürtünme ve tutunma etkileşimlerini daha derinlemesine anlayabilmek için bilimadamları tarafından birçok deneysel yapılar tasarlanmış ve çalışmalar gerçekleştirilmiştir. Buna ilave olarak bu tarz çalışmaların yürütülebilmesi için esas konu, hayvanların ve/veya insanların algılama mekanizmasının doğru kavranmasıdır.

İnsanoğlu, kendisinin çevresiyle iletişim kurmasını ve hayatta kalmasını sağlayacak vazgeçilmez bir algılama mekanizmasına sahiptir. Bu mekanizmanın olmazsa olmaz komponentlerinden biri, dokunsal algılamadaki kritik rolüyle insan derisidir. Özellikle insan vücudunda dokunsal algılama en fazla parmak uçlarındadır ki bunlar yüzey yapısını yaklaşık 1 cm^2 lik temas alanında ve 10-40 kPa gerilme seviyesinde algılayabilirler. Deri, insanın çevresiyle olan etkileşimi üzerinde önemli bir görev üstlenmektedir. Oyle ki çevreyle olan bu etkileşim, bilginin dış uyaranlardan gömülü reseptörlere aktarımı şeklindedir. Derinin dokunsal özellikleri, bu bilginin işlenmesini ve titreşim, basınç dağılımı, sıcaklık gibi fiziki duyulara kendi geribesleme sistemi sayesinde cevap vermesini mümkün kılmaktadır. İnsanın bu doku algılama mekanizmasının enteresan yapısı, son yıllarda araştırmacıları yapay yüzeyler üreterek dokunsal algılamanın taklit edilmesi için cesaretlendirmektedir. Yapay dokularla ilgili çalışmalar, aynı zamanda bilimadamlarına dokunsal algılamanın elde edilebilmesi için prosesin nasıl çalıştığını anlamaya ve otonom olarak yüzey algılama görevi ya da tıbbi görevli robotik alanındaki, tıp, dokuma ve kozmetik alanındaki uygulamaların gelişimine imkan sağlamıştır.

Dokunsal algılamanın elde edilebilmesi için kontakt ve relatif hareket, gerekli başlıklardır. Statik kontakta yüzey yapısı algılama mekanizmasının etkin bir sonucu olmamaktadır. Birbiriyle etkileşim halindeki iki yüzey arasında relatif hareket oluştuğu zaman yani uygun önyükleme ve kayma hızı koşullarında dinamik kontakt olduğunda, yüzey özelliklerinin algılanması olası hale gelmektedir. Dokunsal algılama, doku, şekil, kuvvet, sürtünme, sıcaklık ve ağrı algılamasından oluşan formlarda olmaktadır. Doku algılamanın temel ölçüsü pürüzlülüktür. Yüzey pürüzlülüğü ve dokunsal algılama arasındaki ilişki, birbirleriyle temas halinde bulunan yüzeylerin sürtünme özellikleri göz önünde bulundurularak incelenmektedir. Bir yüzeyin bir diğer yüzey üzerindeki yatay hareketi, pürüzlülüğün algılanmasına olanak tanımaktadır.

Bu yüzden can alıcı bir proses olan dokunsal algılamanın taklit edilmesi, triboloji, titreşim ve kontrolden oluşan disiplinlerarası bir çalışma gerektirmektedir. Yüzey pürüzlülüğü ve dokunsal algılama ile ilgili sürtünme çalışmaları birçok araştırmacı tarafından gerçekleştirildi, oysa sürtünmenin yol açtığı titreşime dayanan desen algılama halen devam eden araştırma konusudur. Bu gelecek vaad eden yaklaşım, sadece dinamik kontaktaki birbirine temas eden yüzeyler arasındaki sürtünme çalışmaları açısından değilde aynı zamanda frekans domaininde veri analizi açısından da ele alınmayı gerektirir. Sonuçta, önyükleme kuvvet kontrolü altındaki sürtünmenin yol açtığı titreşime dayanan desen algılama ile ilgili analiz, triboloji, titreşim ve kontrol alanlarını kapsayan disiplinlerarası çalışmayı içerir.

İnsandan esinlenilmiş mikro desenli yapay yüzey ile cam uç benzeri sert numune arasındaki relatif hareket süresince kayma, sürtünmenin yol açtığı titreşimler olarak adlandırılan titreşimler yaratır. Titreşimler, ilgili mekanoreseptörleri harekete geçirir ki bu reseptörler aracılığıyla titreşimler elektrik darbelerine çevrilir ve objenin yüzey bilgileri beyine aktarılır. Bu aşamalardan sonra insan, pürüzlülüğü de ihtiva eden yüzey yapısının özelliklerini algılayabilir. Bu prosedürü yapay dokulara, desenlerini algılamak maksatlı adapte etmek için yapay mikro desenli yüzeyler, farklı boşluk genişliği, tümsek genişliği, tümsek yüksekliği ve konumu gibi çeşitli ebat ve aralıktaki özelliklere sahip olmaktadır. Yüzey taraması süresince oluşan sürtünmenin yol açtığı titreşimler, yapay derinin desenine ait ve taranan yüzeyin tümseklerinin dalgaboyu ve yüksekliği tarzındaki bilgisini taşıyan frekansın algılanmasına imkan tanımaktadır. Dikkat edilmesi gerekir, zira çok önemli çalışma koşullarından biri sabit önyükleme kuvvetidir. Bunun için araştırmacılar tarafından literatürde ölü ağırlık kullanmak, kirişe davul bağlamak, manuel basamak ya da analog voltmetre kullanmak gibi çeşitli metotlar uygulanmıştır. Çok rastlanan metotlardan biri, ölü ağırlık kullanımıdır. Fakat bu tarz bir yaklaşım, sistem parametresi olan önyükleme kuvvetinin sabit tutulmasını garantilemez. Eğer bu çok önemli çalışma koşulu, bir kuvvet geribesleme kontrolcüsü tarafından gerçekleştirilirse, önyükleme kuvveti önceden tanımlanan değerine ulaştıktan sonra kayma süresince değişmeden kalır. Ayrıca dikkat edilmesi gerekir, zira kontrolcü kullanılması, önyükleme kuvvet hatasının deneylerin her bir aşamasında incelenmesini mümkün kılar. Böylece doğru ve hassas analiz yapılabilmesi sağlanmış olur. Buna ek olarak ölü ağırlık kullanılması, sistemin değişmez bir yapıya sahip olmasına sebep olur ki böyle bir yapıda gerektiğinde önyükleme kuvvet değeri değiştirilemez. Sonuç olarak bir kuvvet geribesleme kontrolcüsü kullanarak önyükleme kuvvetinin yüzey taraması süresince sabit tutulduğu ve gerekli durumlarda bu kuvvetin değiştirilebilindiği yarı otonom bir sistem tasarlamak, bu çalışmanın temel fikrini taşımaktadır.

Bu çalışmada, yapay olarak yapılan yüzey üzerinde sürtünmenin yol açtığı titreşime dayanan desen algılama yaklaşımı detaylarıyla ortaya konmuştur. Öncelikle isteğe göre yapılmış olan yarı otonom sürtünme-yapışma deney düzeneği tasarlandı ve kontrol numunesi olarak üretilen düz şeffaf polimer (PDMS- Polydimethlysiloxane) kullanılarak sert cam uca karşı sürtülüp bu düzenek gerçeklendi. Ayrıca deneysel testlerde kullanılmak üzere insan eli parmak uçlarının yapısından esinlenerek yapay deri tasarlanıp üretildi. Bir yandan insan eli parmak izindeki tümseklerin yüksekliği, dalgaboyu ve çukurların mesafesi baz alındı, ancak diğer bir yandan da deneysel çalışmaların yürütüldüğü laboratuarda yapay doku üretimi için kullanılan üç boyutlu yazıcının üretim kısıtları da göz önünde bulunduruldu. Bu kriterlere göre bir yapay doku üretilmiştir. Önceden de belirtildiği gibi ölçümler esnasında yüzeye uygulanan önyükleme kuvvetinin olabilecek minimum hata oranıyla sabit tutulabilmesi, bu

yöndeki çalışmalar için önemli bir noktayı oluşturmaktadır. Bu sebepten ötürü, yüzey taraması sırasında sabit önyükleme kuvveti için üç farklı kuvvet geribesleme kontrolcüsü, PID (Oransal-Bütünleyici-Türevsel), Adaptif PID, ve SMC (Kayma Modu Kontrolcüsü) tasarlandı ve denendi. Yapılan testler her iki polimer yüzeyde de uygulandı yani hem düz polimer hem de insandan esinlenilmiş ve eşit aralıklarla dağıtılmış tümsekleri olan yapay deri üzerinde uygulandı. Test sonuçlarına göre düz polimer numune kullanıldığında, yüzey taraması süresince yüzeye uygulanan önyükleme kuvvetini her üç kontrolcü de düşük hata oranlarıyla ve birbirlerine çok yakın değerlerde sabit tutabilmiştir. Ancak yine de SMC sayesinde hata oranı, % 1-1.5 seviyelerinde tutulabilinmiştir. Önyükleme kuvvetini yüzey taraması esnasında düz yüzey üzerinde sabit tutabilmekten daha da önemlisi, tümsekli şekilde üretilen diğer yapay doku üzerinde minimum hata oranıyla sabit tutabilmek. Yapılan ölçümlerde PID kontrolcüsünün yaklaşık % 80, adaptif PID kontrolcüsünün ise % 40 seviyelerinde bir hata oranıyla yüzeye uygulanan önyükleme kuvvetini sabit tutmaya çalıştığı gözlemlenmiştir. Ancak bu yüzeyde de yine en iyi sonuca ~ % 16 gibi bir oranla SMC kullanılarak ulaşılmıştır. Yani karşılaştırmalı sonuçlar, SMC kullanılmasının deneylerin sabit önyükleme kuvveti altında minimum hata oranıyla gerçekleştirilmesini mümkün kıldığını göstermiştir.

Sonrasında gezinme aralığı, kayma hızı ve önyükleme kuvveti gibi uygun çalışma koşullarının belirlenmesi için bazı testler gerçekleştirildi. Böylece şeffaf polimer ve sert yüzey arasındaki yapışma-kayma osilasyonlarının oluşma koşulları analiz edildi. Bahsi geçen bu etkilerin, 10 mN önyükleme kuvveti altında ve 0.02 mm/s kayma hızında elde edildiği yapılan denemeler sonucunda görülmüştür. Sabit kayma hızında yüzeye uygulanan kuvvet arttırıldığında, bu osilasyonların giderek yok olduğu ve kararlı kayma haline geçtiği gözlemlenmiştir. Sabit kuvvet altında hız arttırıldığında ise etkilerin genliklerinin giderek azaldığı, statik sürtünmeden dinamik sürtünmeye geçiş süresinin azaldığı ve buradaki eğimin giderek arttığı görülmüştür. Sonuç olarak, bu etkilerin oluşma şartları belirlenmiş olmuştur. Böylece esas yürütülen desen algılama deneyleri, bu koşulların dışında kararlı kayma bölgesinde gerçekleştirilmiştir.

Kayma hızı, önyükleme kuvveti ve uç çapı gibi değişik tasarım parametrelerinin desen algılama ve sürtünme üzerindeki etkileri, PDMS' den yapılan eşit aralıklı ve birbirine paralel tümsekleri olan insandan esinlenilmiş yapay deri üretilerek incelendi. Burada üç farklı çap ölçülerine sahip cam uçlar kullanıldı ve sonuçları karşılaştırıldı. Deneylerde hız etkisini gözlemleyebilmek için 20 mN sabit önyükleme kuvveti altında 0.09-0.49 mm/s arasında değişen hız değerleri, 12 mm gezinme aralığında uygulanmıştır. Kuvvet etkisini inceleyebilmek için ise 0.09 mm/s sabit kayma hızında 5-35 mN arasında değişen farklı önyükleme kuvvetleri yüzeye uygulanmıştır.

Çap ölçüsü 1 mm olan cam uç ile yüzey taraması gerçekleştirildiğinde, bu tipin yapay dokunun tümsekleri arasında gezinebilmesinden dolayı yüzeyin profilinin elde edilebildiği gözlemlenmiştir. Profil bilgisi, tümseklerin dalgaboyu ve yüksekliğini içermektedir. Yüzeye uygulanan önyükleme kuvveti arttırıldıkça, hata oranının % 70 seviyelerinden % 8 seviyelerine düştüğü elde edilmiştir. Hız arttırıldığında ise kuvvet hatası da % 16'dan % 55 seviyelerine artış göstermiş olup desene ait olan dominant frekans değeri de giderek sağa doğru kaymıştır. Desene ait olan bu frekans ile kayma hızı arasındaki doğrusal orantısallık, kayma hızı ve tümseklerin dalgaboyu arasındaki orana ($f = V/\lambda$) dayanarak gösterilmiştir. Bu bağıntı kullanılarak beklenen frekans değerleri hesaplanmıştır ve sürtünme kuvveti verilerine FFT uygulanmasıyla elde

edilen sonuçlardaki gözlemlenen dominant frekans değerleriyle karşılaştırılmıştır. Sonuçta bu her iki değerin de neredeyse aynı olduğu görülmüştür. Yani desene ait olan frekans değeri, ölçüm verilerine yapılan frekans analizi sonucunda da aynı değerlerde gözlemlenebilmiştür. Ayrıca tipin tümsekler arasına girerek yüzeyi taramasından dolayıda frekans sonuçlarında sinyalin harmonikleri de gözlemlenmiştir.

Çap ölçüsü 10 mm değerlerine çıkartıldığında önceki sonuçlara kıyasla genel olarak kuvvet hatalarında azalma kaydedilmiştir. Çap ölçüsünden dolayı tip, tümsekler arasına girememekte, tümseklerin üzerinden gitmektedir. Bu yüzden yapay dokunun sadece tümseklerinin dalgaboyu elde edilebilmektedir. Ayrıca bu deneysel sürtünme sonuçları, numunenin ters mikroskop kullanılarak elde edilen görüntüsüyle karşılaştırıldığında numunenin deseninin doğru bir şekilde tarandığı ispatlanmıştır. Yüzeye uygulanan önyükleme kuvveti arttırıldıkça, hata oranı % 35'den % 7'ye inmiştir. Hız arttırıldığında ise hata oranı % 11'den % 32'ye çıkmıştır. Bu sonuçlar, bir önceki çap ölçüsü kullanıldığında elde edilenlerle karşılaştırıldığında hata oranının azaldığı görülmüştür. Yine aynı şekilde yapılan frekans analizi sonuçlarında dominant frekans değeri beklenen değerlerinde elde edilebilmiştir.

Tip çapı etkisini daha net gözlemleyebilmek için 34.74 mm çapındaki tip ile çalışılmıştır. Sabit kuvvet altındaki iki farklı hız değeri kullanılarak yapılan test sonuçlarında, bu tipin kullanılmasının kuvvet hatasının daha da azalmasında etkili olduğu tespit edilmiştir. Ayrıca sürtünme kuvveti verilerine uygulanan FFT sonuçlarında desene ait olan dominant frekans değeri yine elde edilmiştir. Ancak bir diğer önemli nokta ise bu kadar büyük çaplı tip kullanılmasının, sinyalin harmoniklerinin filtrelenmesinde de etkin rol oynadığını ortaya koymuştur.

Önceden de bahsedildiği gibi test sonuçlarına göre önyükleme kuvveti, düşük kayma hızında ve yüksek kuvvet altında, minimum hata oranıyla sabit tutulabilmektedir. Bu çalışmanın sonucunda, bir yandan yüzeye uygulanan önyükleme kuvveti, kuvvet geribesleme kontrolcüsü tarafından sabit tutulurken, tümseklerin dalgaboyu ve yüksekliği gibi taranan yüzeyin bilgisi, sürtünmenin yol açtığı titreşime dayanan desen algılama yaklaşımı sayesinde elde edilmiştir.

1. INTRODUCTION

Human beings have an indispensable perceptual mechanism which allows them to communicate with the environment and survive. One of the essential components of this mechanism is the human skin with a critical role in the sense of touch [1]. Especially, on the human body the most touch sensing is at the fingertips which can perceive surface texture approximately on a 1 cm^2 area of contact, and at 10-40 kPa stress levels [2]. The skin undertakes a significant task on human interaction with the physical environment by conveying information from external stimuli to the embedded receptors [3-5]. Tactile properties of the skin allow to process this information and respond to physical sensations like vibrations by using its feedback system. Such an interesting feature of human texture perception mechanism encourages the researchers in recent years to emulate the sense of touch by producing artificial tactile skin although it is known to be a challenging and complex process [4-15]. To design artificial tactile systems becomes now promising issue to realize and improve applications in the fields of robotics with an autonomously surface detection task or surgical task, medicine, fabrics, and cosmetics [6].

1.1 Purpose of Thesis

Perceptual features of the skin provide humans to respond to sensations such as vibrations, pressure distribution, and temperature. By using vibration, some details like surface texture, slippage, and puncture enable to convey [5]. This process is taken place by the relevant afferent unit. The mechanoreceptive units which are one of the afferent units located under the skin in human hand are activated by vibrations transduced by mechanoreceptors and respond to the mechanical excitations. Thus, the crucial sense of touch allows assessing object properties including size, shape, texture etc [5, 16].

Tactile properties of human skin highlight the way of developing artificial tactile skin. To investigate the pattern detection on the human-inspired artificial structure by processing the frictional data, artificial polymer surface with evenly spaced parallel

ridges can be fabricated with an intention of mimicking tactile properties of human skin. The resource of the inspiration, including the properties of human touch perception and the dimensional structure of human hand ridges called fingerprint, allows scientists to develop artificial skin and comprehend how the process works to acquire tactile sensation. There are many applications for which the sense of touch is significant such as the improvement of tests for evaluating the tactile sensitivity during diagnosis; the development of artificial tactile sensors for intelligent prostheses or robotic assistants; and the investigation of the contact with objects of everyday life, with the aim of identifying its characteristic parameters [17].

The relationship between surface roughness and tactile sensation has been investigated by many researchers [1, 4, 6, 13, 16-19]. However, the topic of friction induced vibration based pattern detection is an ongoing research subject. The purpose of this thesis is to exhibit pattern detection and frictional properties of the human-inspired artificial polymer surface under different design parameters such as sliding velocity, preload, and diameter of rigid glass tip. The friction induced vibrations, occurred during the dynamic contact of surface scanning between the artificial surface and the rigid glass tip, allow to detect the frequency belonging to the pattern of the artificial skin, and carrying the information of the scanned surface like wavelength and height of ridges while the preload applied to the surface is kept constant by force-feedback controllers.

1.2 Proposal: Friction Induced Vibration Based Pattern Detection by Preload Control

To comprehend the process from touching to sensing like the surface texture, tribological effects between two surfaces contacting to each other and relative motion between them should be analyzed. Some of these effects comprise friction, roughness and surface structure. The essential property for texture perception is the roughness [5, 13, 15, 19, 20]. Thus, in this thesis it is aimed to detect the pattern of the human-inspired artificial surface with evenly spaced parallel polymer ridges made of PDMS (Polydimethylsiloxane).

During the relative motion between the artificial surface and rigid glass tip, the frequency of vibrations called friction induced vibrations will be constituted while the preload applied to the surface is kept constant by the force-feedback controllers.

2

So, controlling the preload during the surface scanning results in obtaining the frequency of vibration which concerns the information of the pattern such as wavelength and height of ridges.

It should be paid attention that one of the crucial working conditions which has to be provided is constant preload as it mentioned before. For this aim, various methods have been carried out by researchers in literature such as using a dead weight, mounting a drum on a beam, using manual stage, or analogue voltage meter [7, 11, 16, 19, 21]. One of the prevalent methods is using a dead weight [11]. However, such an approach does not provide to guarantee to keep the system parameter, preload, consistent. If this essential working condition is carried out by a force-feedback controller, the preload remains unchanged during sliding after reaching to the predefined value. It should be also noted that using a controller enables to investigate the preload error on every step of experiments which allows to have accurate and sensitive analysis. In addition, to use dead weight causes the system to have a fixed structure on which the preload value cannot be changed if it is necessary. As a result, it is aimed to design a semi-autonomous system, on which the preload is kept constant by using a force-feedback controller during surface scanning, and can be changed in necessary situations.

In addition, it is desired to investigate the frictional properties of the dynamic contact between artificial surface and rigid glass tip by observing the effect of the design parameters include diameter of the glass tip, sliding velocity and preload. The necessary relation between the frequency of vibration and the sliding velocity will be the ratio of the sliding velocity and wavelength of the ridges. The frequency related to the pattern is linearly proportional to the sliding velocity. Thus, any changes on the design parameters will play an important role in pattern detection.

Consequently, properly tuned and controlled preload on the human-inspired artificial skin allows to obtain the frequency of vibration called friction induced vibration containing the information of the pattern. During controlling the preload, the filter effect of the tip diameter will result in elimination of the harmonics of the signal.

1.3 Background

Observing and understanding mechanism in nature provide humans new inspiration sources to develop scientific researches by producing artificial systems. One of the most significant subjects for human beings and animals is touch perception. For this perceptual mechanism the essential means is the sense of touch by which they can interact with their physical environment [4, 5]. For instance, spiders can feel vibrations belonging to surrounding and differentiate the vibrations caused by insect or wind [5].

With the aid of the skin, humans can respond to sensations such as vibrations which cause to activate the mechanoreceptive unit in human hand under the skin [6, 17]. After conveying the information of the object surface to the relevant tactile receptors, vibrations are converted into electric impulses which are processed by the brain [17]. Therefore, such a crucial sense of touch attract researchers' attention in recent years to emulate its properties by producing artificial tactile skin, and to apply the developments to the surgical and medical robotics research area although mimicking the sense of touch is known to be a challenging and difficult process [5].

There are some investigations in literature to understand how the human touch perception mechanism work as a neural coding point of view [18, 19, 22]. One of the important afferent units, the mechanoreceptive unit located in the human hand under the skin and responding to mechanical excitations, is explained in details. According to their different depths in the skin, human can feel and differentiate the vibrations at various frequency levels related on the static and dynamic skin deformations.

Therefore, the knowledge about the tactile receptors, the mechanoreceptors, permits scientists to explore the relationship between the surface roughness and tactile sensation in details. To feel the surface of an object, the steps of the touch perception are as follows; 1) human fingertip rubs on the surface, 2) sliding generates vibrations called friction induced vibrations, 3) vibrations activate the related mechanoreceptor, 4) receptor convert these vibrations into electric impulses and convey the information of the object surface to the brain. So, human perceives the properties of the surface structure [16].

To comprehend perceptual mechanism more in details, frequency analysis of the signals obtained by the dynamic contact of the surfaces moved relative to each other

should be exhibited [16, 17]. Related to this point, in one of the pioneer studies to examine the frictional behaviors of the human skin and observe the vibrational frequency spectra induced by the human fingertip-surface scanning, a set of experiments are realized by using real finger and sample surfaces with various roughness and wavelengths values ranging from 0.64 μm to 5.2 μm, and from 0.78 mm to 2.17 mm, respectively. In the study to keep the normal load constant on 1.5 ± 0.7 N during sliding, the finger is fixed and the sample is moved at a constant speed by the machine based on a hydraulic movement system. According to the experimental results, the FFT (Fast Fourier Transform) of the acceleration measured on the finger for different sliding speeds ranging from 10 mm/s to 50 mm/s provides that increasing the speed, the frequency spectra distribution covers larger values meaning that the dominant frequency value shifts to the right. The relation between the sliding velocity and the wavelength of the surfaces ($f = V/\lambda$) is supported with the experimental results as well [17].

Normally, during controlling the normal load, the appropriate diameter size of rigid specimen (glass tip) filters the harmonics of the signal. Although in the study it is noticed that the normal load is kept constant, the normal load controlling mechanism does not work sufficiently such that the harmonics are observable. Furthermore, it is mentioned also that increasing the applied force, sprag-slip and stick-slip behaviors of contact vibrations are measured which are usually prevented by controlling the normal load which is applied on the finger [17]. Thus, under relevant conditions, other than the vibrational frequency of the pattern some effects like stick-slip can be observed on the frequency analysis. For instance, stick-slip effects on soft materials like elastomers are obtained under low sliding velocity with low preload or under high sliding velocity with high preload [23]. If there will be uncontrolled preload conditions, and experiments want to be realized under high sliding velocity with low preload, the value of the preload can be getting higher and then the information of stick-slip vibrations will be obtained on the gathered data sets as well which is an undesirable condition. Because of these reasons, preload control mechanism is significant actually.

Studies about the concept of emulating a human finger for tactile sensation are applied on foundations in cosmetic sector as well [7]. The contact load and sliding velocity values are chosen as 0.05-0.25 N and 1-20 mm/s respectively, by taking into

account the human finger action of rubbing the surfaces. Sample surfaces are made of silicone rubber, and supported by double-cantilever springs that allow the movement of the surfaces. The upper surface is a hemisphere with 16 mm diameter. For non-grooved surface the lower one is a plate with 1 mm thickness. Four types of cosmetic foundations are used. Each sample of foundations is applied homogeneously on the lower surface by a cosmetic powder-puff. For grooved pattern surface, human finger-print like grooved pattern is used by employing it on the lower surface perpendicular to the sliding direction. The contact load is adjusted with the deflection of the related spring, and then the lower surface is moved by a motorized stage in tangential direction [7].

According to the tests on the study, for obtaining tactile sensation related on the cosmetic foundation both static information (like static and dynamic friction coefficients) and dynamic information like frictional vibration are needed for non-grooved and grooved pattern surface experiments. For grooved pattern surface the width of the groove is 0.2 mm, the depth is 0.1 mm, and the pitch (wavelength) is 0.4 mm. Tests showed that two types of vibrations are observed. One of them is the natural frequency called unstable vibration, and the other one is frequency of vibration called forced vibration generated by the grooves [7].

For ungrooved pattern it is obtained that under certain sliding velocity (under 4 mm/s) and contact load (0.20 N), the increase of the velocity causes an increase on the frequency with a constant amplitude corresponding to a stick-slip vibration. When the velocity is higher than 6 mm/s, the frequency is constant corresponding to natural frequency. Increasing the velocity, the amplitude of the frequency increases also [7]. This observation has an additional meaning such that under relevant frictional conditions, there will be stick-slip effects on soft materials like silicone rubber. If the experiments will not be realized under appropriate sliding velocity and contact loads, the effects like stick-slip vibrations will occur as well. As it mentioned on the previous study that sprag-slip and stick-slip behaviors are usually avoided by controlling the normal force during surface scanning. Moreover, if sensitive frequency analysis at low levels on pattern detection is considered, the elimination of all frequencies except vibrational frequency belonging to the pattern becomes an essential subject.

There are some investigations related on the physics behind the tactile sensation and the effect of the texture-induced modulations of friction forces. Thus, the subject of micropatterning effect in solid-solid friction becomes an important issue [9, 24]. In the study the friction dynamics between an elastomer patterned with parallel grooves like human fingerprint ridges and an abraded glass slides are investigated in details at constant velocity (range 0.01-0.5 mm/s) and under constant normal force (range 0.02-2 N). The surface of the elastomer consisted of a periodic square grating of depth 40 μm and spatial period λ = 125, 218, or 760 μm (width λ/2). It is showed that with any nonlinearity in the friction law texture-induced friction force fluctuations developed, and an increase in the modulation of friction with loading force can be obtained [9, 24].

The results showed that if the ridges are located perpendicular to the direction of motion, periodic oscillations occurred consisting of a dominant oscillation frequency and its harmonics. But, if the ridges are located parallel to the direction of motion, this dominant frequency and the harmonics are disappeared. In addition, it is also mentioned that at all loads the patterned elastomer is in contact with the glass slide only at the top, called summit, of the ridges [9]. Controlling the normal load with a controller and using a glass tip with a appropriate diameter for the ridge wavelengths will result in scanning and detecting the pattern in details which means the contact of two surfaces occur not only at the summit of the ridges but also in the grooved region between the ridges. So, the information of the surface structure can be obtained. In addition, using the appropriate diameter size of rigid glass tip will solve the problem observing the harmonics of the signal and filter them.

Mimicking the touch perception of human hand by emphasizing the role of the human fingerprints in the coding of tactile information using a biomimetic sensor is the another important research area [4, 25-27]. The improvements of these studies are essential also for some robotic applications such as grip control. It is designed a biomimetic tactile sensor which is mounted on a rigid base. This sensor is covered with a cap made of elastomer, and its surface is smooth or patterned with regular square waved ridges whose dimensions are as wavelength of the ridges is 220 μm, and depth is 28 μm. By surface scanning with this sensor the dominance of the frequencies is demonstrated that are in the sensing range of Pacinian afferents located in human hand. Experiments are realized at 0.2 mm/s sliding velocity and

under 1.71 N constant load. Using the smooth sensor, a low-pass filter effect is observed. All pressure modulations coming from the texture components of wavelength smaller than ~ 1 mm are weakened. By using the fingerprinted sensor, band-pass filter properties are obtained with spatial frequency $1/\lambda$ and its harmonics [4]. Therefore, if there will be used a force-feedback control mechanism in the study for providing constant load and the appropriate diameter size of rigid glass tip, the harmonics of the signal will be filtered.

In addition, biomimetic touch sensors covered with soft and elastic polymers, called coverings, are used in many robotic applications to improve robostness. Moreover, using such elastic covers with human fingerprint-like structures, results in improving grip and avoiding slip. However, as it exhibited before that elastic covers act as low-pass filters. Due to this property, these covers eliminate the high frequency components belonging to tactile information which cause to desensitize the touch sensors [25]. To solve the desensitization of the touch sensors, it is proposed to use a fluid or gel filled pad in an elastomer constructing a conveying mechanism [26, 27].

2. PATTERN DETECTION

2.1 Texture Perception

Perceptual mechanism has a crucial role in human interaction with the environment. The necessary means, through which the information belonging to external stimuli is conveyed to the relevant tactile receptors, is the human skin [1, 3-6]. Tactile properties of the skin provide humans to have an excellent system which behaves like a closed-loop feedback system. With the aid of this feedback system, the mechanical excitations in the form of vibrations for instance are responded. Thus, human can perceive the properties of the surface structure scanned by finger, or decide how much pressure or force is enough to grasp an object.

To acquire the perception of the related structure, contact and relative motion are required for tactile sense [28] which is the origin of this receiver and transmitter perceptual system. To observe the importance of the sense of touch, a simple experiment is realized on which the volunteers put their hands on an ice block for a while. After that they lost their sense of touch temporarily which results in having difficulties to provide a stable and sensitive grasp of the objects [29, 30]. Lack of this sense causes such unstable and inaccurate conditions.

Therefore, touch is the most critical sense among the others which receives the information from external stimuli, undertakes a role of augmentation of other senses to perceive the contact, motion, shape, and texture. Ability of recognition of texture, shape, and grasping objects are gained to humans by this sense [31]. In other words, tactile perception is a significant mechanism which carries information about the contact, the relative motion of the contacting surfaces, the direction and amount of the forces. These informations are indispensable for texture perception, discrimination, and grasping objects sensitively [10].

As a consequence, static contact, relative motion (dynamic contact) and friction allow humans to process the information and perceive the properties of the structures such as size, shape, roughness, and texture [5, 10, 28, 31]. In other words, the

information like roughness, thickness, and friction affect the human decision in texture perception [6, 32]. Among these, the essential property for texture perception is the roughness [5, 13, 15, 19, 20]. Thus, the artificial micropatterned surfaces which are designed to emulate the human sense of touch, understand the frictional properties of the structure, and detect the pattern have various features in size and spacing such as different groove width, ridge width, ridge height and orientation.

2.2 Human Touch Perception

To be able to apply the texture perception mechanism of humans to artifacts, mimicking the properties and the process of human sense of touch by producing artificial tactile skins attract scientists' attention in recent years. Related to this subject, there have been carried out many investigations to date [4, 7, 9, 16, 17, 25].

The skin carries an essential role in the sense of touch, and has an important task on human interaction with the physical environment by conveying information from external stimuli to the embedded receptors [1, 3-5]. In human hand under the skin, various types of afferent units are located in various layers of the skin which are mechanoreceptive units (for pressure/vibration), the thermoreceptive units (for temperature), and the nociceptive units (for pain/damage) [5, 17]. The glabrous skin of the hand has the most nerve endings, and about 17,000 mechanoreceptors are located inside the skin. These receptors have four types of tactile receptors comprising Meissner's Corpuscles, Merkel Disks, Ruffini Organs, and Pacinian Corpuscles shown in Figure 2.1. They are classified based on their receptive fields, the speed, and the intensity through which they can adapt to static stimuli [33].
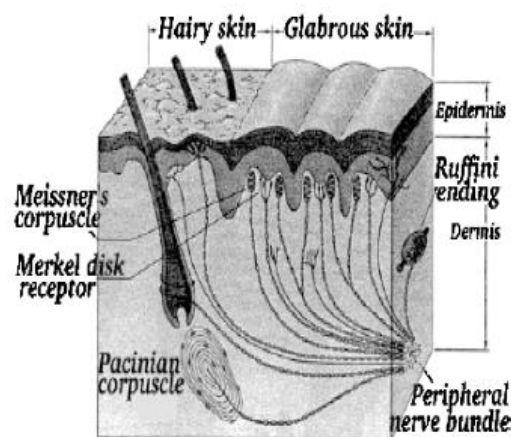
Figure 2.1 : The locations of mechanoreceptors in human hand under the skin [33].

10

The mechanoreceptors can be divided into two groups related on their adaptation; rapidly adapting units (RA) with no static response, and slowly adapting units (SA) with static response [5, 17]. According to their receptive fields, they are categorized in two types such as Type I named for small receptive fields, called near field also, and Type II named for large fields, called far field also. These receptors are located under the skin at different depths, and depending on these depths they are activated at different frequency levels shown in table 2.1 [17, 31].

Table 2.1 : Response properties and frequency ranges of receptors [31].

Type of Receptor	Response Characteristics
Merkel (SA I) (near field; continuous, irregular discharge)	Slow, fine details, 1-16 Hz
Meissner (RA I) (near field; On-off discharge)	Slightly faster, grip control, 2-60 Hz
Ruffini (SA II) (far field; continuous, regular discharge)	Slow speed, stretching, 100-500 Hz
Pacinian (RA II) (far field; On-off discharge)	Fast, vibration, dynamic texture, 40-500 Hz

These tactile receptors, called mechanoreceptors, are activated by contact vibrations. The RA I units are excited between 2 and 60 Hz which located at a depth of 0.5-0.7 mm in the skin. They respond to dynamic skin deformations like increase and decrease of indentation, and are insensible to static contacts. RA I can discriminate fine spatial details, and are required for grip control due to providing the slip information. Because the RA II units are located in the deeper dermis layer with 1.5-2.0 mm, they are very sensitive to mechanical vibrations of higher frequencies with a range of 40-500 Hz. They have the ability of detecting the acceleration vibration [17].

The SA I and SA II respond to static skin deformations. SA I units are excited between 1 and 16 Hz which are sensitive to fine spatial details. They are able to detect the local stress-strain field, and the conveyed information is the pressure. The SA II units react from 100 to 500 Hz, and are sensitive to remote lateral stretching of the skin due to the fact that their long axis is parallel to the skin surface. They support the perception of object motion, direction, and finger position [17]. Furthermore, the transduction mechanism in the human skin has chemical attributes.

But the result of the stimulations like force, position, size, softness/hardness, roughness, and texture shows that the result is a response of electrical discharge. Then these responses are conveyed to the brain [5].

When there is no relative motion between two surfaces contacting to each other, just SA units are activated continuously, whereas RA units are activated at the beginning of the contact. When there is a relative motion, SA units are activated, and RA units are activated by the friction induced vibrations due to dynamic contact [16].

To understand and observe the frictional properties of the texture perception mechanism of humans, the researchers try to design various artificial tactile surfaces like skin in similar dimensions as human has. Human fingerprints have ridges with dimensions circa 0.1 mm in height and 0.3-0.5 mm in width. Their shape is a combination of a trapezoid and semicircle [6]. In addition, humans can discriminate the particles size of a diameter range 180-710 μm [28]. Therefore, to study the frictional properties of the artificial skin and to detect the pattern of this surface, the relationship between surface roughness and tactile sensation should be analyzed.

2.3 Relation between Surface Roughness & Tactile Sensation

To acquire tactile sensation, contact and relative motion are necessary subjects [28]. In a static contact, the surface texture perception mechanism does not have an effective result. When a relative motion between two surfaces contacting to each other occurs which means dynamic contact takes place under relevant preload and sliding velocity, perception of the surface characteristics becomes possible [16].

Tactile sensing takes some forms comprising the detection of texture, shape, force, friction, temperature, and pain. Fundamental dimension of the texture perception is the roughness [5, 13, 15, 19, 20]. The relation between surface roughness and the tactile sensation is investigated by taking into account the frictional properties of the surfaces contacting to each other. Lateral motion of the surface over the other one permits to perceive the roughness [8, 16, 17, 28]. Meanwhile, scanning the surface with fingertip or rigid glass tip generates vibrations, the friction induced vibrations, which propagate in the skin [1, 6, 7, 16, 17, 34]. Then, the information belonging to the surface structure is conveyed to the mechanoreceptors which convert the vibrations into electric impulses. These impulses are processed by brain [17].

Thus, it is obvious that to comprehend the touch perception mechanism, only the frictional studies between the contacting surfaces in a dynamic contact are not sufficient. Frequency analysis of the generated vibration signals, which carry the clues about surface information such as roughness, should be developed in details.

2.3.1 Friction induced vibration based pattern detection

Tactile properties of human skin attract researchers' attention, and become an inspiration source to emulate the human sense of touch by producing artificial surfaces. Studies related on the artifacts allow scientists also to comprehend how the process works to acquire tactile sensation, and to improve applications in the fields of robotics with an autonomously surface detection task or surgical task, medicine, fabrics, and cosmetics [4-7, 10-13, 15, 21, 26, 27, 30, 31, 35-37].

Therefore, the crucial and complex process, emulating the sense of touch, needs a multidisciplinary study comprising tribology, vibration, and control. Frictional studies related on the surface roughness and tactile sensation have been carried out by many researchers [17, 19, 21, 28], whereas the subject of friction induced vibration based pattern detection is rarely investigated to date. This promising research topic needs to consider not only the frictional studies between the contacting surfaces in a dynamic contact but also data analysis in frequency domain. Consequently, analysis about the friction induced vibration based pattern detection by preload control includes multidisciplinary study containing tribology, vibration, and control.

During the relative motion between the human-inspired micropatterned artificial surface and rigid glass tip, sliding generates vibrations called friction induced vibrations [1, 6, 7, 16, 17, 34]. Vibrations activate the related mechanoreceptor through which these vibrations are converted into electric impulses and conveyed the information of the object surface to the brain. After these steps, human can perceive the properties of the surface structure including the roughness [16]. To adapt this procedure to the artifacts for detecting their pattern, the artificial micropatterned surfaces have various features in size and spacing such as different groove width, ridge width, ridge height and orientation [1, 4, 7, 13, 14, 16, 17, 19]. The friction induced vibrations occurred during the dynamic contact of surface scanning allow to detect the frequency belonging to the pattern of the artificial skin, and carrying the

information of the scanned surface like wavelength and height of ridges while the preload applied to the surface is kept constant by the force-feedback controllers. During controlling the preload, the filter effect of the tip diameter will result in elimination of the harmonics of the signal. As a consequence, the steps from sliding to pattern detection can be summarized in the following Figure 2.2.
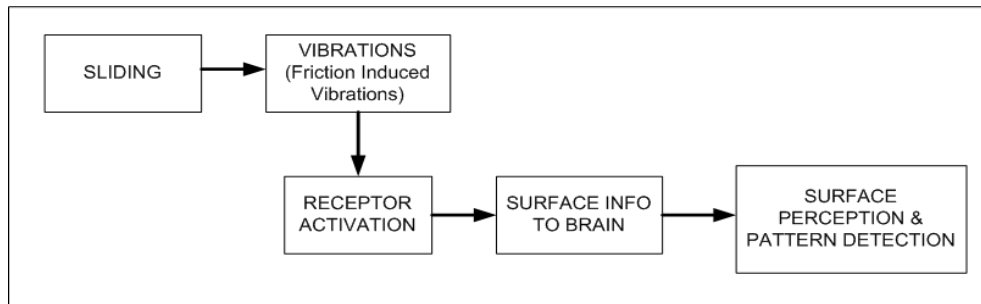
Figure 2.2 : Steps from surface sliding to pattern detection.

Furthermore, it is desired to investigate the frictional properties of the dynamic contact by observing the effect of design parameters include diameter of the glass tip, sliding velocity and preload. The necessary relation between the frequency of vibration and the sliding velocity will be the ratio of the sliding velocity and wavelength of the ridges ($f = V/\lambda$). The frequency related to the pattern is linearly proportional to the sliding velocity [4, 6, 7, 9, 16, 17]. Thus, any changes on the design parameters will play an important role in pattern detection.

2.4 Applications

The process of human touch perception mechanism becomes the inspiration source for researchers in recent years to mimic the sense of touch by developing artificial tactile skin, and to apply the improvements to the surgical and medical robotics research area although mimicking the sense of touch is known to be a challenging process [5]. The other applications for which the sense of touch is significant are as follows; the improvement of tests for evaluating the tactile sensitivity during diagnosis; the development of artificial tactile sensors for intelligent prostheses or robotic assistants; and the investigation of the contact with objects of everyday life, with the aim of identifying its characteristic parameters [17].

To comprehend the process from touching to sensing like the surface texture, tribological effects (comprising friction, roughness and structure) between two

surfaces contacting to each other and relative motion between them should be analyzed. However, to achieve this aim, a multidisciplinary approach is needed to investigate the frictional studies between two surfaces in a dynamic contact, and carry out frequency analysis of the generated vibration signals, which have the clues about surface information such as roughness.

To understand how the human touch perception mechanism works, there are some investigations in literature based on the neural coding system [18, 19, 22]. The mechanoreceptors, located in the human hand under the skin, are activated by vibrations, and respond to mechanical excitations. According to their different depths in the skin, human can feel and differentiate the vibrations at various frequency levels related on the static and dynamic skin deformations.

Based on the knowledge about the tactile receptors, researchers begin to examine the relation behind the surface roughness and tactile sensation. To understand perceptual mechanism more in details, frequency analysis of the signals obtained by the dynamic contact of the surfaces are exhibited [16, 17]. Thus, in the study experiments are realized by using real finger and sample surfaces with various roughness, 0.64 - 5.2 μm, and wavelengths, 0.78 - 2.17 mm, to observe the frictional behaviors of the human skin, and the vibrational frequency spectra induced by the human fingertip-surface scanning. The normal load is kept constant on 1.5 ± 0.7 N by fixing the finger, whereas the sample is moved at a constant speed by the machine. The frequency analysis of the acceleration data measured experimentally on the finger for different sliding speeds, 10-50 mm/s, demonstrated that increasing the speed, the frequency spectra distribution covers larger values meaning that the dominant frequency value shifts towards the right. The frequency of vibration is formulated based on the relation between the sliding velocity and the wavelength of the surfaces ($f = V/\lambda$) [17].

The other application area of the concept of emulating a human finger for tactile sensation is the foundations in cosmetic sector [7]. The design parameters, contact load and sliding velocity, are so chosen that they matched with the human finger action of rubbing the surfaces (for load as 0.05-0.25 N and for velocity 1-20 mm/s). The upper surface is a hemisphere with 16 mm diameter. Sample surfaces made of silicone rubber are designed as non-grooved and grooved surfaces. Four types of cosmetic foundations are used each of them is applied homogeneously on the lower

surface by a cosmetic powder-puff. The contact load is adjusted with the deflection of the related spring. The dimensions of the grooved pattern surface are as follows that the width of the groove is 0.2 mm, the depth is 0.1 mm, and the wavelength is 0.4 mm. The results showed that two types of vibrations are observed. One of them is the natural frequency called unstable vibration, and the other one is frequency of vibration called forced vibration generated by the grooves [7]. For ungrooved pattern it is obtained that under certain sliding velocity (under 4 mm/s) and contact load (0.20 N), the increase of the velocity causes an increase on the frequency with constant amplitude corresponding to a stick-slip vibration. But, when the velocity is higher than 6 mm/s, the frequency is constant corresponding to natural frequency. Increasing the velocity, the amplitude of the frequency increases too.

The physics behind the tactile sensation and the effect of the texture-induced modulations of friction forces is an another subject carried out by some researchers [9]. In the study the friction dynamics between an elastomer surface patterned with human fingerprint-like parallel grooves and an abraded glass slides are investigated in details at constant velocity (range 0.01-0.5 mm/s) and under constant normal force (range 0.02-2 N). A periodic square grating on the elastomer surface is in dimension of depth 40 μm and spatial period λ = 125, 218, or 760 μm (width $\lambda/2$). It is showed that with any nonlinearity in the friction law texture-induced friction force fluctuations developed, and an increase in the modulation of friction with loading force can be obtained [9, 24]. The results showed that the directional location of the ridges is important. If the ridges are located perpendicular to the direction of motion, periodic oscillations occurred consisting of a dominant oscillation frequency and its harmonics. But, if the ridges are located parallel to the direction of motion, this dominant frequency and the harmonics are disappeared [9].

The improvements of the studies related on the mimicking the touch perception of human hand is essential also for some robotic applications such as grip control. On these studies the role of the human fingerprints in the coding of tactile information using a biomimetic sensor is emphasized [4, 25-27]. It is designed a biomimetic tactile sensor which is mounted on a rigid base. This sensor is covered with a cap made of elastomer, and its surface is smooth or patterned with regular square waved ridges whose dimensions are as wavelength of the ridges is 220 μm, and depth is 28 μm. Sliding velocity is 0.2 mm/s, and load is kept constant on 1.71 N. By surface

scanning with this sensor the dominance of the frequencies is demonstrated that are in the sensing range of Pacinian afferents located in human hand. Using the smooth sensor, a low-pass filter effect is observed. By using the fingerprinted sensor, band-pass filter properties are obtained with spatial frequency $1/\lambda$ and its harmonics [4].

Consequently, as it is demonstrated that there are various studies in the literature related to this subject. However, they have the common point which is lack of controlling preload during sliding with a force-feedback control algorithm. When the results are examined, it can be seen that on the frequency analysis the dominant frequency of vibration is obtained but with its harmonics. Actually, during controlling the preload, the filter effect of the appropriate diameter size of rigid specimen (glass tip) will result in elimination of the harmonics of the signal. Thus, keeping the applied load constant on the surface by force-feedback controller allow to obtain the frequency of vibration called friction induced vibration containing the information of the pattern such as wavelength and height of ridges.

In addition, it is also known that stick-slip effects on soft materials like elastomers are obtained under low sliding velocity with low preload or under high sliding velocity with high preload [23]. Therefore, if there will be uncontrolled preload conditions, and experiments want to be realized under high sliding velocity with low preload, the value of the preload can be getting higher and then the information of stick-slip vibrations will be obtained on the gathered data sets as well which is an undesirable condition. As it mentioned that sprag-slip and stick-slip behaviors are usually avoided by controlling the normal force during surface scanning. Furthermore, if sensitive frequency analysis at low levels on pattern detection is considered, the elimination of the high frequency components belonging to the pattern becomes an essential subject.

Thus, the purpose of this thesis is to exhibit pattern detection and frictional properties of the human-inspired artificial polymer surface under different design parameters such as diameter of the glass tip, sliding velocity and preload. The friction induced vibrations occurred during the dynamic contact of surface scanning between the artificial surface and the rigid glass tip allow to detect the frequency belonging to the pattern of the artificial skin, and carrying the information of the scanned surface like spacing between ridges while the preload applied to the surface is kept constant by the force-feedback controllers. During controlling the preload, the filter effect of the

appropriate diameter size of rigid specimen (glass tip) will result in elimination of the harmonics of the signal.

To achieve the aim of this thesis, it is mentioned before that a multidisciplinary approach is needed to investigate the frictional studies between two surfaces in a dynamic contact, and carry out frequency analysis of the generated vibration signals, which have the clues about surface information such as roughness.

.

3. SURFACE FRICTION OF SOFT MATERIALS: POLYMERS

3.1 Basics of Polymer Friction

Development in science and technology results in being able to study complex and multidisciplinary processes in recent years. Moreover, the size of means decreased down to micro/nanometer scale used in experimental investigations. As a consequence of this situation, comprehension of tribology at molecular level becomes essential.

Friction is one of the basic engineering discipline and a part of the multidisciplinary science of tribology. This phenomenon is considered if a relative motion occurs at the interface of surfaces, and provides a resistive effect on this type of motion. The friction force is in the opposite direction of motion and tangential to the interface of the surfaces [38].

3.1.1 Principle laws of friction

During the Renaissance period, Leonardo da Vinci supported the study of friction by his scientific works. He is a pioneer on this area by introducing for the first time the concept of friction coefficient which is known as the ratio of the friction force to normal force $\mu = F/N$. Although he was never referred to friction force, his observations written on his notes are parallel with the statement of the first laws of friction which are named after the French engineer Guillaume Amontons in the seventeenth century. The two basic laws of friction are provided by Amontons in 1699 as follows;

1. The force of friction is directly proportional to the applied load.
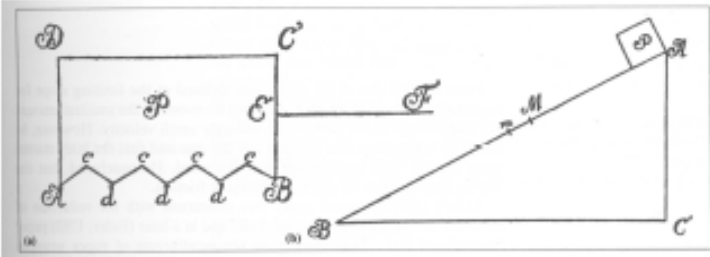2. The coefficient of friction is independent of the apparent area of contact.

Amontons used in his studies copper, iron, lead, and wood in various combinations as test specimens shown as in Figure 3.1 [39]. Similar to Leonardo's observations about constant friction coefficient of 1/4, Amontons exhibited that materials used in experiments have a constant coefficient of friction of 1/3. Amontons thought that

surface irregularities caused to the frictional resistance. In addition, he thought also to initiate the sliding, a force is needed for relative motion means lifting the asperities of one surface over the other one. Amontons' 1/3 rule was known as deviation with variations in materials, surface quality, and the type of lubricant. Related to this point, the deviation of cohesive forces is explained by John Theophilus. His proposal is that cohesion can be related to sliding friction by its contribution.
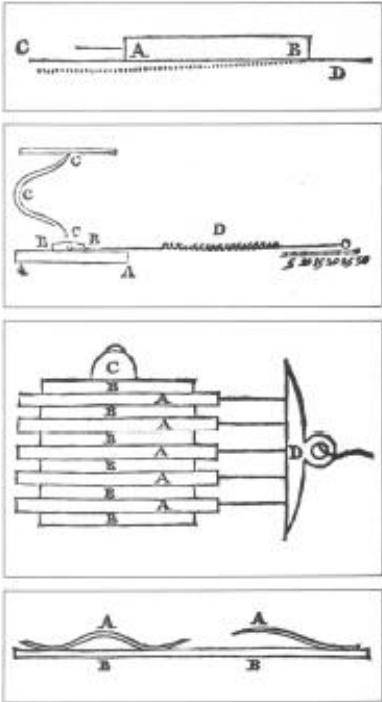
Figure 3.1 : Original sketches of Amontons' friction experiments [39].

In 1748, other important studies about friction are exhibited by Leonhard Euler. His suggestion was that the surface asperities have a triangular shape with a slope of α pointed by Amontons shown in Figure 3.2 [38].

Figure 3.2 : Studies of friction belonging to Euler [38].

Euler introduced to the coefficient of friction with the relation of $\mu = \tan\alpha$. By studying on the sliding motion down an inclined plane shown in Figure 3.2, concept

20

of static and kinetic friction became more understandable. He stated that the kinetic friction must be smaller than the static friction [38].

Charles Augustine Coulomb thought that mechanical interlocking is the cause of friction, and adhesion had also a role in friction. Desaguliers introduced to the idea of adhesive forces, and developed a general expression for friction with adhesion as follows

$$F = A + \frac{P}{\mu}$$ (3.1)

where the first term is related to adhesive effects and the second one is the deformation action. Due to the fact that he observed the friction is independent of the size of the surfaces, the contribution from adhesive forces is very small and can be neglected. The other discussion point of Coulomb is the relationship between kinetic and static friction. He thought a tangential force at an interface is the cause of the asperities of both surfaces. After a certain amount of deformation, sliding begins. This results the situation that frictional force depends on the nature of the asperities and load, however not the size of the contact area. Once sliding is started, the asperities fold over. It decreases the slope and causes that the kinetic friction to be lower that static one [38]. So, the third law of friction is developed;

3. Kinetic friction is independent of the sliding velocity.

In 1785, a professor at Cambridge Samuel Vince concluded that kinetic friction is independent of the sliding speed but not entirely independent of the apparent area of contact. This statement constituted the relation as $\mu_s = \mu_k + $ adhesion.

Starting from Leonardo and Amontons there are many studies and findings on friction. However, for more understanding on the concept of the friction, detailed characterization and molecular level studies of surfaces and interfaces are required. In the 1920's with the aid of Langmuir's work on this subject, surface chemistry became more understandable. In 1929, an approach about molecular adhesion is exhibited by Tomlinson, and the suggestion of the linear relation of the friction force and normal load depending on the number of the interacting atoms is supplied.

Then, Bowden and Tabor developed the adhesion theory of friction. According to their statement, two surfaces make contact only at points of asperities [38, 40]. Under

very high stresses plastic deformations occur. The average normal pressure, P, and friction force, F, can be written as

$$P = A * H \tag{3.2}$$

$$F = A * S \tag{3.3}$$

$$\mu = \frac{F}{P} = \frac{S}{H} \tag{3.4}$$

where A is the real contact area, H is the hardness of the softer material, and S is the shear strength of the bond. This approach was not sufficient for all experimental studies due to lack of details about deformation and even interactions. But, to include the mechanical properties of the materials was a significant progress. Then, plastic flow occurred at the asperities even for small static loads are showed by Bowden and Tabor [38].

Furthermore, adhesion and friction are the subjects which should be discussed together on some cases. If the used material is a polymer, then adhesion, deformation, and some another effects become to be subject.

Polymer friction is different from the other friction cases. Because of their elastic and viscoelastic behaviour (deformation) Amontons' laws does not confirm generally. Friction of rubber increases with sliding speed which is discovered by Arino in 1929. Then, Derieux confirmed in 1934. After a certain velocity, stick-slip sliding and the sliding friction coefficient decreased with load were observed by Roth and coworkers in 1942. The relationship is as follows

$$F = k * P^n \tag{3.5}$$

$$\mu = \frac{F}{P} = k * P^{n-1} \tag{3.6}$$

(n-1) is between 0.2 and 0.3 for many polymers in static frictional case and k is a constant [38]. μ decreases when the normal load increases which results from the plastic deformation. In 1952, Schallamach had an approach to this case which stated the polymers' frictional behaviour resulted from an elastic deformation of spherical surface asperities. As in Amontons' laws, at higher loads the asperities had a shape of flat and so, true contact area is the same as apparent contact area which is termed as single point contact. Here, friction force is proportional to the true contact area. As a result of the elastic deformation, it is

$$A\alpha\left(P^{2/3}\right) \tag{3.7}$$

$$F\alpha\left(P^{2/3}\right) \tag{3.8}$$

$$\mu = k * P^{-1/3} \tag{3.9}$$

Due to the fact that the Johnson-Kendall-Roberts (JKR) theory was not developed yet on which the surface forces are included, these relations were based on a Hertzian contact.

In equation 3.9, for viscoelastic deformation the exponent may be written as 2/3 which is a proposal of Pascoe and Tabor in 1956 on which $2 < m < 3$ because $m = 2$ plastic and $m = 3$ at elastic contact. Viscoelastic behaviour is more suitable for polymers whose μ can be written as follows [38]

$$\mu = k * P^{(2-m)/m} \tag{3.10}$$

Consequently, if there is not an adhesional effect, classical friction theory can be considered, static and dynamic frictional theory as follows. According to the experimental investigations of Coulomb, static friction is required to set in motion a body in a state of rest, the force of static friction F_S must be overcome which is proportional to the F_N shown in Eq.3.11 [39],

$$F_s = \mu_s * F_N \qquad\qquad (3.11)$$

Dynamic friction force F_R is the resisting force and acts on a body after static friction force has been overcame which is proportional to the normal force [39];

$$F_R = \mu_K * F_N \qquad\qquad (3.12)$$

However, if some complex materials like polymers are used, then static and dynamic friction forces should be analyzed using the relation about the shear strength and the contact area as follows on equations 3.13 and 3.14;

$$F_S = \tau * A_S \qquad\qquad (3.13)$$

$$F_K = \tau * A_K \qquad\qquad (3.14)$$

3.1.2 Nonlinear effect on surface sliding

The relation between contact area and force, mentioned in Eqn. 3.7 and 3.8, result in obtaining a nonlinear effect on surface sliding at the contact area. During sliding, the contact area decreases while increasing the friction force (Figure 3.3) [41].
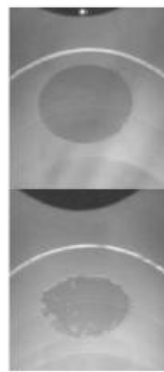
Figure 3.3 : Contact area reduction during surface sliding [41].

Therefore, working on soft polymers such as PDMS requires to use a complementary approach related to contact mechanics to describe the dependency of the contact area and load. The appropriate theory utilized for the comparison test in Chapter 6 is

called JKR adhesive contact theory defined by Tabor parameter [42-45]. The nondimensional Tabor parameter is used to decide which theoretical model Johnson-Kendall-Roberts (JKR), Derjaguin-Muller-Toporov (DMT), or transition model is appropriate for the tip-sample contact. The relevant relation is given below

$$\mu = \left(\frac{R\Delta\gamma^2}{E_r^2 z_0^3} \right)^{1/3}$$

(3.15)

$$\frac{1}{E_r} = \frac{1-\upsilon_i^2}{E_i} + \frac{1-\upsilon_s^2}{E_s}$$

(3.16)

where R is the radius of curvature of two surfaces in contact, $1/R = [1/R_1 + 1/R_2]$, $\Delta\gamma$ is the work of adhesion of sample surface, E_r is the reduced modulus of the sample, z_0 is the equilibrium separation of the surfaces (on the order of 0.3 to 0.5 nm). E_i and E_s are the Young's modulus, υ_i and υ_s are the Poisson ratio of surface 1 and surface 2, respectively. According to the nondimensional Tabor parameter, for $\mu < 0.1$ the DMT theory, and for $\mu > 5$ the JKR theory is used. In between cases, the transition model can be used [43]. In the experiments of this study, $\mu \gg 5$ is obtained and so, the JKR theory is used. The JKR contact model is described by the equations as follows

$$a^3 = \frac{R}{K}\left(P + 3\pi WR + \sqrt{6\pi WRP + (3\pi WR)^2} \right)$$

(3.17)

$$\delta - \delta_0 = \frac{a^2}{3R} + \frac{2P}{3aK}$$

(3.18)

$$\frac{1}{K} = \frac{3}{4}\left[\frac{1-\upsilon_1^2}{E_1} + \frac{1-\upsilon_2^2}{E_2} \right]$$

(3.19)

where a is the contact radius, R is the radius of curvature of the two surfaces in contact, K is the effective modulus, W is the work of adhesion of the sample, P is the preload applied to surface, δ_0 is zero point of the indentation. On the relation of effective modulus, E_i and υ_i are the Young's modulus and Poisson ratio of surface 1 and surface 2, respectively [45].

3.2 Occurrence of Stick-Slip Phenomenon on Soft Materials

The mechanism of soft materials is different from the hard materials [23]. When a body is in relative motion with a soft material, due to its viscoelastic properties of this material Schallamach waves (detachment waves) occur which is actually relative displacement between two surfaces [23, 46]. It can be observed from the Figure 3.4 that the contact area decreases with the occurrence of these waves [23, 47].
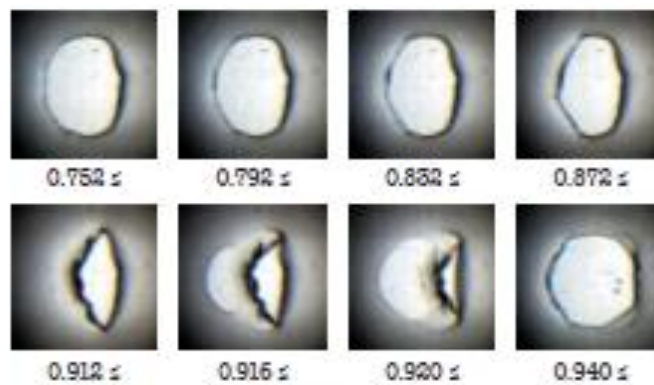
Figure 3.4 : Contact area images [23, 47].

If a rigid probe slides on a soft material like polymer, one of the three possible displacement mechanisms (true sliding, stick-slip, Schallamach waves) may occur which is shown in Figure 3.5 [48]. By exceeding a critical initiation force, called static force, true sliding proceeds. Then, sliding continues at a constant kinetic force shown in Figure 3.5 (a).

However, on the second displacement mechanism, stick-slip, there is not a continuous sliding, but rather sawtooth vibrations. Stick-slip is the common situation on soft materials which have similar properties with the human skin.

The schematic of the energy translation during surface sliding of the rigid spherical probe on the soft skin can be observed on Figure 3.6 [49]. During surface sliding, the rigid probe moves on the sliding direction and presses into the soft skin. Then skin is

stressed and elastic energy is taken up. Under the low sliding speed, most of the energy is released when the stress is removed. This means that hysteretic friction is small due to only a small part of the energy is lost. However, under the high sliding speed, deformation is difficult to overcome and recover because the deformation rate of the skin also increases. So, hysteretic friction increases. These situations may be the reason of increasing of friction coefficient as sliding speed increases.
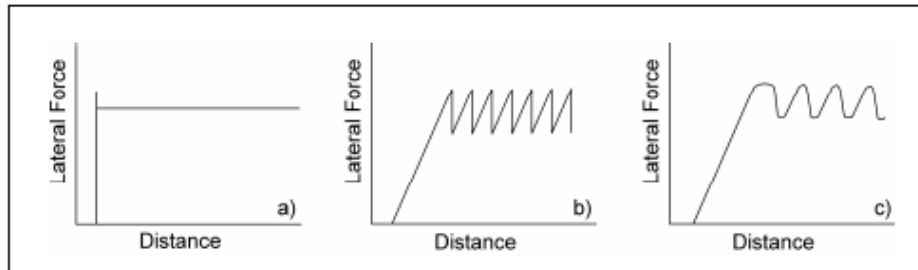
Figure 3.5 : Frictional results for true sliding (a), stick-slip (b), Schallamach waves (c) [48].
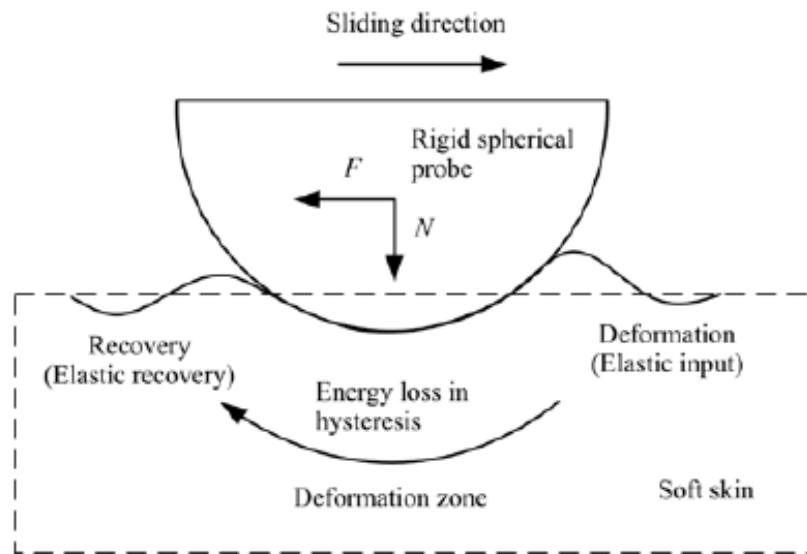
Figure 3.6 : Energy translation during the surface sliding [49].

Therefore, the friction coefficient does not remain constant. However it causes to form oscillation. When sliding speed increases, the oscillation becomes greater. This is known as stick-slip phenomenon [49].

When a rigid support slides on the soft material such as PDMS, Schallamach waves are generated in the surface shown in Figure 3.7. It is known that these waves derive from the viscoelastic property of the soft material, and result in a relative

displacement between the two surfaces. As it can be seen in Figure 3.8 [23], in soft materials stick-slip has two parts. One results from the Schallamach waves, and the other one results from the natural vibration of the system.
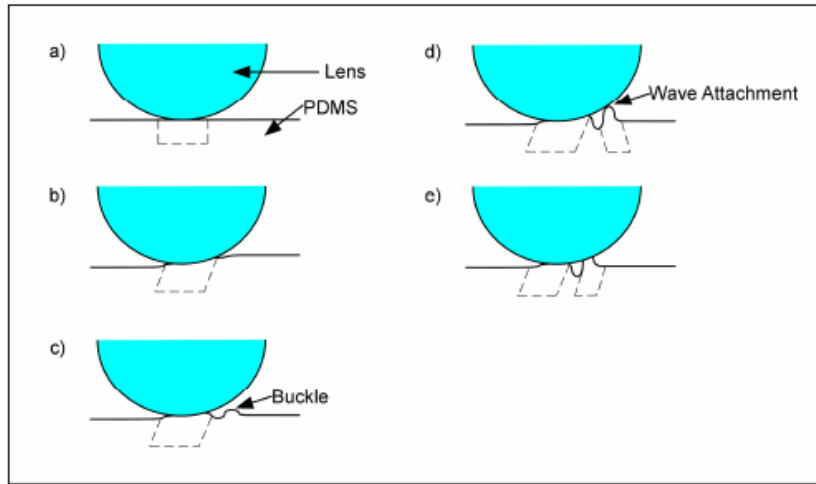

Figure 3.7 : The view of the formation, attachment, and propagation of Schallamach waves [48].
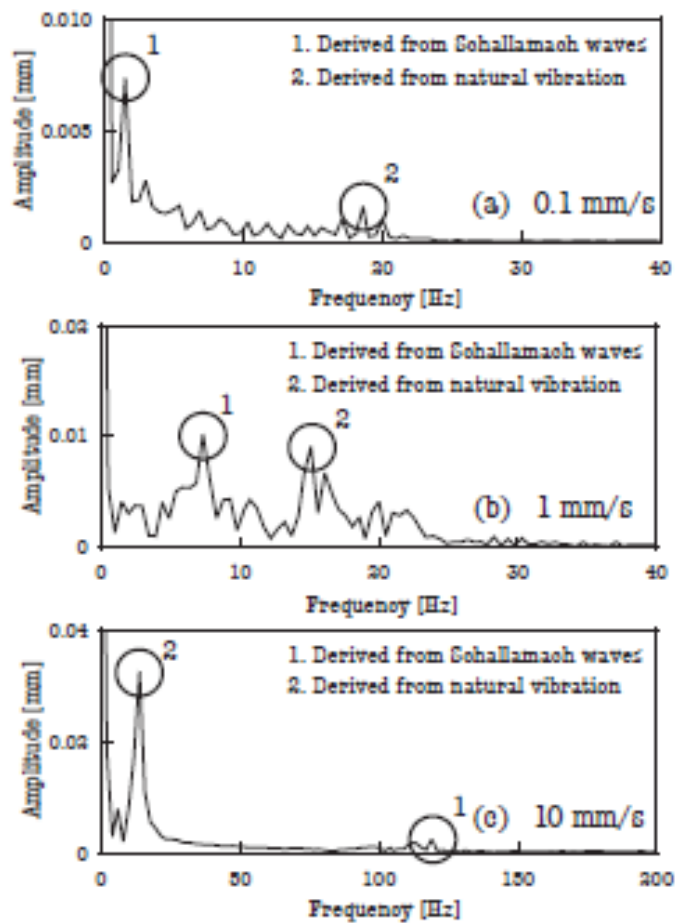
Figure 3.8 : Frequency analysis of stick-slip [23].

3.2.1 Effect of normal load

Under high load, the first peak shown in Figure 3.8 does not occur due to the fact that the contact area is larger than the Schallamach wave. Despite the occurrence of the Schallamach wave, the contact area remains constant. However, the second peak does not affected by this wave because it comes from the natural vibrations in the system. The results are in Figure 3.9 [23].
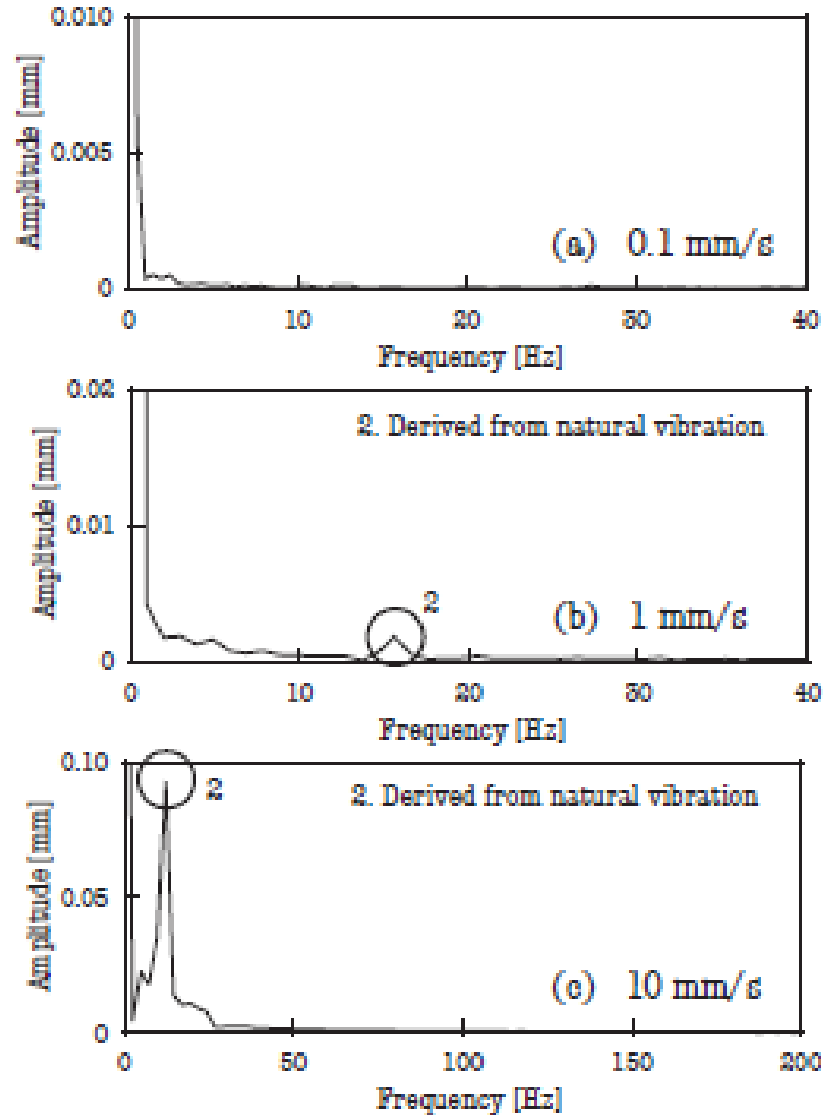
Figure 3.9 : Frequency analysis of stick-slip under high load (20 mN) [23].

3.2.2 Effect of sliding velocity

In contrast to the hard materials, in soft materials stick-slip occurs under high sliding velocity and high contact load, or under low sliding velocity and low contact load (Figure 3.10). Steady sliding is observed under low sliding velocity and high contact load [23].
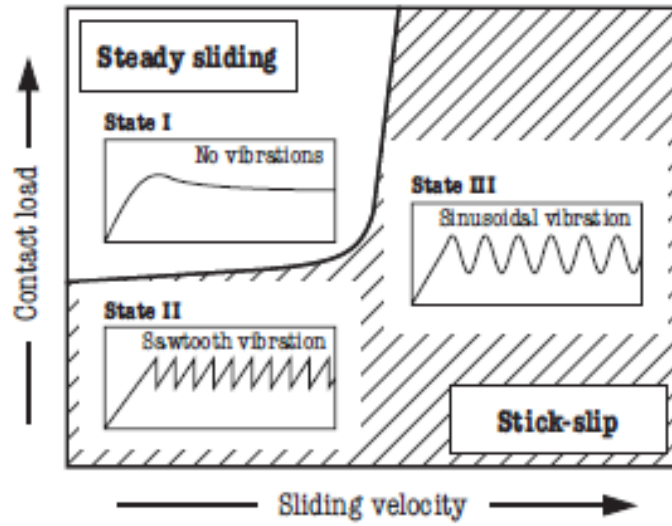
Figure 3.10 : Stick-slip conditions of soft materials [23].

4. EXPERIMENTAL SYSTEM

4.1 Design of Experimental Set-Up

A custom built semi-autonomous friction-adhesion set-up is developed by using high precision measurement devices, and constructed on a vibration isolation table (Smart Table, Newport) to exhibite pattern detection and frictional properties of a fabricated human-inspired artificial tactile polymer surface with parallel ridges (Figure 4.1). The components of the experimental set-up as illustrated in Figure 4.2 consist of two linear DC servomotors (MFA-CC, Newport) for vertical and horizontal motion with a 17.5 nm resolution [50] connected to a controller (XPS-C8, Newport), 100 g and 250 g loadcells (GSO-100 and GSO-250, Transducer Techniques) for gathering preload and friction force data, glass tip (N-BK7 Half-Ball Lens, Edmund Optics). Relative motion between rigid glass tip and polymer surface contacting to each other is supported by two linear micromotors drived by a custom written software which allows to control preload on artificial sample during surface scanning. Therefore, force and displacement data are gathered while the preload applied to the surface is kept constant by the force-feedback controllers.
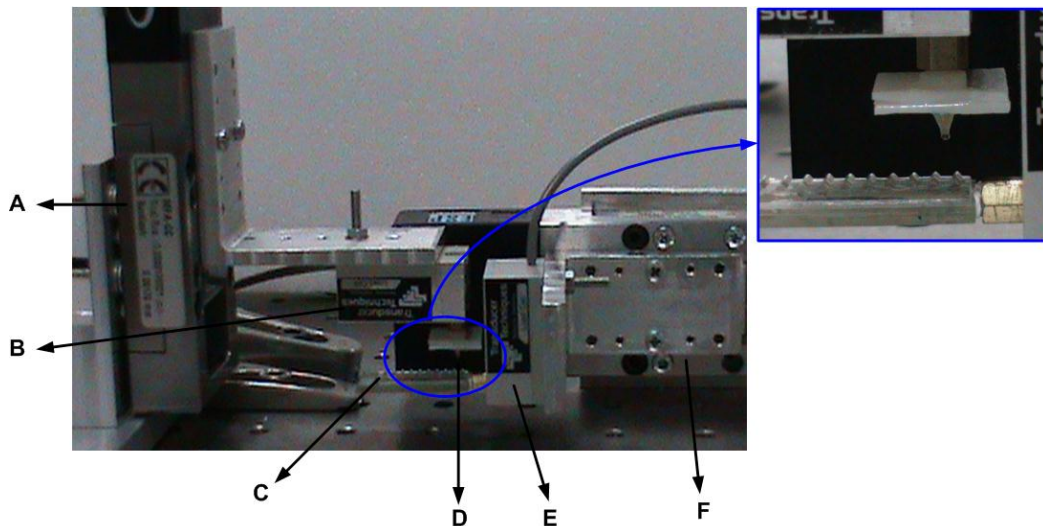

Figure 4.1 : Experimental set-up; A: Linear DC motor for vertical motion, B: Loadcell 1 with 250 g capacity, C: Artificial skin, D: Rigid surface (glass tip), E: Loadcell 2 with 100 g capacity, F: Linear DC motor for horizontal motion.
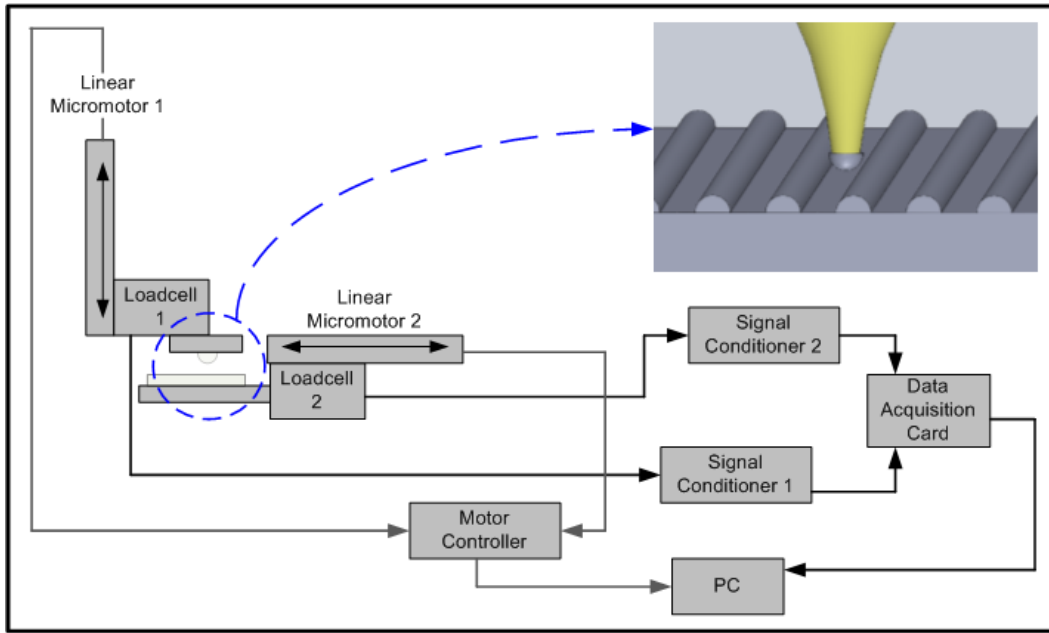
**Figure 4.2 :** Illustration of experimental set-up.

Detailed view of the tip components can be seen on Figure 4.3. In addition, Figure 4.4 shows tip-sample contact and dimensions of the evenly distributed artificial ridges made of PDMS. The diameter of the ridges and the space between the ridges are 1 mm and 1.4 mm, respectively. Peak-to-peak value of two ridges is 2.4 mm. Meanwhile, the travel length is chosen approximately 12 mm amounts to five ridges. Different sizes of tip diameters are used such as 1 mm, 10 mm, and 34.74 mm. One of them is illustrated on the Figure 4.4.
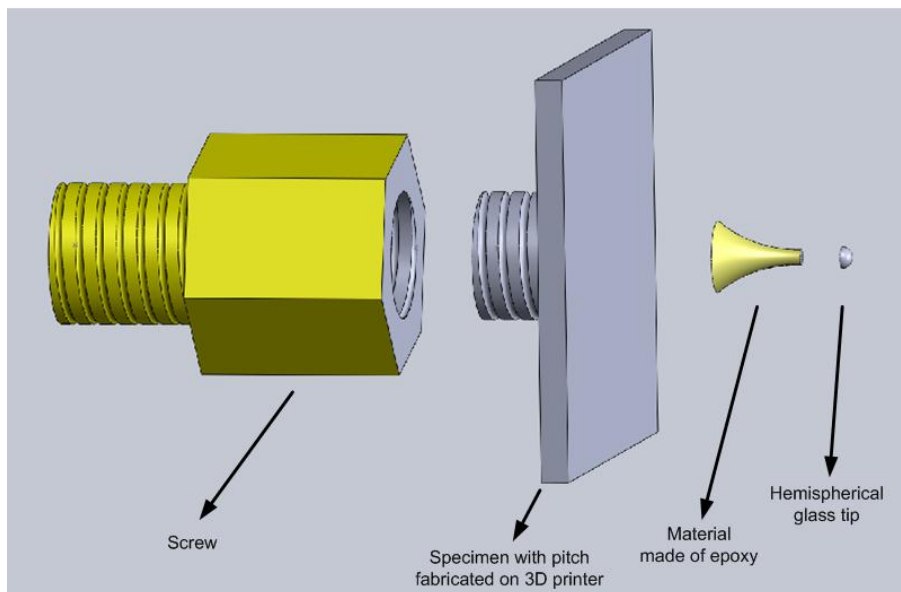
Figure 4.3 : Detailed view of tip components.
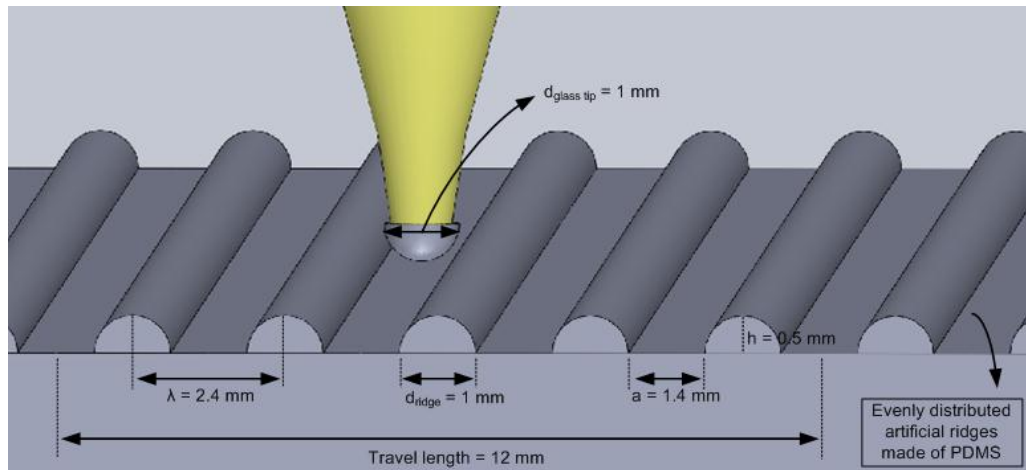
(a)
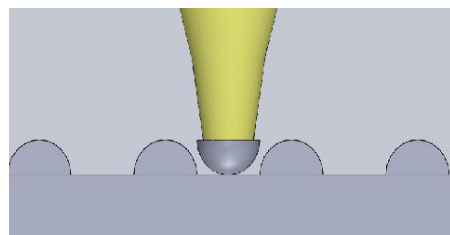
(b)

Figure 4.4 : Dimensions of the evenly distributed ridges scanned by glass tip (a), a close-up view of ridges (b).

In order to obtain appropriate working conditions such as travel interval, and sliding velocity, some performance tests of linear motors are realized. To determine optimal distance to the origin of the motorized stage, position errors are obtained for each start point from the origin. First, the motor is positioned to the start point of choice which is shown in Figure 4.5. Then, a constant velocity reference is performed, and the motor is positioned until the end of the stage. This test is repeated for each start point from the origin. After the results of these tests are acquired, the percent position errors are calculated. It is obvious that the errors increase with respect to the distance from the origin (Figure 4.5). Additionally, the position errors are dependent to the velocity of the linear motor. It is clear that as the velocity and distance increase the errors become larger. As a consequence, for the experiments of this study the distance is chosen close to the origin.

To minimize the velocity error, optimal velocity value is determined. For this case, the motor is commanded to go to the origin of the stage, and then a position reference of 25 mm is given with various velocity profiles. Although the optimal choice of the velocity is 2 mm/s, the percent velocity error is just 0.9 at 0.5 mm/s sliding velocity

(Figure 4.6). This result allows to perform the experiments at low sliding velocities with negligible error values.
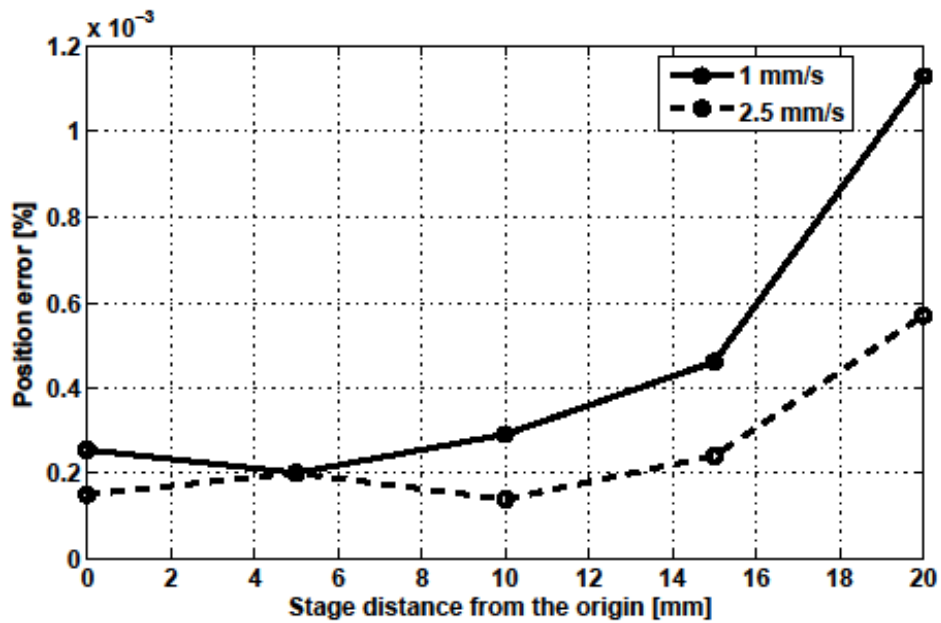
Figure 4.5 : Position errors with respect to different distances from the origin of the motorized stage.
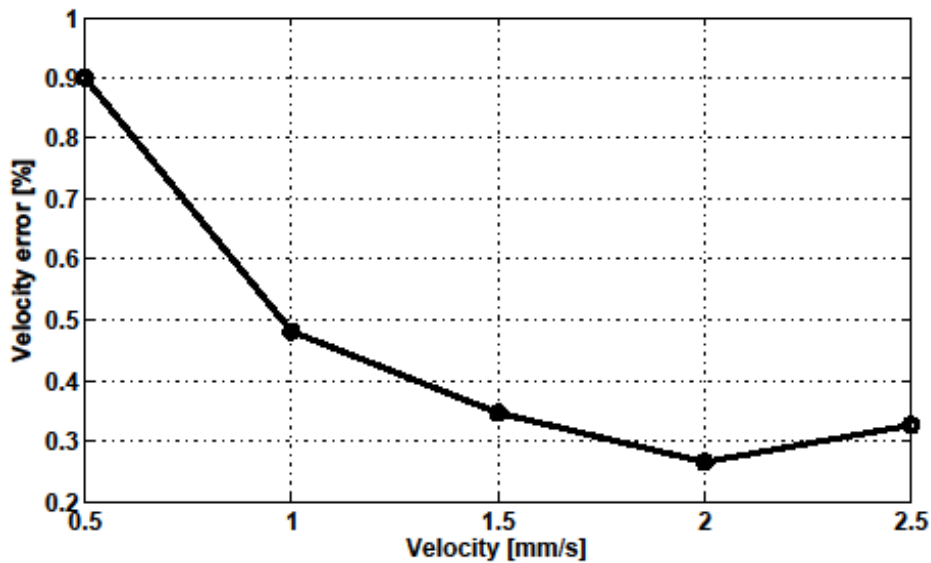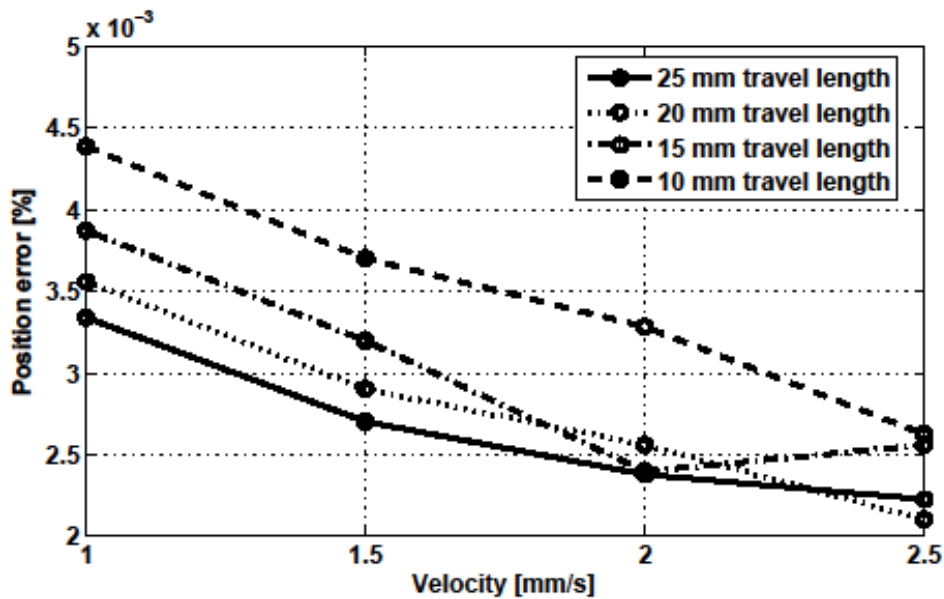

Figure 4.6 : Velocity errors with respect to different velocity values.

In addition, another test is realized to investigate the position errors with respect to different velocity values for various travel lengths (Figure 4.7). The tests are repeated for four different travel lengths (10, 15, 20, and 25 mm). The results showed that the position errors increase with the increasing travel length. Consequently, to minimize

the position and velocity errors in the experiments of this study, the travel length is kept at min. in the range of 8-12 mm.


Figure 4.7 : Position errors with respect to different velocity values for various travel lengths.

4.2 Design & Fabrication of Human-Inspired Artificial Skin

Artificial sample is designed by inspiring human skin tactile properties to develop artificial polymer skin. Human ridges are 0.1 mm in height and 0.3-0.5 mm in width [6]. The artificial soft polymer surface with parallel ridges is fabricated from PDMS (Sylgard 184, Dow Corning) 0.5 mm in height and 1 mm in width. Peak-to-peak value of two ridges called wavelength is 2.4 mm, and the space between the ridges is 1 mm. The backing layer of the sample is approximately 0.8 mm. The required first mold is printed by using three dimensional printer (Rapid Prototyping 3D Printer, Objet) with a 0.1-0.2 mm resolution (Figure 4.8). The sample surfaces are obtained with a technique used in literature [51]. First, the negative of the mold is obtained using silicone rubber (HS II Base, Dow Corning) with a mix ratio of the base material to the curing agent 20:1. Silicone rubber is cured in 24 hours at room temperature, and peeled off from the mold to obtain a second mold. Then, soft polymer PDMS is prepared with a mix ratio of the base material to the curing agent 10:1. The mixture is poured onto the silicone rubber mold and cured in 48 hours at room temperature to get the positive of the first mold as artificial skin with parallel ridges shown in Figure 4.9. Meanwhile, the images obtained by using an inverted

optical microscope (Eclipse Ti-S Inverted Microscope, Nikon) can be seen on the Figure 4.10 on which the diameter and height of the ridge, the backing layer of the sample can be followed as well.
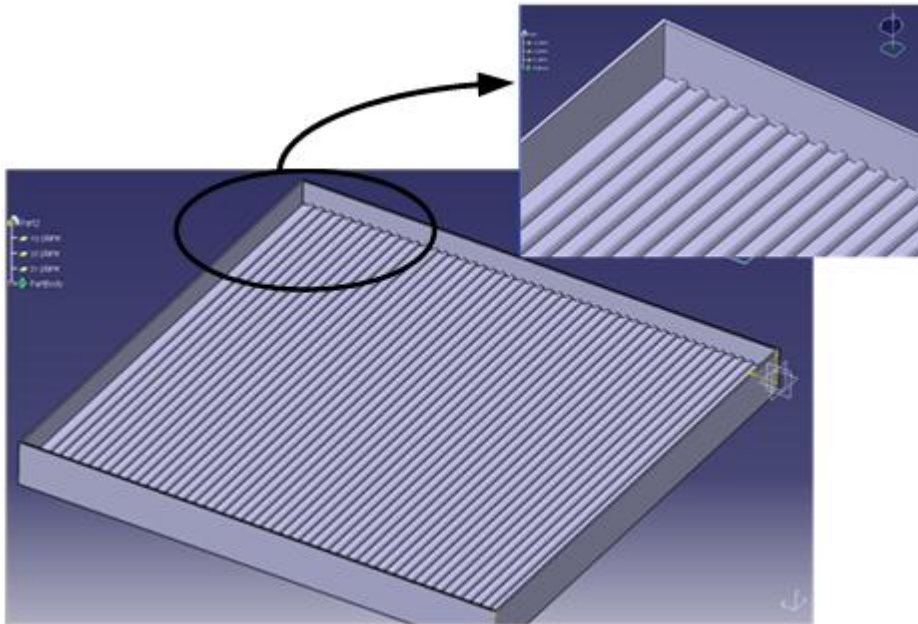
Figure 4.8 : The mold fabricated by using Rapid Prototyping 3D Printer.

Figure 4.9 : Front-view of the artificial skin made of PDMS
which is the positive of the mold.

4.3 Measurement Procedure

According to the motion cycle of the linear motors, first the vertically placed motorized stage is moved down to the artificial sample. When the glass tip came to the contact with the sample, it is pressed till the preload reached to its predefined value. Afterwards, the horizontally placed motor started to move, and the relative motion between glass tip and polymer sample is occurred in a predetermined travel interval. At the end of this motion, the first motorized stage is pulled up, and two surfaces separated from each other.

During relative motion between glass tip and polymer sample, displacement data of the motors are gathered continuously from their encoders with the aid of the software which has 2 kHz sampling frequency. In addition, after amplifying the output signals

of the loadcells using signal conditioners, signals gathered from the loadcells are transmitted to an internal data acquisition card. By analyzing the captured preload, friction force, and displacement data, pattern detection on the artificial surface, and frictional properties of the surface are investigated in details. So, the gathered friction force data is analyzed in time and frequency domain.

Different design parameters such as different sizes of tip diameter, sliding velocity, and preload are studied on the experiments to observe frictional properties, and pattern detection on the artifically made polymer surface. The sliding velocity effect is discussed using five different velocities, i.e. 0.09, 0.15, 0.26, 0.34, and 0.49 mm/s under constant preload (20 mN). The preload effect is investigated at constant sliding velocity (0.09 mm/s) using six different velocities, i.e. 5, 10, 20, 25, 30, and 35 mN.

(a)

(b)
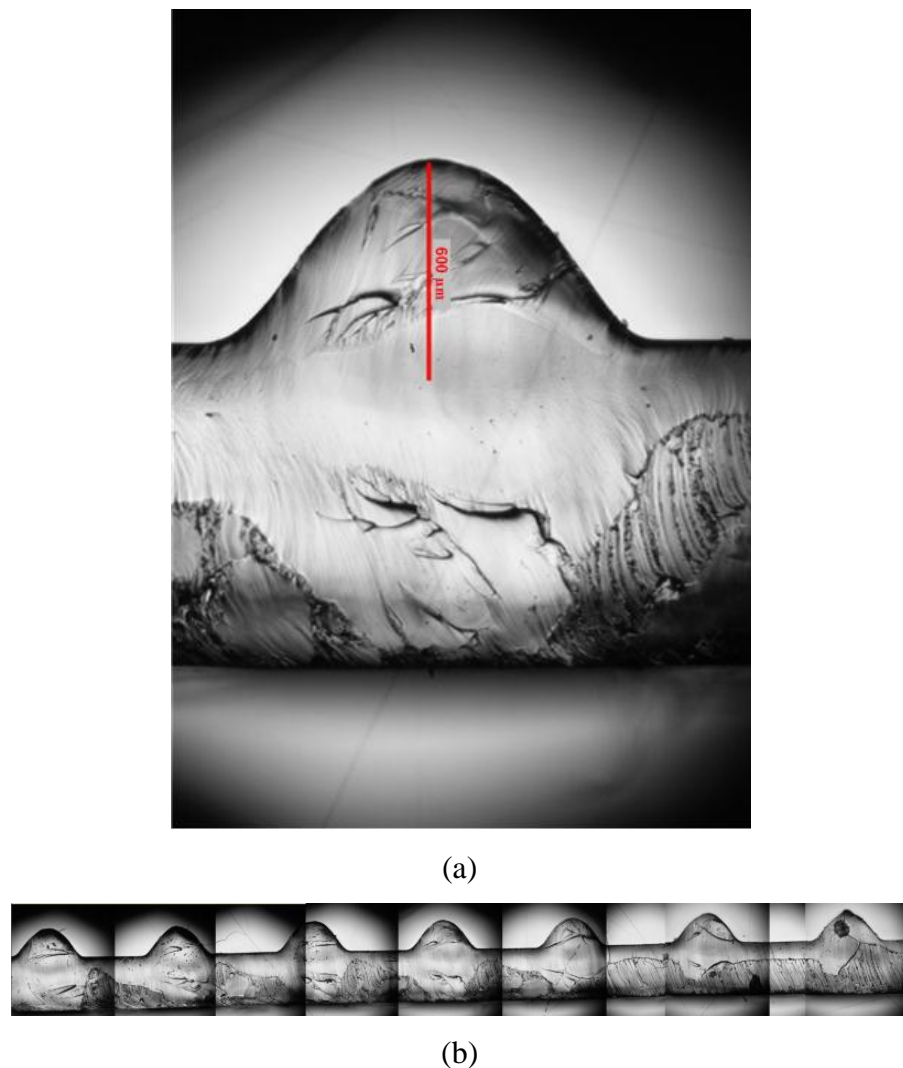
Figure 4.10 : Side-view optical inverted microscope image of the artificial polymer ridge (a), and of the total sample patterned with evenly distributed ridges (b).

5. CONTROLLER DESIGN FOR CONSTANT PRELOAD

5.1 Preload Control with PID, Adaptive PID, and SMC

In order to keep preload constant during surface scanning, three different control methods are studied, and compared according to their tracking error performance; Proportional-Integral-Derivative (PID) Control, Adaptive PID Control, and Sliding Mode Control (SMC).

PID controllers are well-known controller type used in industry, especially in control process industries. Due to their simple structure and robust performance in various working conditions, they are useful and can be applied to most control systems [52, 53]. Generally, PID is preferred to use in linear systems. This type of controller can be used in nonlinear systems where their coefficients should be adjusted for each operating points. PID controllers introduce three parameters, i.e. proportional gain (K_p), integral time constant (T_i), and derivative time constant (T_d) such as

$$u(t) = K_p e(t) + K_i \int e(t) dt + K_d \frac{d}{dt} e(t) \tag{5.1}$$

where ($K_p = K$) stands for proportional gain, $K_p = K * (1/T_i)$ for integral gain, and $K_d = K * (T_d)$ for derivative gain. The system gives fast responses by increasing the proportional effect however this effect may induce oscillations. The integral term eliminates the steady-state error. Nevertheless, this kind of an action will introduce low frequency which causes oscillations. The derivative term reduces oscillations, and increases the stability. However, high values of this term may cause the system to go saturation. Some application areas of this type of controller are cruise control in a car, house thermostat, industrial ovens, plastics injection machinery, hot stamping machines, and packing industry [52].

Owing to the structure of the PID controller the parameters are tuned before process which results that they will be fixed during control. However, this type of control method may not be able to control the systems that have changing parameters, and

require on-line retuning. For such cases, another kind of controllers is preferred to use called Adaptive PID controllers [53].

Adaptive PID controllers actually have similar structure to traditional PID, but their parameters are changed by using an adaptation law. The adaptive control method is based on dealing with uncertain systems or time-varying systems by estimating the uncertain plant parameters on-line, with the aid of measured system signals. This approach let the adaptive control system be an on-line parameter estimation, and adjusting system which results in having a coherent control mechanism against of any uncertainty or unknown variation in plant parameters. These control systems are actually nonlinear even though they are advanced whether linear or nonlinear systems [54, 55]. There are some control tasks which exhibit the basic role of the adaptive control such as robot manipulation, ship steering, aircraft control and process control. In robot manipulation systems, parameter uncertainty is an important issue to be overcame. In spite of having these systems uncertainty at the beginning of the process, this subject has to be solved by an adaptation or estimation mechanism. Otherwise, instable or inaccurate situations might appear on the control systems. The other well-known example is on aircraft flies. During flight, as a result of fuel consumption the mass of the plane will decrease. To be able to adapt to such time-varying system parameters, using the adaptive control method becomes essential [54, 55].

One of the categories of feedback adaptive control is gain scheduling which is also used on the comparison tests of this study such as

$$u(t) = K_p e(t) + K_i \int e(t) dt + K_d \frac{d}{dt} e(t) \qquad \text{(5.2)}$$

where $K_p = \gamma_p * e(t)$, $K_i = \gamma_i * e(t)$, and $K_d = \gamma_d * e(t)$. The adaptation gains are γ_p, γ_i, and γ_d. Behind the approach of gain scheduling lies to control nonlinear systems by using linear control methodology. So, changing adaptation gains on the controller based on this mechanism, the required adjustments will be accomplished.

Sliding Mode Control (SMC) approach is a nonlinear and variable structure control method based on switching logic, and mostly used for controlling nonlinear systems [54]. The main advantage of this control method is the robustness meaning that it is resistant to external disturbances, parameter variations, and uncertainties. The other

advantages are the order reduction, simplicity and the high efficiency for designing such robust controllers which can be operated for high-order nonlinear systems [54, 56-58]. SMC has a wide range of area to be successfully applied including robot manipulators, power systems, automotive transmissions and engines, high performance electric motors, and underwater vehicles [54, 58].

The idea behind the sliding mode control is to obligate the state variables of the system to reach and stay on a surface called sliding or switching surface where the predefined function of the error is zero [56, 57]. Such a system behaviour indicates an ideal sliding motion. Furthermore, one of the well-known drawbacks of the sliding mode approach is the chattering effect which is actually high frequency oscillations in the control input occurred as a result of problems in switching devices and delays [57]. Due to the fact that this effect might excite the high frequency dynamics of the system, it is an undesirable subject. To avoid chattering, there are two methods which can be applied such as using a saturation function, or using a boundary layer [54].

The sliding surface can be defined as follows, where e is the tracking error, and λ is the coefficient determining the bandwidth of the controller;

$$s = \frac{de}{dt} + \lambda e \tag{5.3}$$

The switching control law yields to

$$u(t) = u_e(t) - k * \mathrm{sgn}(s) \tag{5.4}$$

$$k = \left| \hat{F} \right| + \mu \tag{5.5}$$

where μ is a strictly positive coefficient that determines the reaching time to the sliding surface, and $\hat{F}$ represents the uncertainty in the system model [54].

In this study, the idea of keeping the preload constant during surface scanning by using a force-feedback controller is exhibited in details with the aid of the experimental results. For this aim, to determine which type of controller should be used in experiments, three different control methods including PID, Adaptive PID,

and SMC are compared according to their tracking error performance. The comparison tests are carried out as two case studies by using two different samples composed of flat PDMS, and human-inspired wavy PDMS sample patterned with parallel ridges.

5.2 Performance Comparison of Controllers on Flat Elastomer (PDMS)

In the first case study, tests are realized under 23 mN constant preload applied to flat PDMS sample which is rubbed against a 6 mm diameter rigid glass tip at 0.15 mm/s sliding velocity. The travel length is approximately 8 mm.

During surface sliding, preload remains constant on flat PDMS with approximately 1-1.5 % error using sliding mode controller as shown in Figure 5.1 and Figure 5.3. However, using Adaptive PID and PID Controllers result in ~ 1.5-2 % and 2 % error values, respectively.
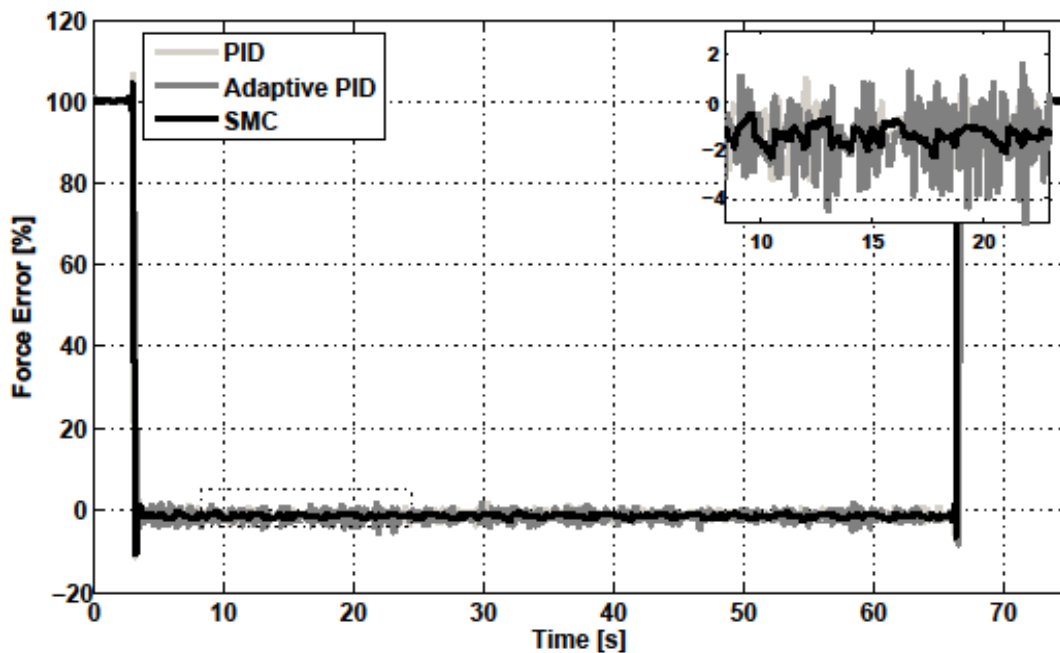
Figure 5.1 : Force error results for PID, Adaptive PID, and SMC on flat PDMS sample scanned by 6 mm diameter glass tip under 23 mN preload at 0.15 mm/s sliding velocity for 8 mm travel length.

In addition, tracking errors of these three controllers are examined. According to the results of the experiment shown in Figure 5.2 (a), the sum of absolute error in force is minimum in SMC. Besides, the Adaptive PID Controller shows better performance than the PID Controller. The second experiment is tracking a sine with given

frequencies such as 0.5, 1, and 2 Hz. Thus, the three controllers are examined according to their tracking errors as shown in Figure 5.2 (b). The highest tracking error is at 1 Hz, while the error is minimum at 2 Hz for each controller.
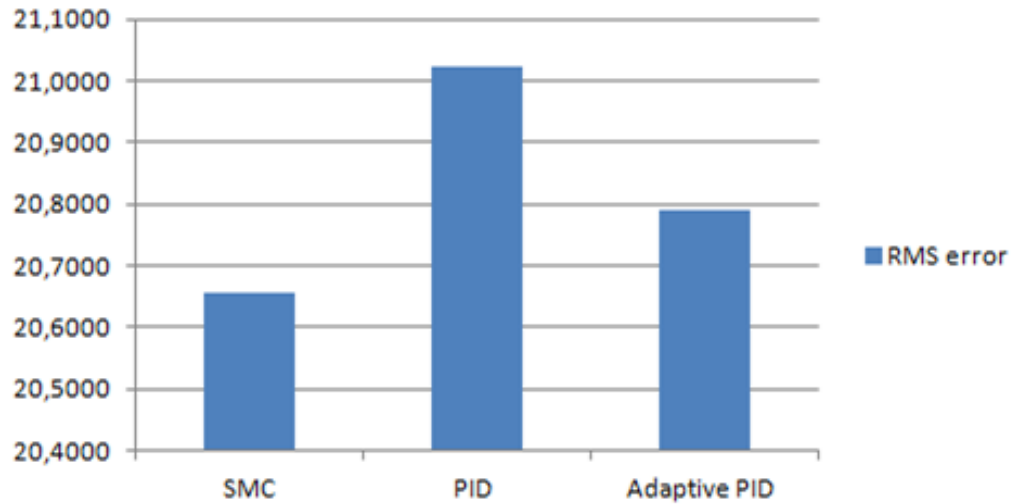
(a)
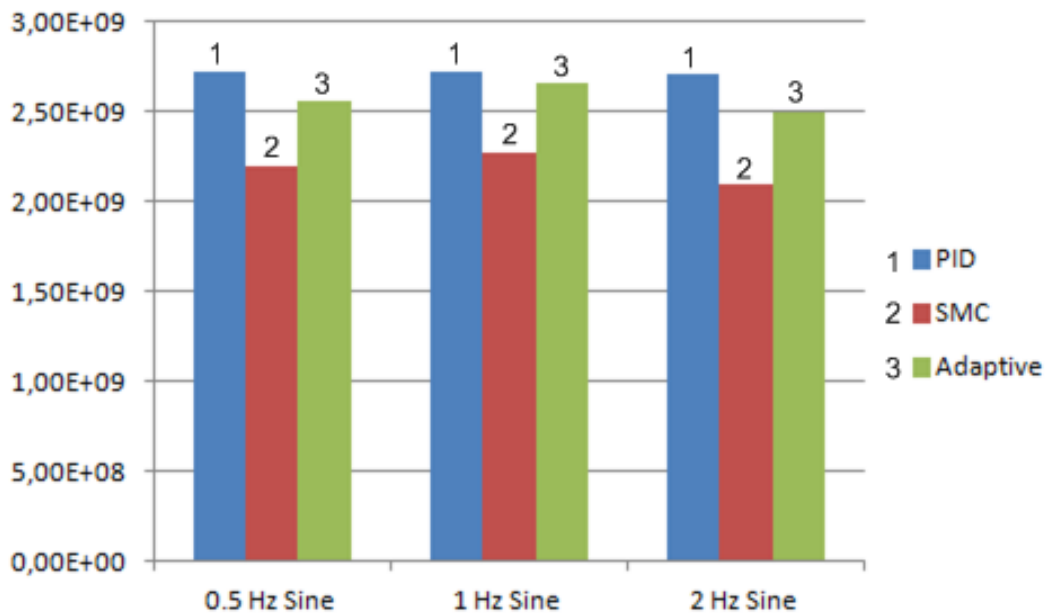
(b)

Figure 5.2 : Tracking errorsof the three different controllers; (a) comparative results with step reference signal, (b) comparative results with sine reference signal at different frequencies.
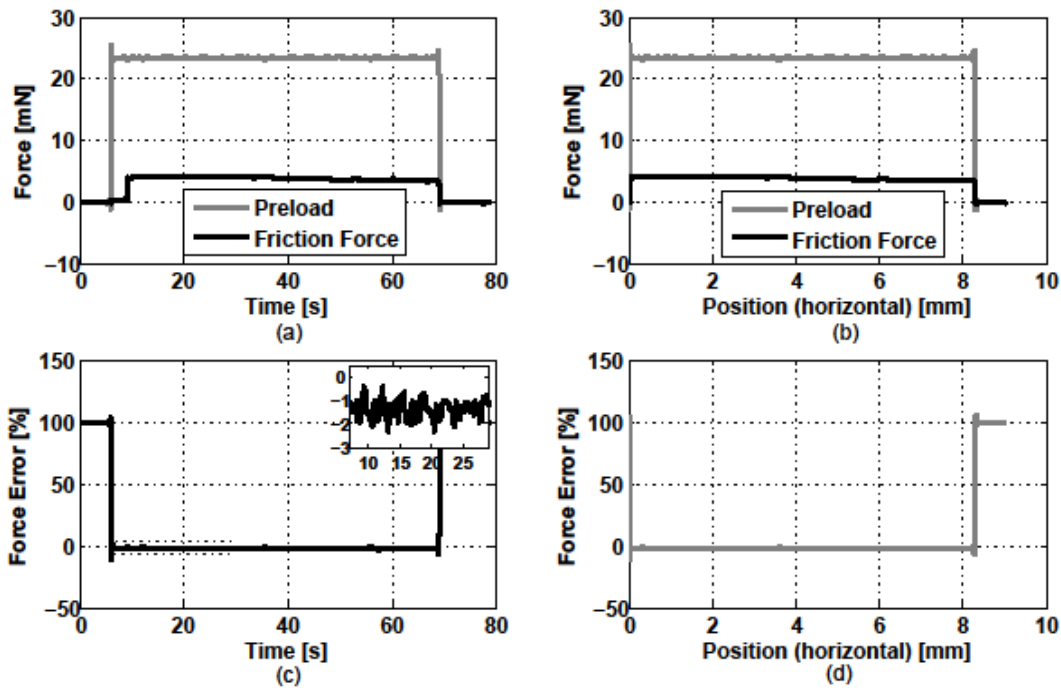
Figure 5.3 : Results for Sliding Mode Controller (SMC) on flat PDMS sample scanned by 6 mm diameter glass tip under 23 mN preload at 0.15 mm/s sliding velocity for 8 mm travel length.

5.3 Performance Comparison of Controllers on Artificial Skin Patterned with Evenly Distributed Ridges

In the second case study, tests are realized under 20 mN constant preload applied to PDMS sample with evenly distributed ridges which is rubbed against a 1 mm diameter rigid glass tip at 0.09 mm/s sliding velocity. The travel length is approximately 12 mm amounts to five ridges.

Although appropriate coefficients of PID controller are chosen to give the system fast responses, and deal with the steady-state error under reduced oscillations, the results showed that the preload does not remain constant. The force error is approximately 80 % as shown in Figure 5.4.

It should be noted that the artificial surface patterned with ridges is scanned by the 1mm diameter glass tip. According to the tip position data gathered by encoder of the linear motor, the wavelength of the ridges, 2.4 mm, and the height of them, 0.5 mm, can be detected, and obtained as the profile of the sample approximately.

Therefore, to be able to control and adapt the time-varying parameters such as preload, tip position, the motion of linear motor and tip, an adaptive PID controller is

examined, and the parameters of the controller are tuned based on an adaptation law. According to this mechanism, different number of operating points are so selected that they comprise the range of the system operation. Then, linear time-invariant approximation to the plant dynamics are realized at these points, and a linear controller is designed. In addition to adjusting PID coefficients, the adaptation gains on the controller are changed based on the gain scheduling. Thus, controlling nonlinear systems by using linear control methodology is carried out by the approach of this scheduling. The results are better than that of the traditional PID controller. The preload is kept constant with ~ 40 % error (Figure 5.4).
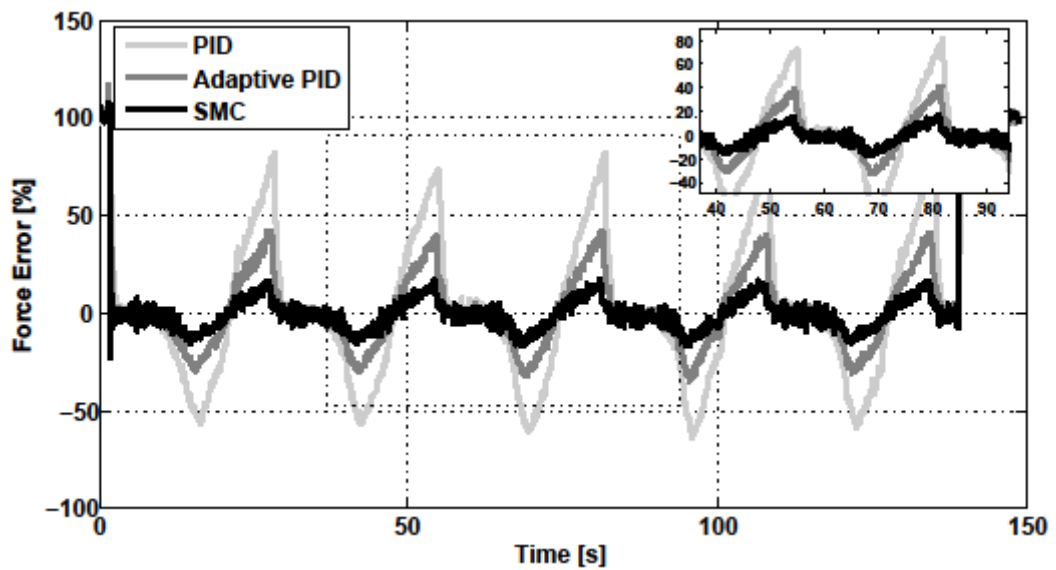
Figure 5.4 : Force error results for PID, Adaptive PID, and SMC on rough PDMS sample called artificial skin with parallel ridges scanned by 1 mm diameter glass tip under 20 mN preload at 0.09 mm/s sliding velocity for 12 mm travel length.

Nevertheless, due to the inadequate control effects of the PID and adaptive PID controllers, the other control method, SMC, is applied (Figure 5.4 and Figure 5.5). The main characteristic of this method, which is to be robust to external disturbances and parameter variations, provides to overcome the complexity of feedback design. This kind of control method introduces also a property of order reduction which amounts to transforming a nth order system, consisting of tracking problem, into a first order system dealing with stabilization problem. Because the sliding mode controller performs based on a model, the model parameters of the system are embedded to the controller. Empirically, first to determine the reaching time to the sliding surface, μ is increased which provides the system to be faster but also

unstable. When the chattering effect is observed, the boundary layer width φ is increased to diminish the oscillations. However, it should be noted that this kind of an action makes the system slower. Thus, the appropriate values of these coefficients are tuned. According to the results, sliding mode control method allowed to keep the preload consistent during surface scanning with a reduced force error compared to the other two controllers, PID and adaptive PID controllers (Figure 5.4). The preload error is obtained approximately 16 %. In addition, it should be paid attention that under the light loads (~ 20 mN) the force-feedback controller can keep the preload with approximately 16 % error. This value decreases under high loads.
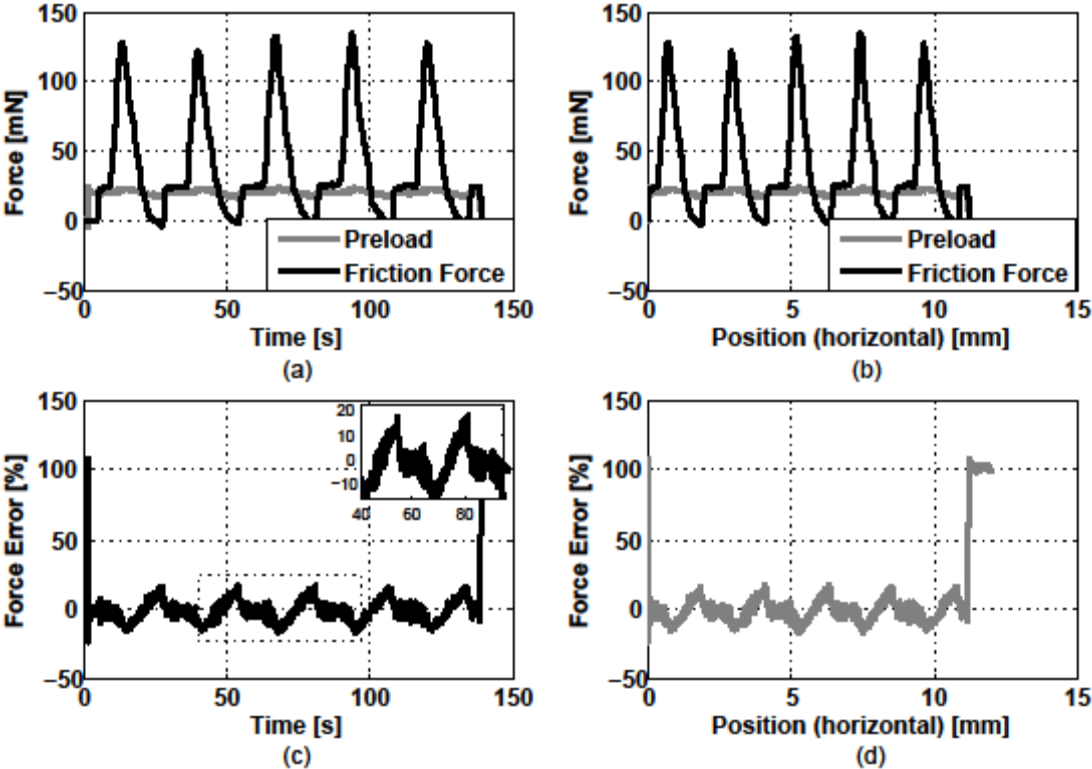
Figure 5.5 : Results for Sliding Mode Controller (SMC) on rough PDMS sample called artificial skin with parallel ridges scanned by 1 mm diameter glass tip under 20 mN preload at 0.09 mm/s sliding velocity for 12 mm travel length.

6. VALIDATION OF EXPERIMENTAL SYSTEM

6.1 Friction Tests on Flat Elastomer (PDMS)

The phenomenon of friction is considered if a relative motion occurs between two surfaces contacting to each other, and provides a resistive effect on this type of motion [38]. A clear understanding of the developments starting from classical friction theory by Leonardo da Vinci to adhesion theory of friction by Bowden & Tabor highlights the way of investigating an approach of soft material friction.

The guiding fundamentals of the classical friction theory are constructed by Leonardo da Vinci by introducing for the first time the concept of friction coefficient as the ratio of the friction force to normal force $\mu = F/N$ [38]. After this concept was rediscovered by Amontons in seventeenth century, he provided two basic laws of friction related on the direct proportionality of the friction force to applied load, and the independency between the friction coefficient and the apparent contact area. The direct proportionality was also verified by Coulomb in eighteenth century. Both Leonardo da Vinci and Amontons suggested that materials used in experiments have a constant coefficient of friction, regarded as a material property, of 1/4 and 1/3, respectively [38, 48]. Then, some ideas about the relationship between surface asperities and friction provided to result in introducing to the friction coefficient with the relation of $\mu = \tan\alpha$. Furthermore, studies about kinetic and static friction are developed, and the third law of friction is stated by Amontons including the independency between the kinetic friction and sliding velocity [38]. Although Amontons' laws and the other approaches provided to comprehend the basis about the phenomena of the friction, they are inadequate to describe the idea behind the soft material friction [48].

The role of adhesion in friction is suggested during the last period of the eighteenth century. Developments about this kind of an approach allow to exhibit various studies related on surface chemistry, especially on molecular adhesion in twentieth century. Then, Bowden and Tabor developed the adhesion theory of friction.

According to their statement, two surfaces make contact only at points of asperities. The relationship is as follows

$$F = \tau * A \qquad \text{(6.1)}$$

where F is the friction force, τ is the interfacial shear strength, and A is the true contact area [38, 40].

Furthermore, it is stated that the frictional behaviour of polymers resulted from an elastic deformation of spherical surface asperities. By taking into account this statement, and the suggestion about the proportionality between the friction force and the true contact area, the relevant relation is described such as A α $P^{2/3}$ and F α $P^{2/3}$ [38]. These proportionalities result in obtaining a nonlinear effect on surface sliding at the contact area. During sliding, the contact area decreases while increasing the friction force [41]. Therefore, working on soft polymers such as PDMS requires to use a complementary approach related to contact mechanics to describe the dependency of the contact area and load. The appropriate theory utilized for the comparison test is called JKR adhesive contact theory defined by Tabor parameter [43, 45].

The test for validation of the experimental system is carried out using flat PDMS as a control sample which is rubbed against a hemispherical glass tip with 6 mm diameter. When the tip is brought into contact with the sample, the relation between the contact radius and various applied preloads can be expressed as

$$a^3 = \frac{R}{K}\left(P + 3\pi WR + \sqrt{6\pi WRP + (3\pi WR)^2} \right) \qquad \text{(6.2)}$$

$$\frac{1}{K} = \frac{3}{4}\left[\frac{1-\upsilon_1^2}{E_1} + \frac{1-\upsilon_2^2}{E_2} \right] \qquad \text{(6.3)}$$

where a is the contact radius, R is the radius of curvature of the glass tip, K is the effective modulus, W is the work of adhesion of the sample, P is the preload applied to surface, E_i and υ_i are the Young's modulus and Poisson ratio of surface 1 (glass tip) and surface 2 (PDMS), respectively [45].

In order to observe that the experimental result about the relationship between preload and friction force fits to a cubic polynomial function (Figure 6.1), various preload values in the range of 25-140 mN are applied on the sample during sliding. It is clear that there is a cubic polynomial relation between applied preload, and friction force. Thus, the result of the curve fit to the experimental data indicates increasing the preload, friction force increases nonlinearly.
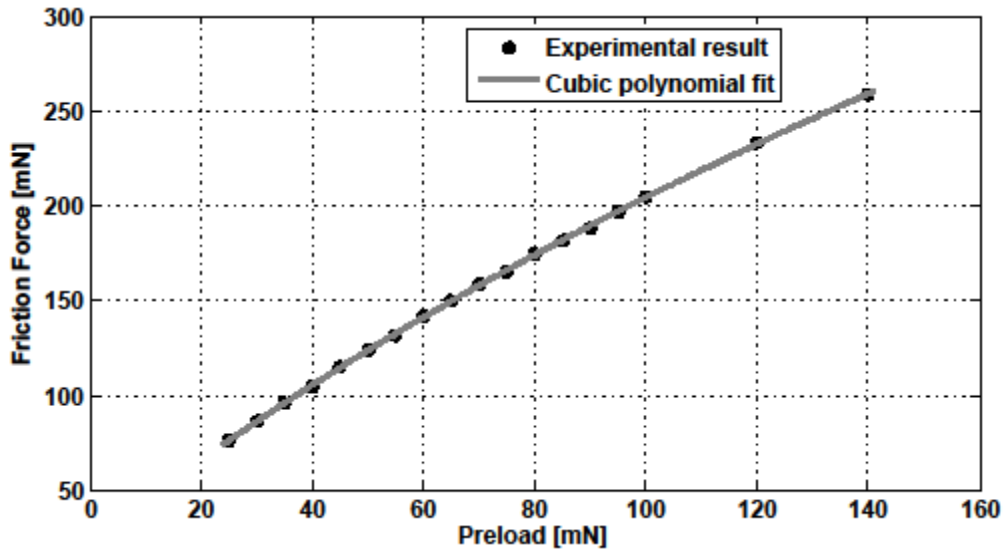
Figure 6.1 : Curve fit to the experimental result for various preload values at 1 mm/s sliding velocity on flat PDMS sample.

7. STICK-SLIP EXPERIMENTS ON FLAT ELASTOMER (PDMS)

7.1 Transition from Stick-Slip Oscillations to Steady Sliding

The occurrence circumstances of stick-slip oscillations and steady sliding between soft polymer and rigid surface are analyzed. As the details of this topic is discussed on the chapter 3.2, if a rigid probe slides on a soft material like polymer, one of the three possible displacement mechanisms may occur such as true sliding, stick-slip, and Schallamach waves [48]. The stick-slip phenomenon is based on energy translation during the surface sliding. The movement of the rigid spherical probe on the sliding direction results in accumulation and release of energy [49]. In contrast to hard materials, stick-slip occurs under high sliding velocity and high contact load, or under low sliding velocity and low contact load in soft materials. Steady sliding is observed under low sliding velocity and high contact load [23].

To investigate under which conditions (such as sliding velocity and preload) stick-slip oscillations occur, some tests are realized using high sensitive two load cells with 25 g and 50 g capacities for horizontally and vertically motion, respectively. To be able to detect the stick-slip oscillations, the friction force data is gathered by using the load cell with 25 g capacity, while the friction force data for pattern detection experiments is gathered by a load cell with 100 g capacity. The tests for stick-slip topic are carried out using flat PDMS as a control sample which is rubbed against a hemispherical glass tip with 6 mm diameter.

7.1.1 Effect of preload

To observe the stick-slip oscillations and transition from stick-slip to steady-sliding, the tip is brought into contact with the sample and the friction force data is analyzed under different preload values at 0.02 mm/s sliding velocity. The preload effect is examined by using various preload values ranging from 10 mN to 110 mN, while the preload on the flat PDMS sample is kept constant during sliding by using SMC based on the comparative results on the chapter 5.

The experiments show that the stick-slip oscillations are observed under 10 mN preload at 0.02 mm/s sliding velocity as shown in Figure 7.1 (b). On this displacement mechanism called stick-slip there is not a continuous sliding, but rather sawtooth vibrations.
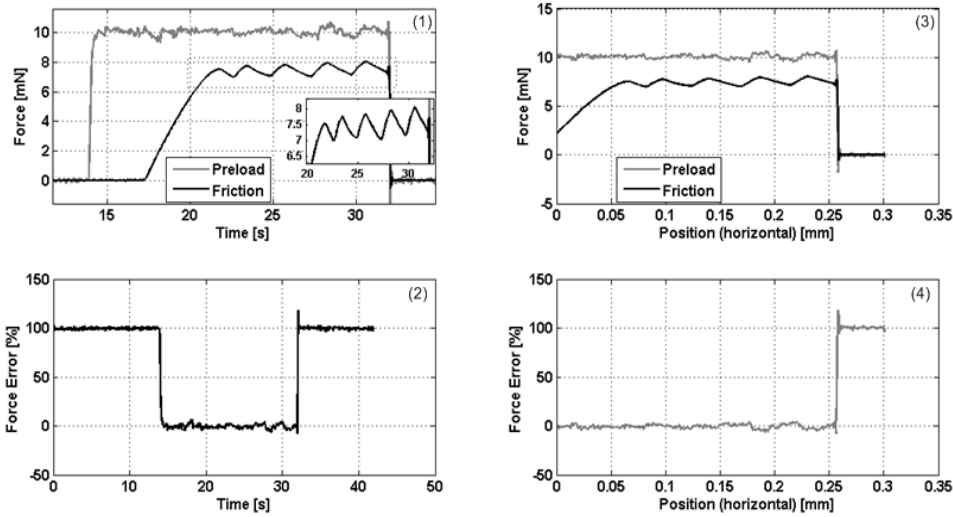

(a)
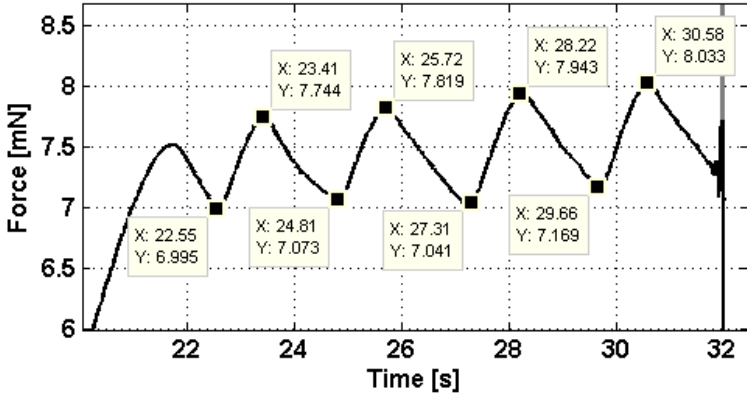
(b)

Figure 7.1 : Stick-slip oscillations under 10 mN preload at 0.02 mm/s sliding velocity; force vs time graph (1), force error vs time graph (2), force vs displacement graph (3), force error vs displacement graph (4) shown in (a), and close-up view of stick-slip oscillations shown in (b).

According to the observed stick-slip oscillations, it can be seen that the period of stick-slip is ~ 2.3 s which results in expecting a dominant frequency at 0.43 Hz based on the relation of f = 1/t. When FFT is applied to the friction force data between four peaks, the dominant frequency is observed at 0.4247 Hz which matches to the expected frequency shown in Figure 7.2 (a). Mentioned four peaks comprise the data

gathered from 23.41 s to 30.58 s as shown in Figure 7.1. When FFT is applied to the all friction force data, the dominant frequency is observed at 0.4029 Hz which is very close to the expected frequency shown in Figure 7.2 (b).
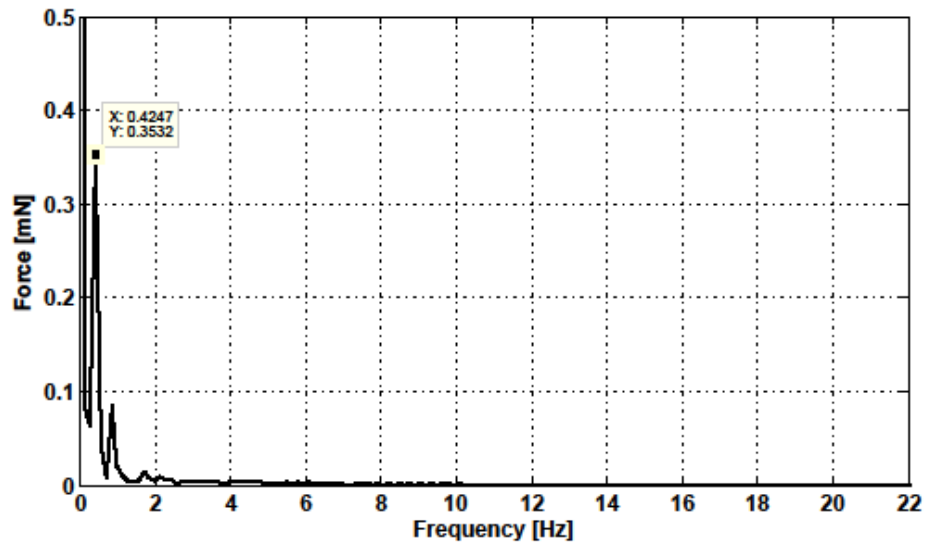
(a)
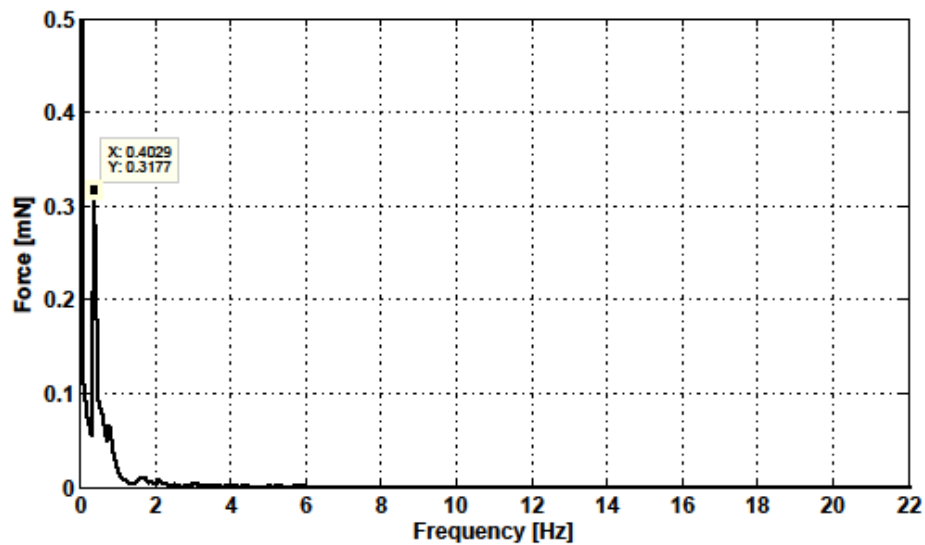
(b)

Figure 7.2 : Frequency analysis of the friction force data belonging to stick-slip oscillations; FFT result applied to the friction force data between four peaks (a), FFT result applied to the all friction force data.

According to the tests for preload effect on the stick-slip, increasing the preload results in obtaining steady-sliding. The stick-slip effects (shown in Figure 7.1) are disappeared when the preloads increased. As an example, a close up view of the frictional data for 20 mN, 60 mN and 110 mN preload values at 0.02 mm/s can be followed on the Figure 7.3. Consequently, transition from stick-slip to steady-sliding

is obtained by increasing the preload in the range of 10-110 mN at 0.02 mm/s shown in Figure 7.4.
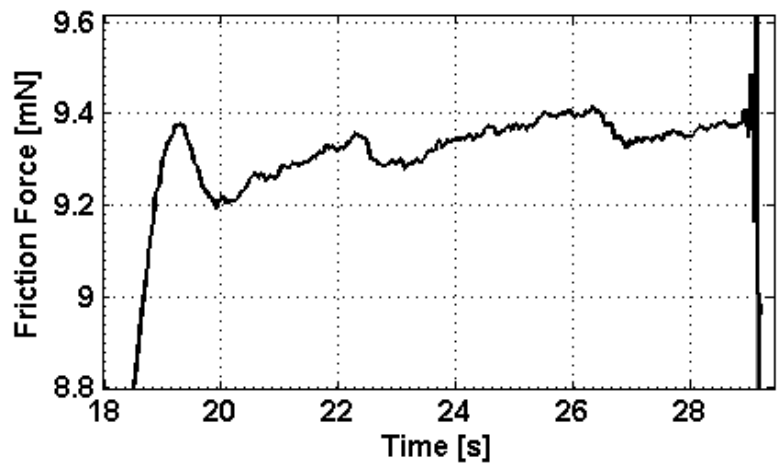
(a)
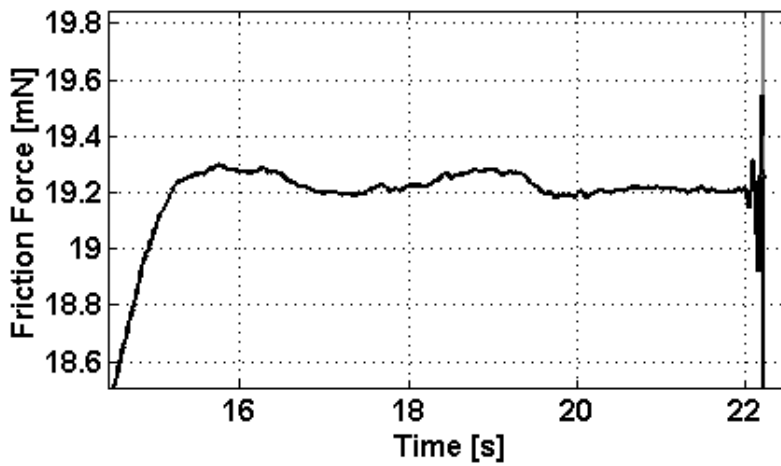
(b)
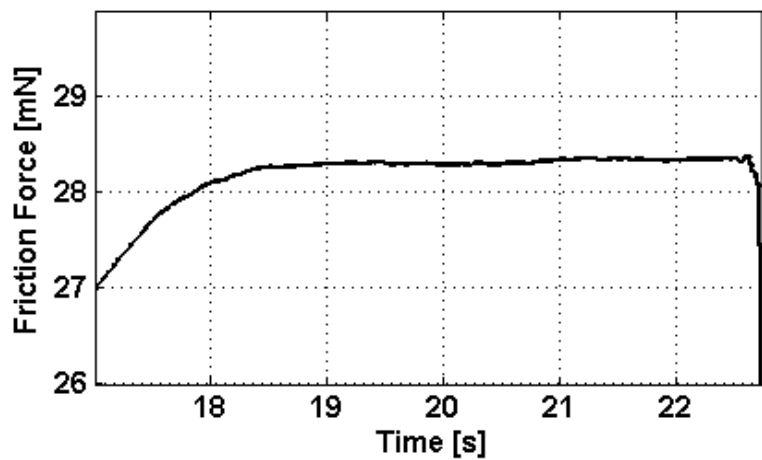
(c)

Figure 7.3 : A close-up view of the friction force data for 20 mN (a), 60 mN (b) and 110 mN (c) preloads at 0.02 mm/s sliding velocity.
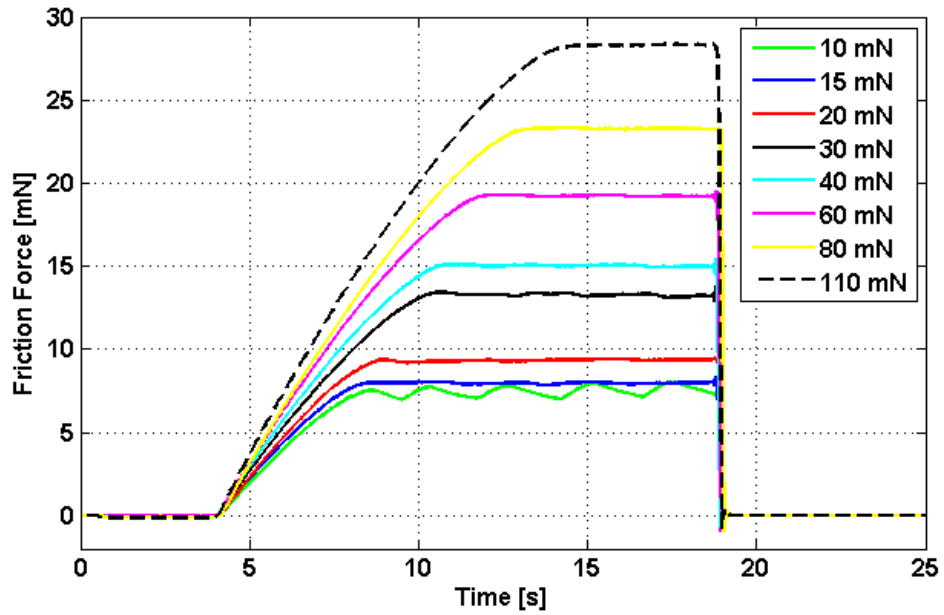
Figure 7.4 : Transition from stick-slip to steady-sliding under various preload values at 0.02 mm/s sliding velocity.

7.1.2 Effect of sliding velocity

The tests for sliding velocity effect on the stick-slip are realized by increasing the velocity values from 0.02 mm/s to 0.5 mm/s under 10 mN constant preload for a duration of 15 s. According to the tests, increasing the sliding velocity results in decreasing the amplitude of the stick-slip effects while they oscillate in the same range of friction force shown in Figure 7.5, Figure 7.6 and Figure 7.7.
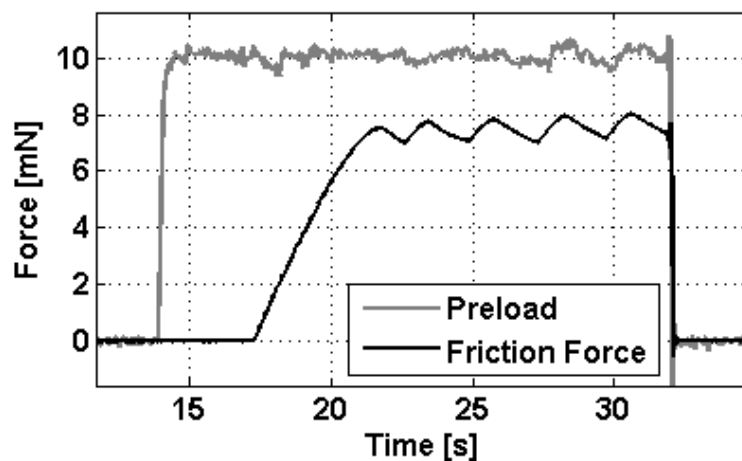
(a)

Figure 7.5 : Stick-slip effects under 10 mN constant preload at 0.02 mm/s (a), 0.03 mm/s (b), and 0.05 mm/s (c) sliding velocities.
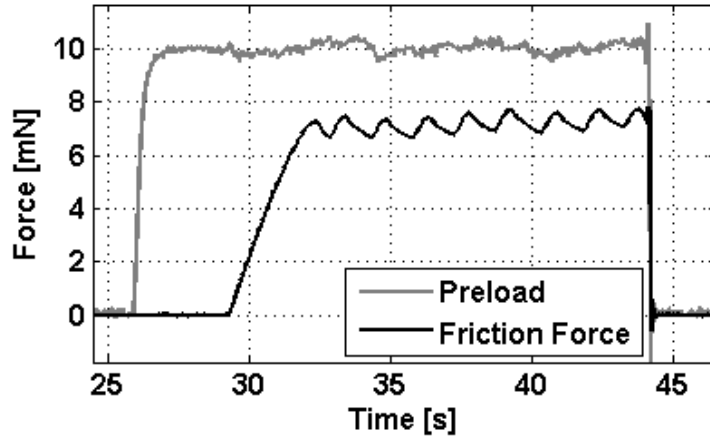
(b)
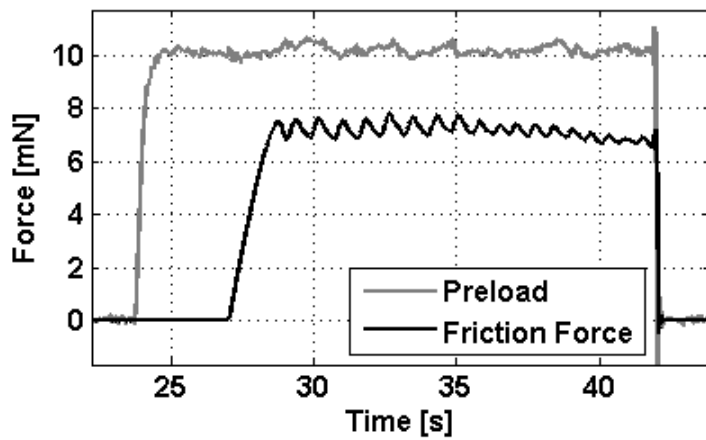
(c)

Figure 7.5 (continued): Stick-slip effects under 10 mN constant preload at 0.02 mm/s (a), 0.03 mm/s (b), and 0.05 mm/s (c) sliding velocities.
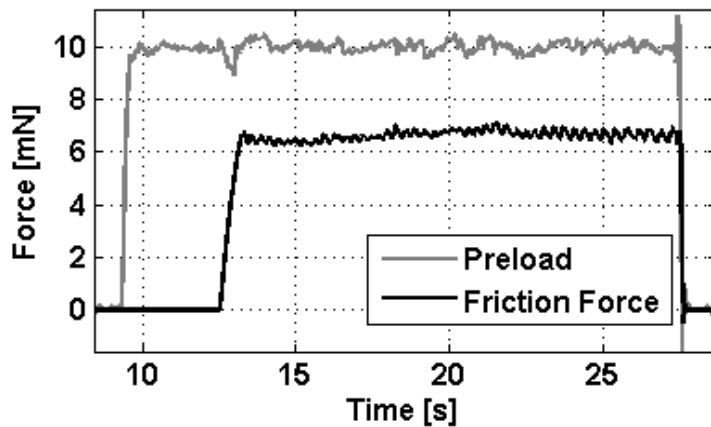
(a)

Figure 7.6 : Stick-slip effects under 10 mN constant preload at 0.1 mm/s (a), 0.2 mm/s (b), and 0.5 mm/s (c) sliding velocities.
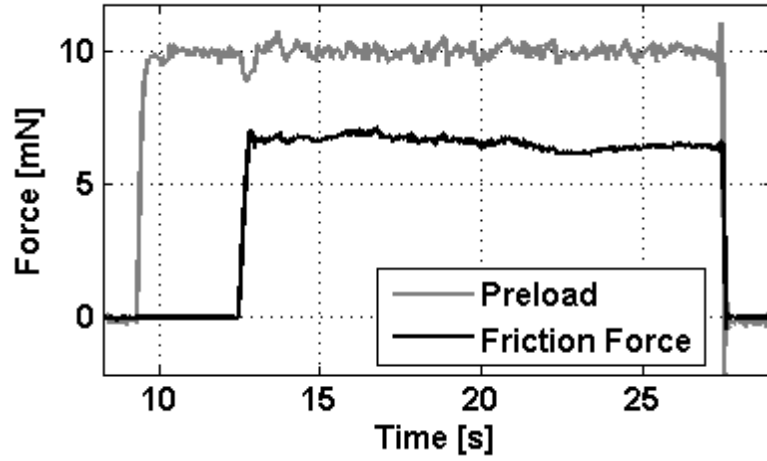
(b)
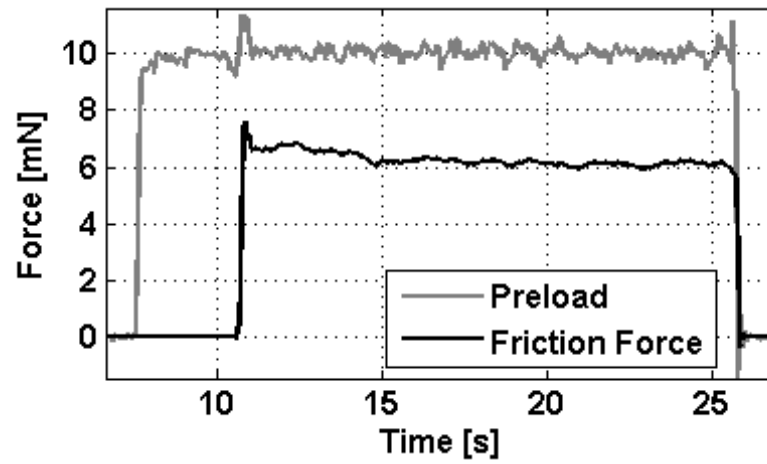
(c)

Figure 7.6 (continued) : Stick-slip effects under 10 mN constant preload
at 0.1 mm/s (a), 0.2 mm/s (b), and 0.5 mm/s (c)
sliding velocities.
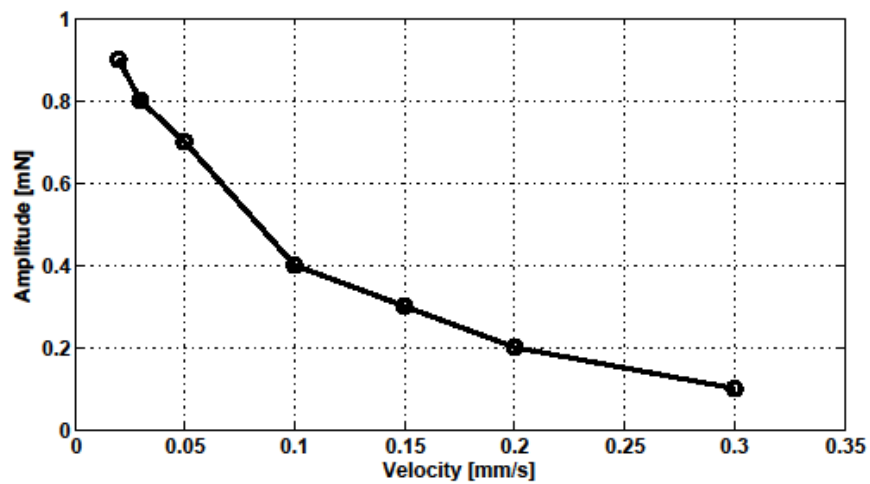
Figure 7.7 : Amplitudes of stick-slip effects at different
sliding velocities under 10 mN constant preload.

In addition, increasing the velocity causes to decrease the time spent for transition from the static friction to the kinetic friction which can be observed by the increase of the graphs' slopes (Figure 7.8).
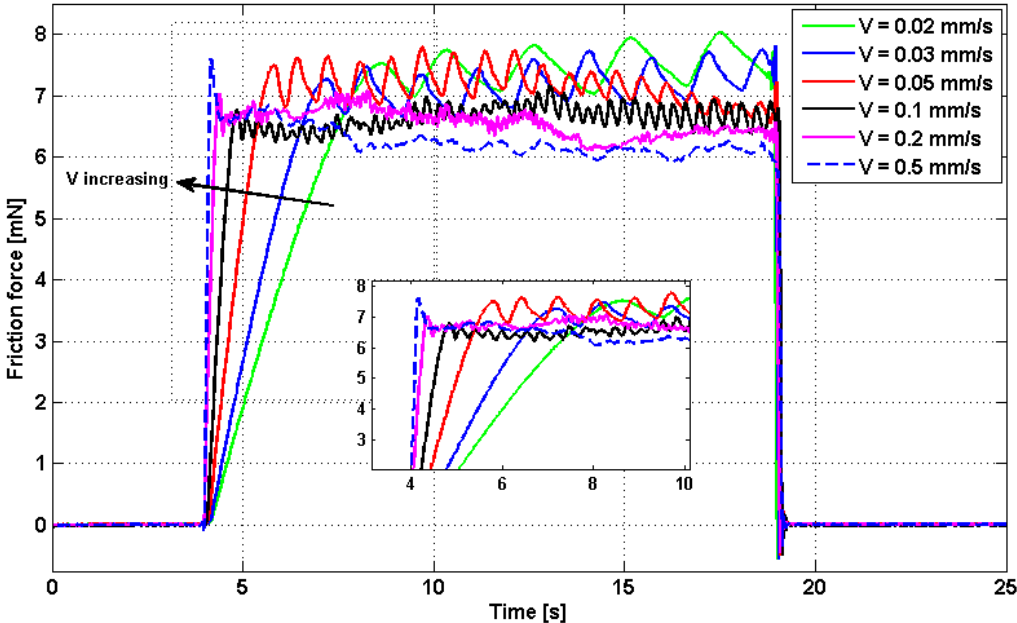
Figure 7.8 : Stick-slip effects at various sliding velocities under 10 mN constant preload.

8. PATTERN DETECTION EXPERIMENTS ON ARTIFICIAL SKIN PATTERNED WITH EVENLY DISTRIBUTED RIDGES

To exhibit pattern detection and frictional properties of the human-inspired artificial skin which is designed to have evenly distributed ridges made of PDMS, some tests are realized using high sensitive two load cells with 100 g and 250 g capacities for horizontally and vertically motion, respectively. As it mentioned on chapter 2, during the relative motion between the micropatterned artificial surface and rigid glass tip, sliding generates vibrations called friction induced vibrations [1, 6, 7, 16, 17, 34]. These vibrations allow to detect the frequency belonging to the pattern of the artificial skin, and carrying the information of the scanned surface like wavelength and height of ridges while the preload applied to the surface is kept constant by the force-feedback controller SMC.

In this study, the pattern detection experiments are carried out by observing the effect of the different design parameters such as sliding velocity, preload, and diameter of rigid glass tip. On this chapter it can be obviously seen that the preload error changes with these design parameters. During sliding, preload can be kept constant with a min. percentage of error at low sliding velocity and under high preload value. During controlling the preload, the filter effect of the tip diameter will result in elimination of the harmonics of the signal.

In addition, due to the fact that the occurrence circumstances of the stick-slip oscillations are exhibited in details on the previous chapter, all of the tests about pattern detection are realized outside of these working conditions. In other words, the tests are realized on the steady-sliding region.

The dimensions of the designed artifact are such that the diameter of the ridges and the space between the ridges are 1 mm and 1.4 mm, respectively. Peak-to-peak value of two ridges called wavelength is 2.4 mm shown in Figure 8.1. Meanwhile, the travel length is chosen approximately 12 mm amounts to five ridges. Different sizes of tip diameters are used such as 1 mm, 10 mm, and 34.74 mm.

8.1 Frictional Results & Frequency Analysis Using Tip Diameter of 1 mm

In order to detect the pattern and investigate the frictional results of the artificial skin, the hemispherical glass tip with a diameter of 1 mm is brought into contact with the sample shown in Figure 8.1. Thus, by using such a glass tip with given dimensions allows the tip to travel between the ridges of the sample, and to get the information of the surface structure called roughness. The gathered friction force data is analyzed in both time domain and frequency domain.
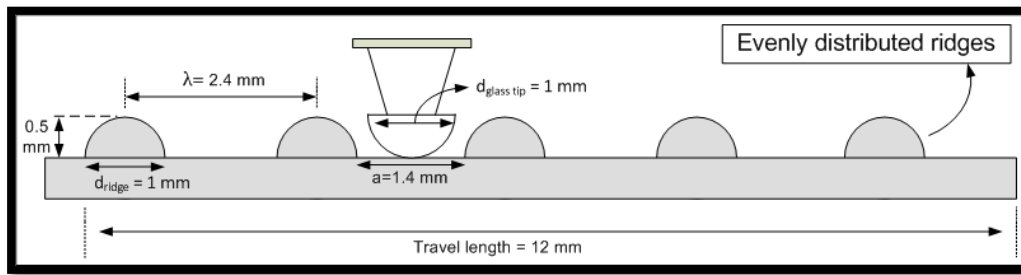
Figure 8.1 : Illustration of the tip-sample contact and dimensions of the artificial skin.

8.1.1 Effect of sliding velocity

The tests for sliding velocity effect on the pattern detection are realized by increasing the velocity values from 0.09 mm/s to 0.49 mm/s under 20 mN constant preload for a travel length of 12 mm amounts to five ridges. As it mentioned before that the preload applied to the surface is kept consistent using the force-feedback controller SMC. According to the tests, increasing the sliding velocity results in increase on the preload error shown in Figure 8.2. During surface scanning, preload remains consistent with a min. percentage of error at low sliding velocity which can be seen both on the Figure 8.2 and Table 8.1. When the artificial skin with evenly distributed ridges is scanned by the 1 mm diameter glass tip at different sliding velocity values, the values of preload errors are observed in the range of ~ 16-55 %.

Table 8.1 : Preload error during surface scanning with 1 mm diameter glass tip at different sliding velocities under 20 mN preload.
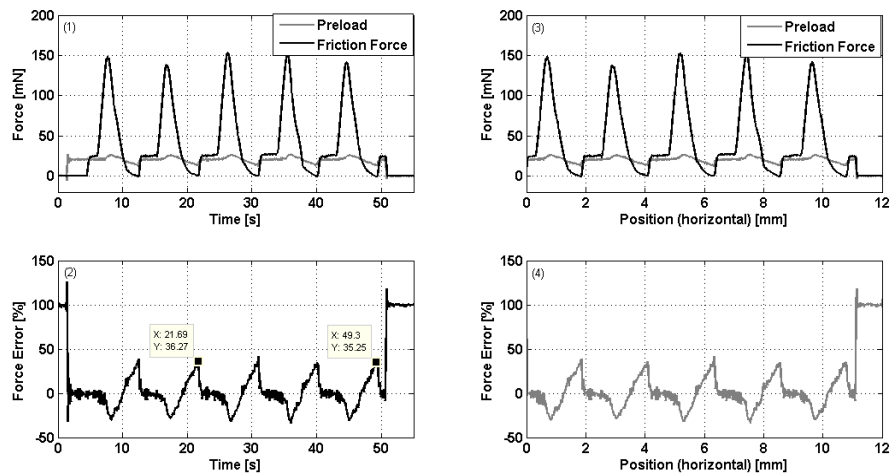
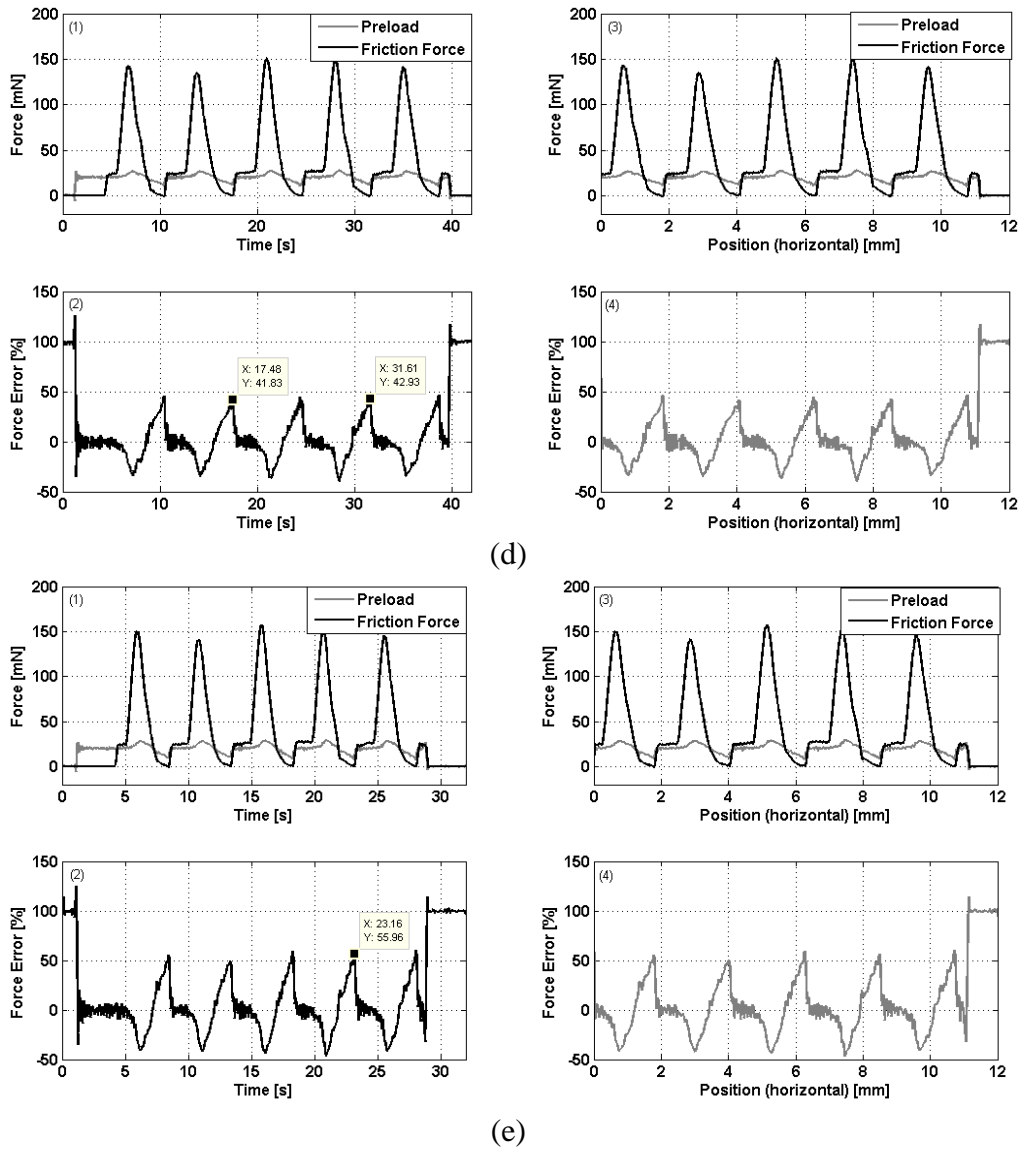| Sliding Velocity (mm/s)	Preload Error (%)
0.09	~ 16
0.15	~ 20
0.26	~ 36
0.34	~ 42
0.49	~ 55
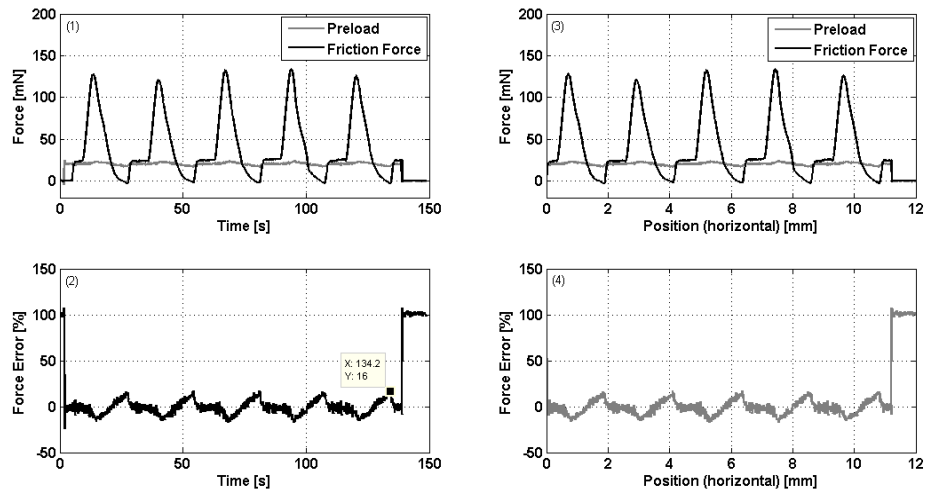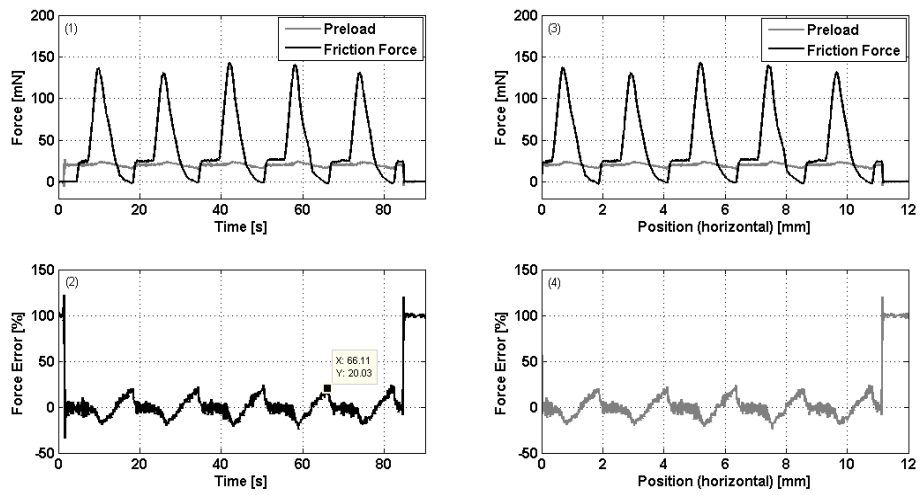
Figure 8.2 : Velocity effect on pattern detection using 1 mm diameter glass tip under 20 mN preload at 0.09 mm/s (a), 0.15 mm/s (b), 0.26 mm/s (c), 0.34 mm/s (d), and 0.49 mm/s (e) sliding velocity by using force vs time graph (1), force error vs time graph (2), force vs displacement graph (3), force error vs displacement graph (4).

Figure 8.2 (continued) : Velocity effect on pattern detection using 1 mm diameter glass tip under 20 mN preload at 0.09 mm/s (a), 0.15 mm/s (b), 0.26 mm/s (c), 0.34 mm/s (d), and 0.49 mm/s (e) sliding velocity by using force vs time graph (1), force error vs time graph (2), force vs displacement graph (3), force error vs displacement graph (4).

The results indicate when the artificial sample is detected by the glass tip with a 1 mm diameter, the information of this sample about the height and wavelength of the ridges is obtained. In other words, the profile of the sample is obtained shown in Figure 8.3.

To investigate the friction induced vibrations generated during sliding, dynamic contact between the artificial surface and the rigid glass tip is analyzed in frequency domain. When FFT is applied on the friction force data, the frequency belonging to the pattern of the artificial skin is observed based on the relation of

$$f = V / \lambda \qquad\qquad (8.1)$$

where f is the frequency belonging to the pattern of the surface, V is the sliding velocity, and λ is the wavelength of the ridges. Depending on the various velocity values, the expected frequencies are computed using the Eq. 8.1. The frequency analysis of the friction force data at 2 kHz sampling frequency indicates that the observed frequencies are relatively same with the expected frequency values. The reason behind the little difference between the expected and observed frequencies is that the system is a coupled system. Furthermore, the polymer type, PDMS, used for fabrication of the artificial skin can cause to obtain this mentioned difference. As the velocity increases in the range of 0.09-0.49 mm/s, the dominant frequency shifts towards right shown in Figures 8.4-8.8. This result matches with the literature as well [7, 16, 17]. In addition, increasing the sliding velocity results in increase on the force amplitude of the frequencies. Due to the fact that the tip travels between the ridges of the sample, the harmonics of the signal are also observed based on the frequency analysis as shown in the Figures 8.4-8.8.
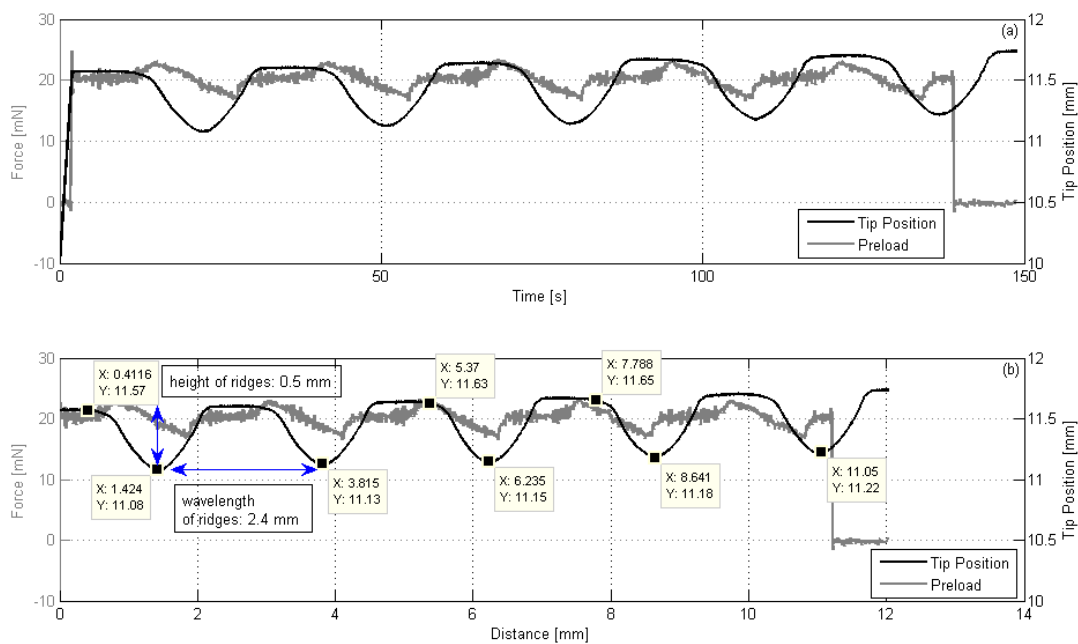
Figure 8.3 : The profile of the sample scanned with 1 mm diameter glass tip under 20 mN preload at 0.09 mm/s sliding velocity by using tip position and force vs. time graph (1), and tip position and force vs. distance graph (2).

Frequency analysis of friction force data for different sliding velocities is as follows;

- For V = 0.09 mm/s;
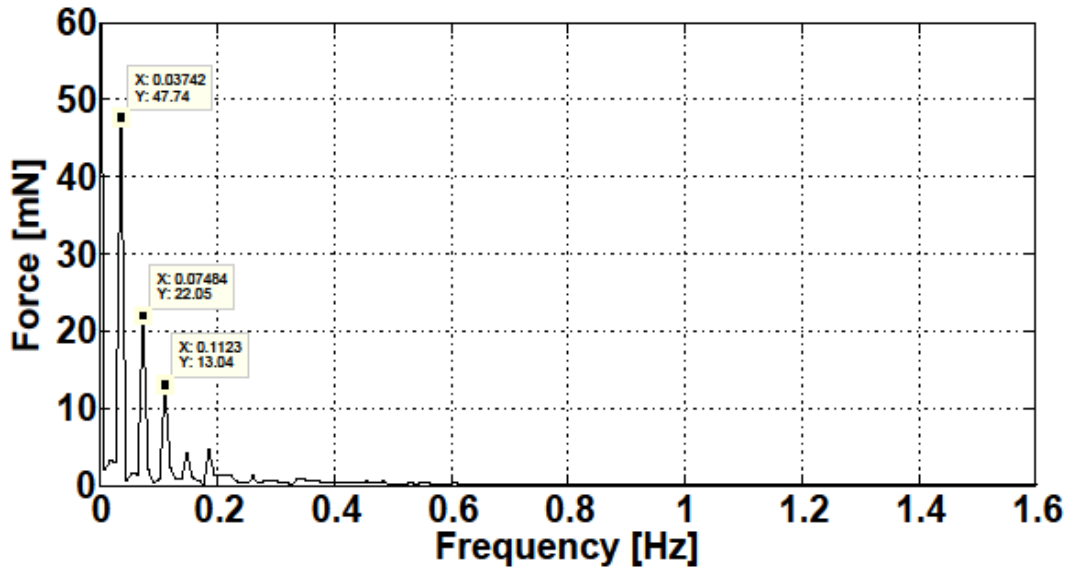
  f(expected) = V/λ = 0.09/2.4 = 0.03750 Hz

  f(observed) = 0.03742 Hz

Figure 8.4 : Frequency result for 0.09 mm/s sliding velocity.

- For V = 0.15 mm/s;

  f(expected) = V/λ = 0.15/2.4 = 0.06250 Hz

  f(observed) = 0.06299 Hz
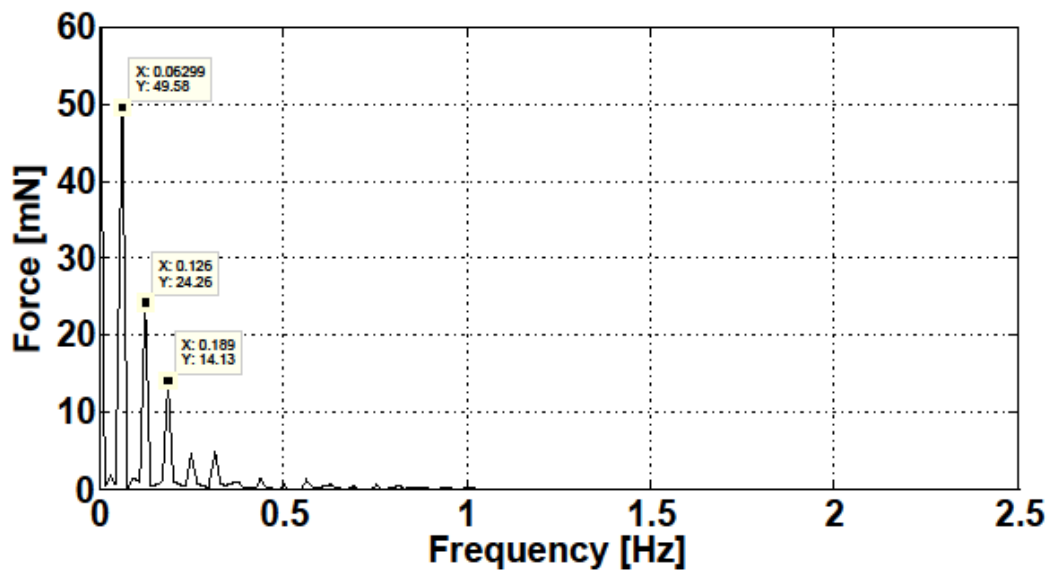
Figure 8.5 : Frequency result for 0.15 mm/s sliding velocity.

- For V = 0.26 mm/s;

  f(expected) = V/λ = 0.26/2.4 = 0.1083 Hz

  f(observed) = 0.1091 Hz
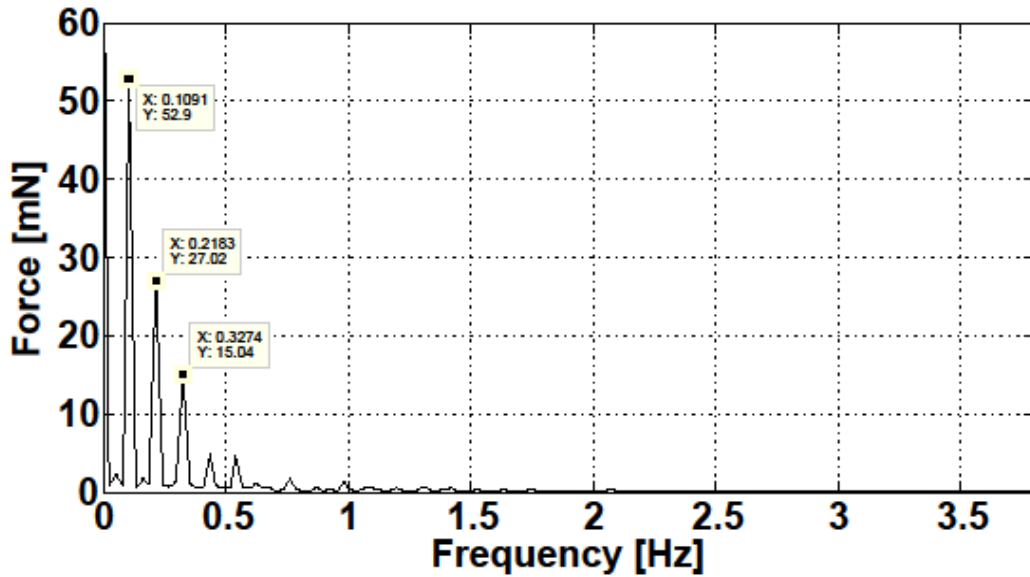
Figure 8.6 : Frequency result for 0.26 mm/s sliding velocity.

- For V = 0.34 mm/s;
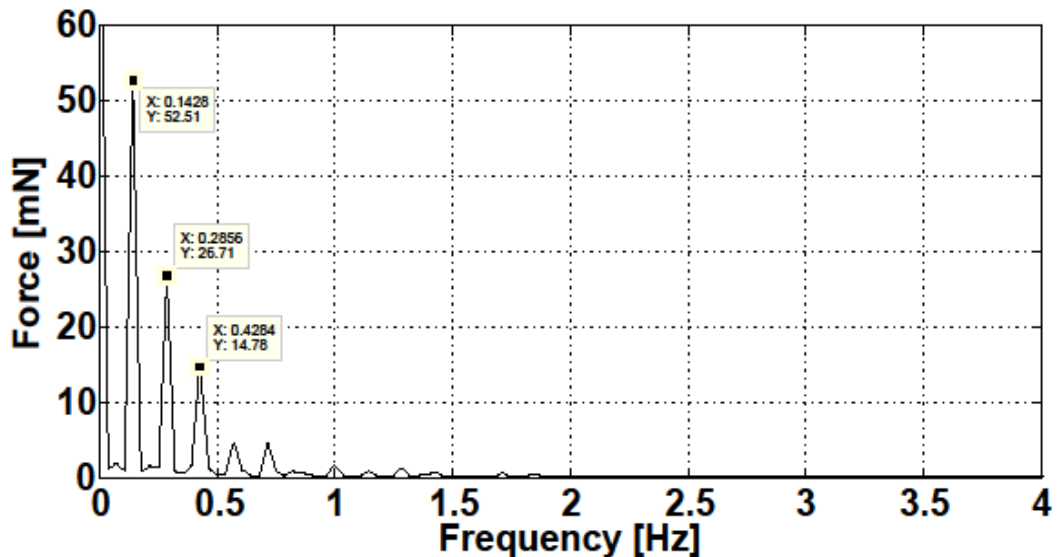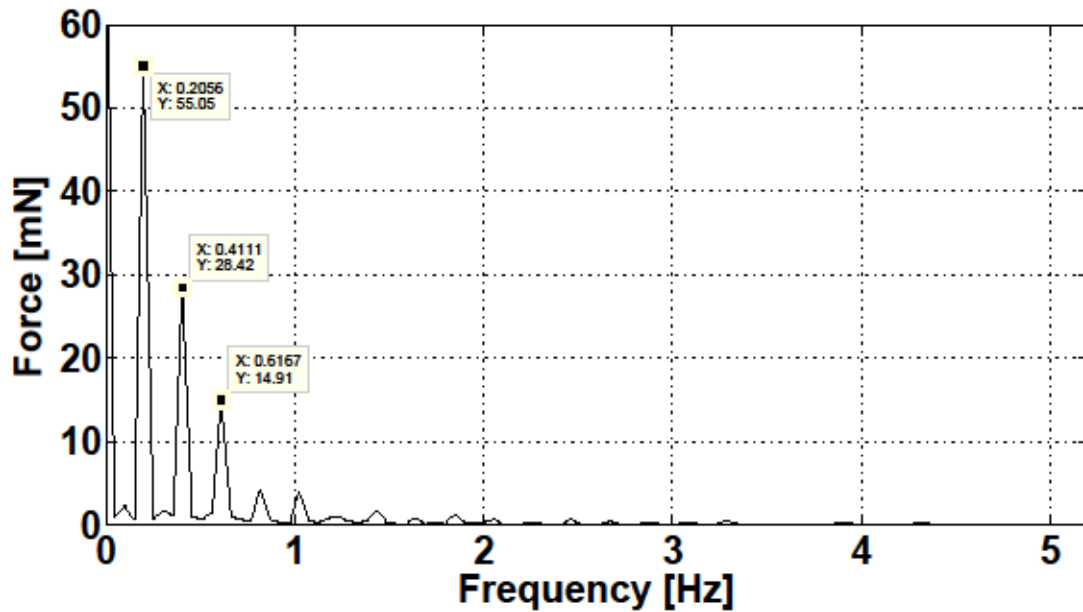
  f(expected) = V/λ = 0.34/2.4 = 0.1417 Hz

  f(observed) = 0.1428 Hz

Figure 8.7 : Frequency result for 0.34 mm/s sliding velocity.

- For V = 0.49 mm/s;

  f(expected) = V/λ = 0.49/2.4 = 0.2042 Hz

  f(observed) = 0.2056 Hz

Figure 8.8 : Frequency result for 0.49 mm/s sliding velocity.
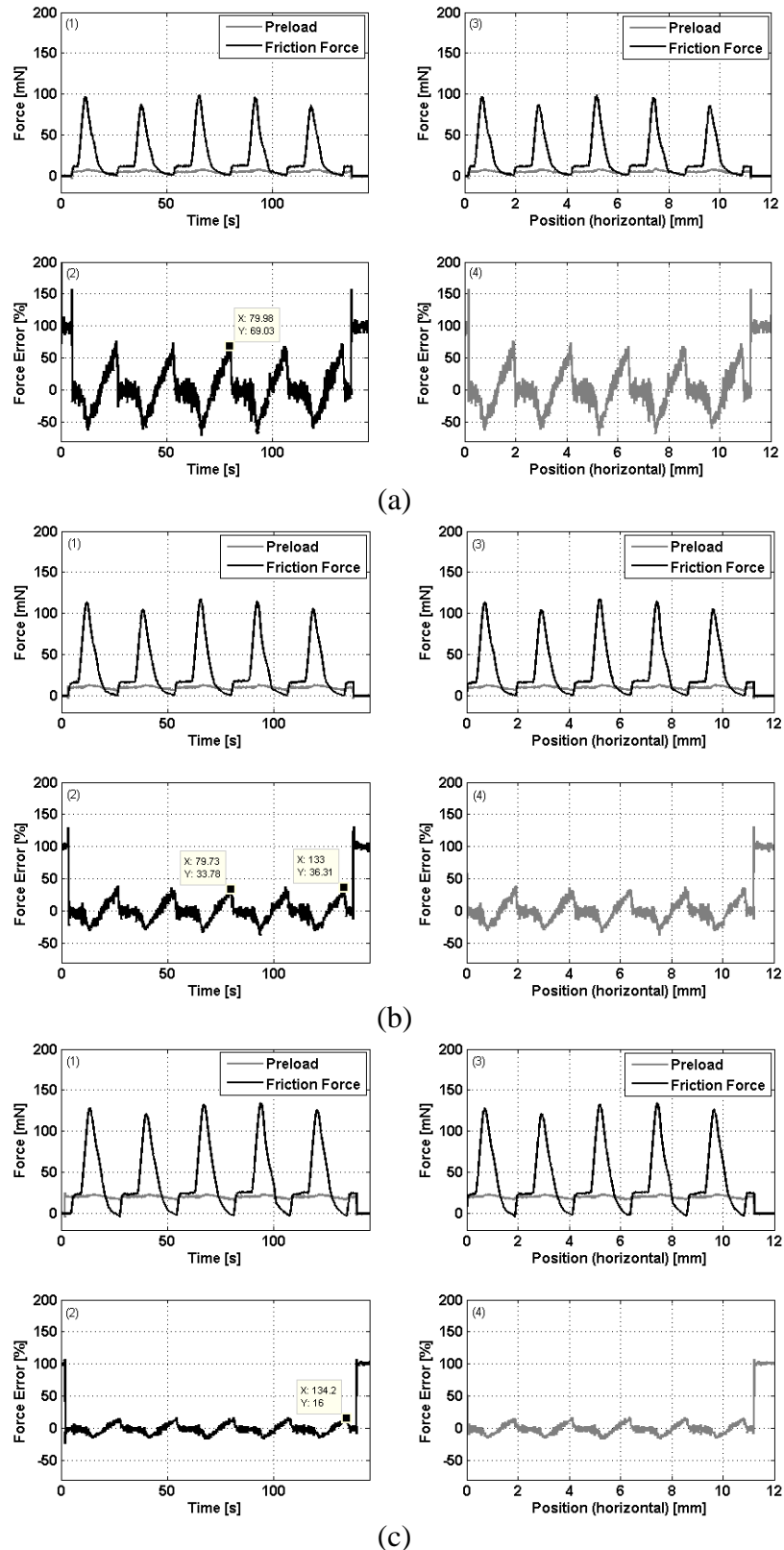
8.1.2 Effect of preload

During the dynamic contact of surface scanning between the artificial surface and the rigid glass tip, different preload values are applied on the surface at 0.09 mm/s constant sliding velocity to observe the preload effect on pattern detection. According to the Figure 8.9, it is obvious that there is an inverse relationship between the preload and preload error. As the preload increases in the range of 5-35 mN, the preload error decreases from ~ 70 % to ~ 8 %.

Total results for preload error can be followed both on the Figure 8.9 and Table 8.2. It is clear that during surface scanning the preload remains unchanged with a min. percentage of error under high preload value. For instance, an approximately 8 % of preload error is observed under 35 mN preload value.

Table 8.2 : Preload error during surface scanning with 1 mm diameter glass tip under different preload values at 0.09 mm/s sliding velocity.

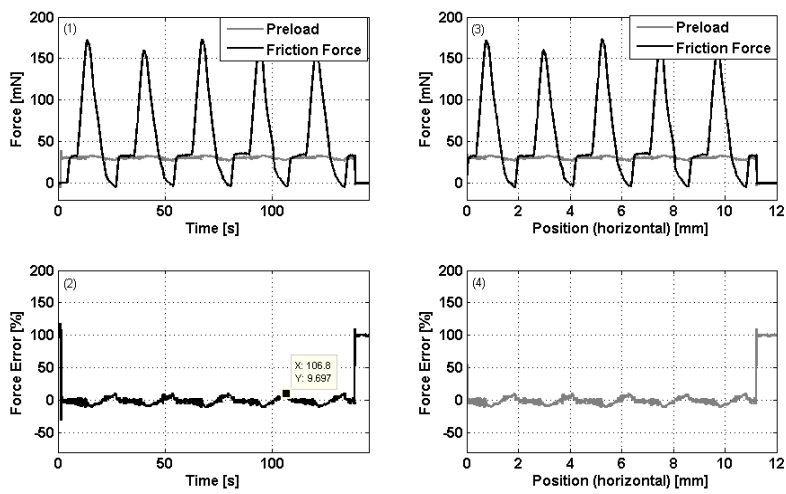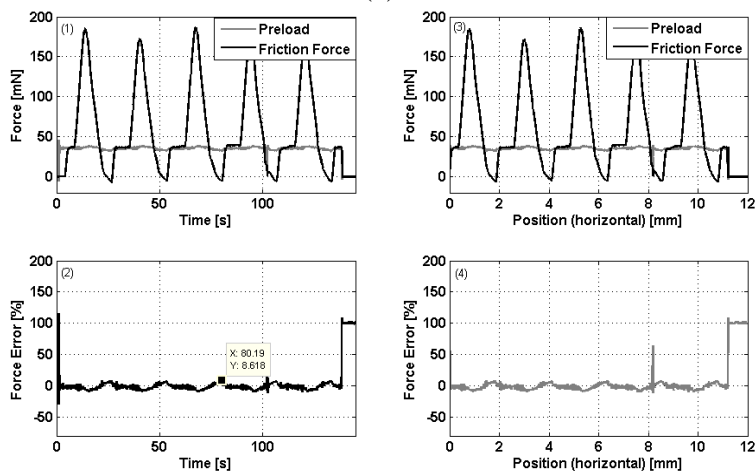| Preload (mN)	Preload Error (%)
5	~ 70
10	~ 35
20	~ 16
25	~ 12
30	~ 10
35	~ 8

Figure 8.9 : Preload effect on pattern detection using 1 mm diameter glass tip at 0.09 mm/s sliding velocity under 5 mN (a), 10 mN (b), 20 mN (c), 25 mN (d), 30 mN (e), and 35 mN (f) preload by using force vs time graph (1), force error vs time graph (2), force vs displacement graph (3), force error vs displacement graph (4).
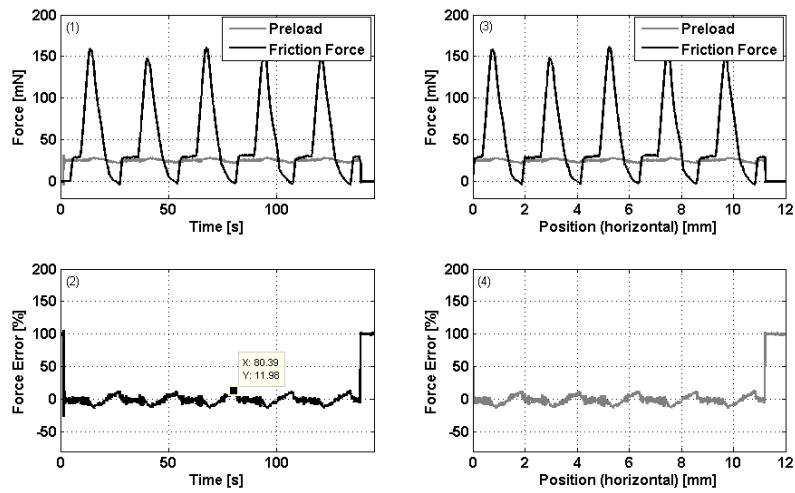
Figure 8.9 (continued): Preload effect on pattern detection using 1 mm diameter glass tip at 0.09 mm/s sliding velocity under 5 mN (a), 10 mN (b), 20 mN (c), 25 mN (d), 30 mN (e), and 35 mN (f) preload by using force vs time graph (1), force error vs time graph (2), force vs displacement graph (3), force error vs displacement graph (4).

In addition, during measurements of preload and sliding velocity effect one of the important conditions is to move the related linear motor with a constant velocity. As it mentioned on the chapter 2 that during relative motion between glass tip and artificial sample, displacement data and velocity data of the motors are gathered continuously from their encoders with the aid of the custom written software which has 2 kHz sampling frequency. To ensure that the motors are driven at a constant velocity, the data about velocity gathered from the encoders of the motors is checked. So, it is proven that the horizontally placed motor, which carries the artificial sample, moves at constant velocity with an approximately $\pm 4 \times 10^{-5}$ percentage of error during sliding as shown in Figure 8.10. This sample result is obtained when the artifact is scanned by the glass tip under 20 mN preload and 0.09 mm/s sliding velocity.

Furthermore, frequency analysis of friction force data using FFT is exhibited in details on the following Figures 8.11-8.16. It is clear that the dominant frequency values are observed as they are expected. Meanwhile, because the tests of preload effect are realized at a constant sliding velocity, 0.09 mm/s, the expected frequencies with their harmonics remain unchanged. In addition, increasing the preload values from 5 mN to 35 mN results in increase on the force amplitude of the frequencies.
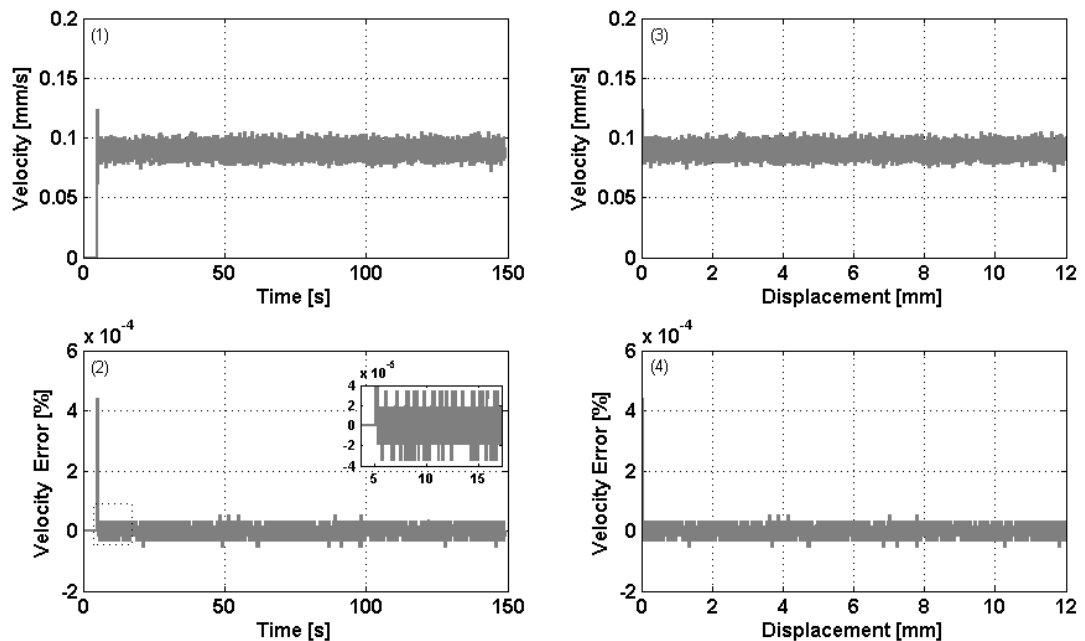
Figure 8.10 : Velocity graphs of the horizontally placed motor during sliding under 20 mN preload and at 0.09 mm/s sliding velocity by using velocity vs time graph (1), velocity error vs time graph (2), velocity vs displacement graph (3), velocity error vs displacement graph (4).

Frequency results are as follows;

- For P = 5 mN;

    f(expected) = V/λ = 0.09/2.4 = 0.03750 Hz

    f(observed) = 0.03793 Hz

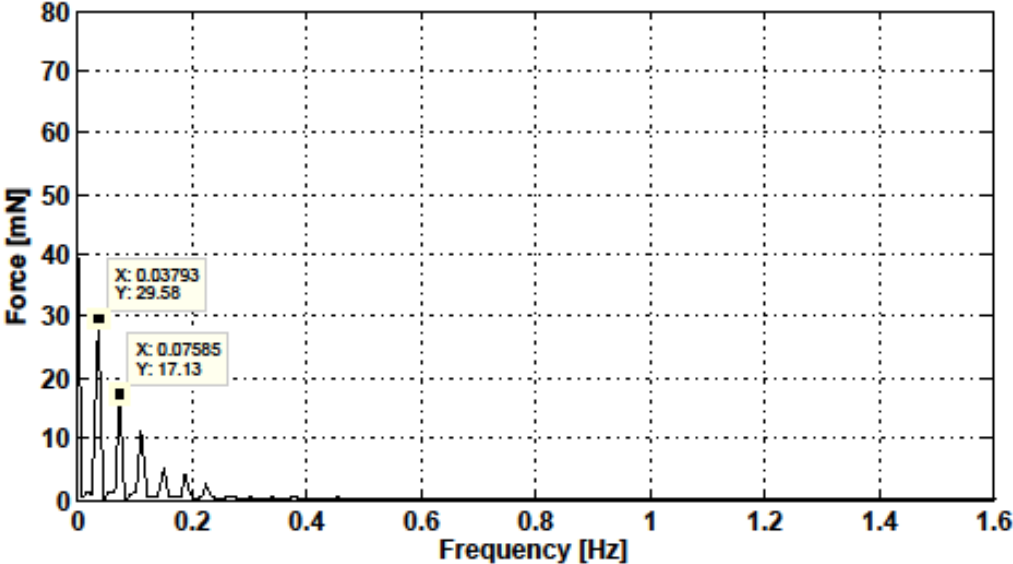**Figure 8.11 :** Frequency result for 5 mN preload.

- For P = 10 mN;

    f(expected) = V/λ = 0.09/2.4 = 0.03750 Hz

    f(observed) = 0.03789 Hz
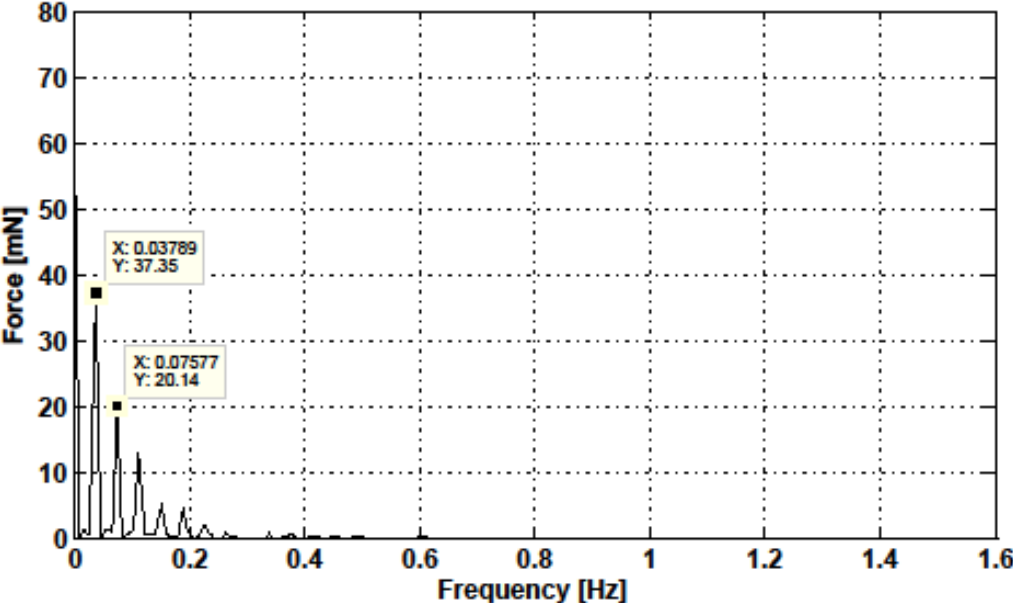
Figure 8.12 : Frequency result under 10 mN preload.

- For P = 20 mN;

  f(expected) = V/λ = 0.09/2.4 = 0.03750 Hz

  f(observed) = 0.03742 Hz
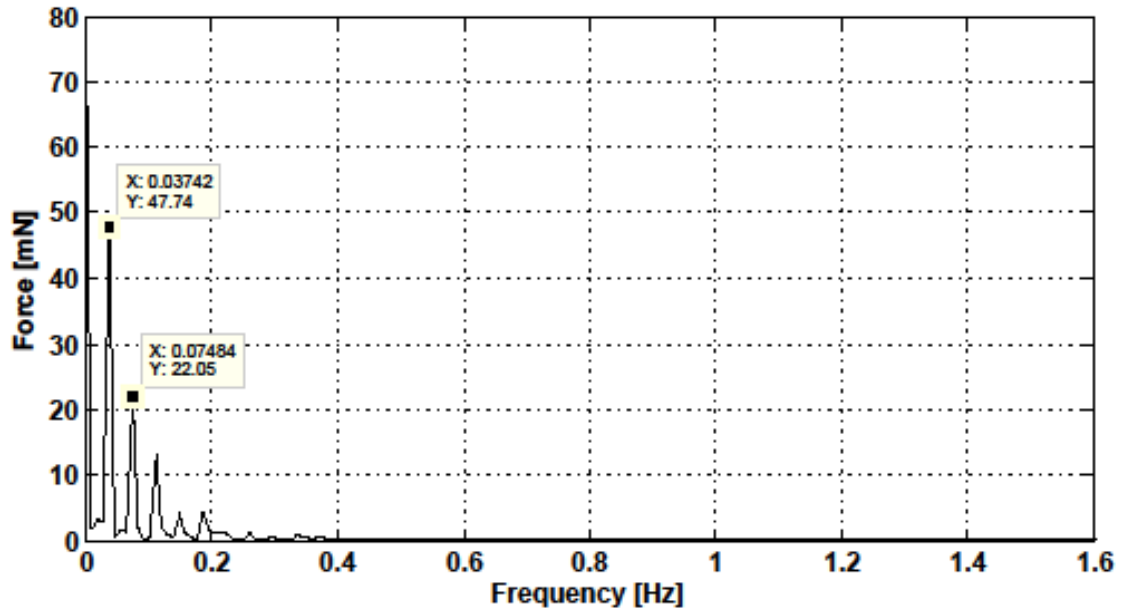
Figure 8.13 : Frequency result for 20 mN preload.

- For P = 25 mN;

  f(expected) = V/λ = 0.09/2.4 = 0.03750 Hz

  f(observed) = 0.03779 Hz
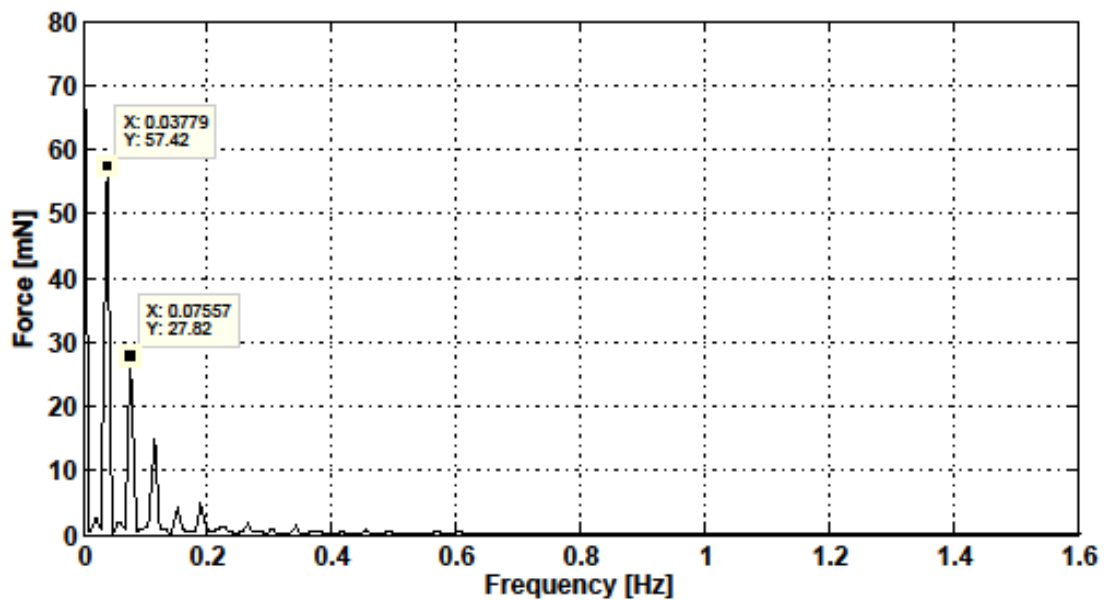
Figure 8.14 : Frequency result for 25 mN preload.

- For P = 30 mN;

  f(expected) = V/λ = 0.09/2.4 = 0.03750 Hz → f(observed) = 0.03802 Hz
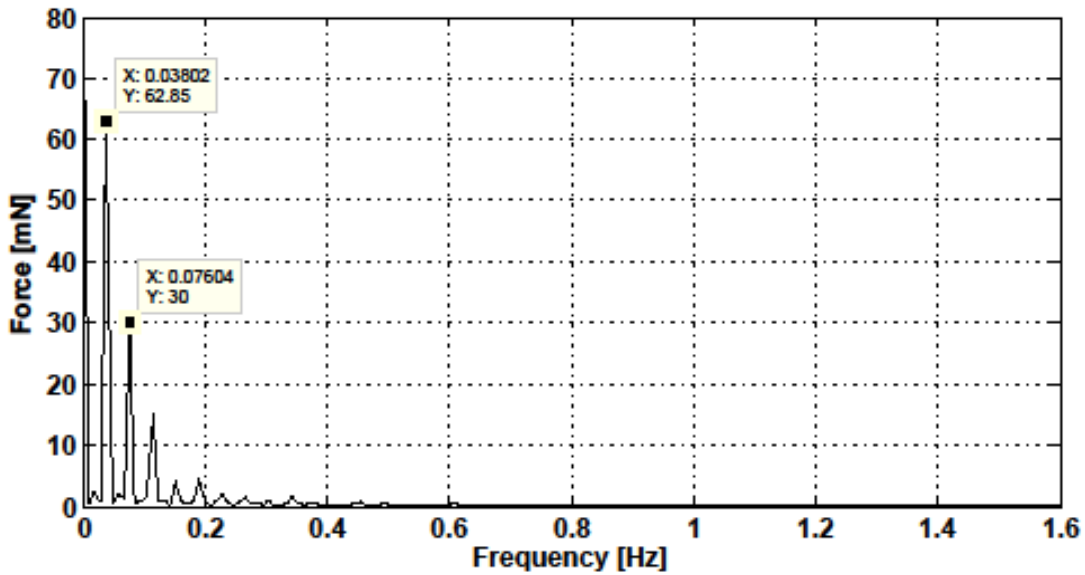
Figure 8.15 : Frequency result for 30 mN preload.

- For P = 35 mN;

  f(expected) = V/λ = 0.09/2.4 = 0.03750 Hz → f(observed) = 0.03791Hz

Figure 8.16 : Frequency result for 35 mN preload.

To summarize the results of the tests on this section, the following statements are considered. As the sliding velocity increases in the range of 0.09-0.49 mm/s,

- preload errors increase from ~ 16 % to ~ 55 %,
- dominant frequency belonging to the pattern of the artificial skin shifts towards right,
- force amplitude of the dominant frequency increases.

As the preload applied to the sample surface increases in the range of 5-35 mN,

- preload errors decrease from ~ 70 % to ~ 8 %,

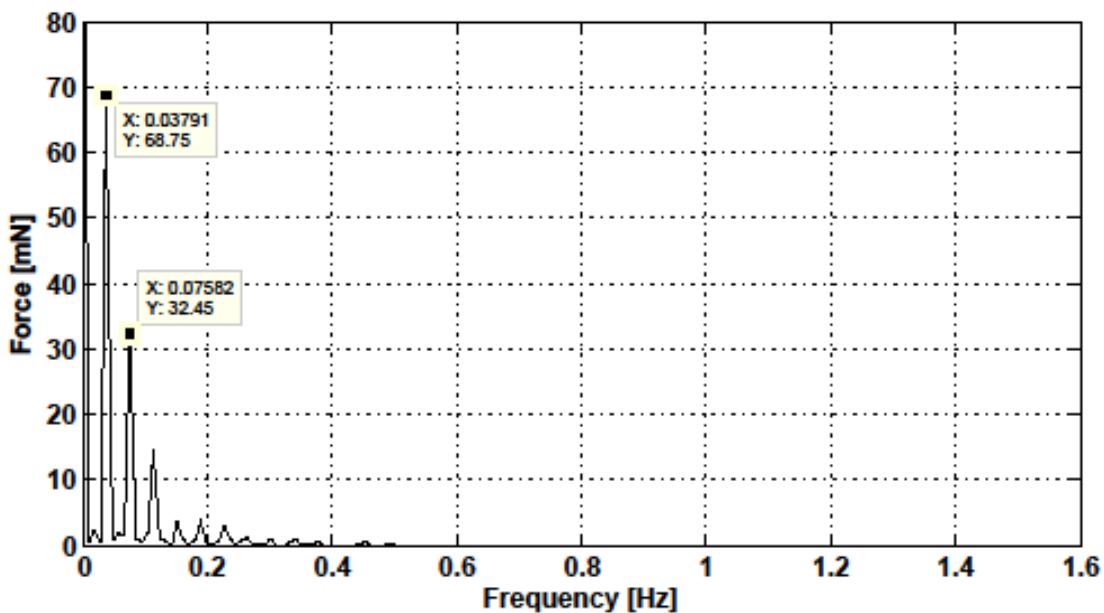- expected frequencies with their relatively unchanged values are obtained,

- force amplitude of the dominant frequency increases.

Using a glass tip with a diameter of 1 mm allows

- the tip to travel between the ridges of the artificial sample,

- obtaining the information about the height and wavelength of the ridges,

- the observed frequencies to be relatively same with the expected frequency values,

- to observe harmonics of the signal due to the fact that the tip travels between the ridges.

8.2 Frictional Results & Frequency Analysis Using Tip Diameter of 10 mm

To observe the tip diameter effect which is the one of the design parameters, relative motion between the artificial sample and the hemispherical glass tip with a diameter of 10 mm is analyzed (Figure 8.17). In addition, sliding velocity and preload effects are also investigated.
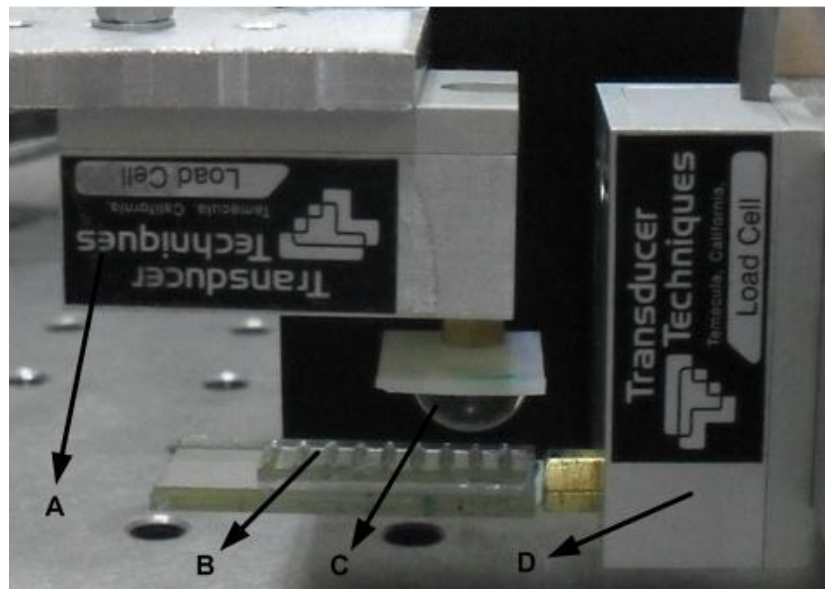
(a)

Figure 8.17 : (a) A close-up picture of the experimental set-up; A: Loadcell 1 with 250 g capacity, B: Artificial skin with evenly distributed ridges, C: Hemispherical glass tip with 10 mm diameter, D: Loadcell 2 with 100 g capacity. (b) Illustration of the tip-sample contact with detailed dimensions.
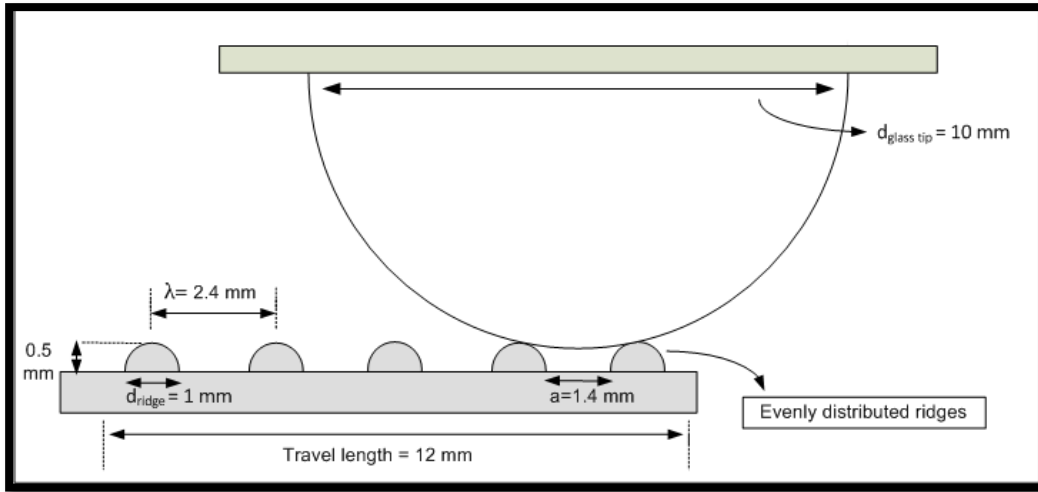
(b)

Figure 8.17 (continued): (a) A close-up picture of the experimental set-up;
A: Loadcell 1 with 250 g capacity, B: Artificial skin with evenly distributed ridges, C: Hemispherical glass tip with 10 mm diameter, D: Loadcell 2 with 100 g capacity.
(b) Illustration of the tip-sample contact with detailed dimensions.

Moreover, as it is mentioned on the previous chapters that the artifact used on this study is designed by inspiring human skin tactile properties to develop artificial polymer skin with evenly distributed ridges. In addition, according to the literature on the human body the most touch sensing is at the fingertips which can perceive surface texture approximately on a 1 cm^2 area of contact, and at 10-40 kPa stress levels [2]. As it is explained in details there are some steps from touching to sensing the properties of the surface structure including the roughness [16]. Thus, to adapt this tactile perception mechanism to the artifacts for detecting their pattern, artificial micropatterned sample with suitable dimensions is designed. Meanwhile, appropriate working conditions are used. For instance, the preload values are so chosen that they correspond to the 10-40 kPa stress levels of the human fingertips as shown on Table 8.3. The related computations are realized by using JKR adhesive contact theory. The details of this theory are given on Chapter 3 and 6. The contact radius for each preload value is computed based on the Eq. 6.2. Meanwhile, the pressure levels corresponding to each preloads is obtained by the relation of

$$P = \frac{F}{A}$$

(8.2)

where P is the pressure, F is the preload, and A is the contact area.

74

Table 8.3 : Results of contact radius, contact area, and pressure values for each preloads applied to the sample surface.
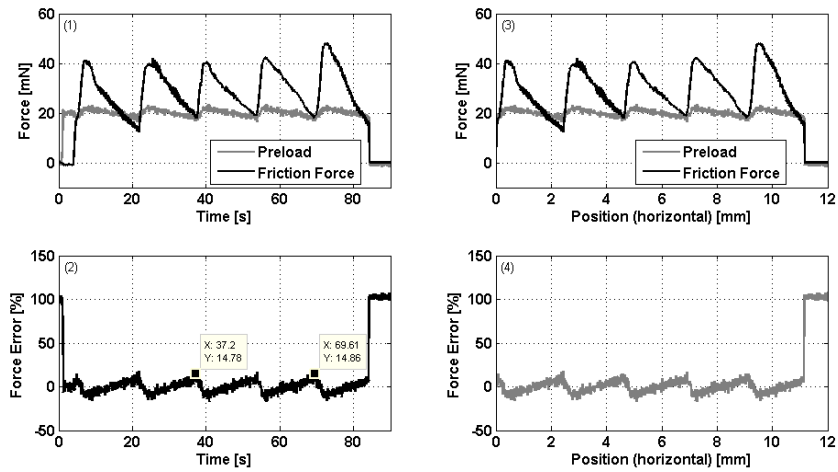
Preload (mN)	Contact radius (mm)	Contact area (mm²)	Pressure (kPa)
5	0.38	0.45	11
10	0.44	0.61	16.4
20	0.52	0.86	23.1
25	0.56	0.97	25.7
30	0.58	1.07	27.9
35	0.61	1.17	29.9

8.2.1 Effect of sliding velocity

The sliding velocity effect is exhibited by using the same velocity values in the range of 0.09-0.49 mm/s under 20 mN constant preload for a travel length of 12 mm as they are used on the previous case study. According to the tests, the preload errors increase with increasing the velocity. However, if the values of the errors are compared with that of the errors gathered by the 1 mm diameter glass tip, the errors diminish. Thus, it indicates that using large diameter of tip allows to decrease the preload errors as shown in Figure 8.18 and Table 8.4.

(a)
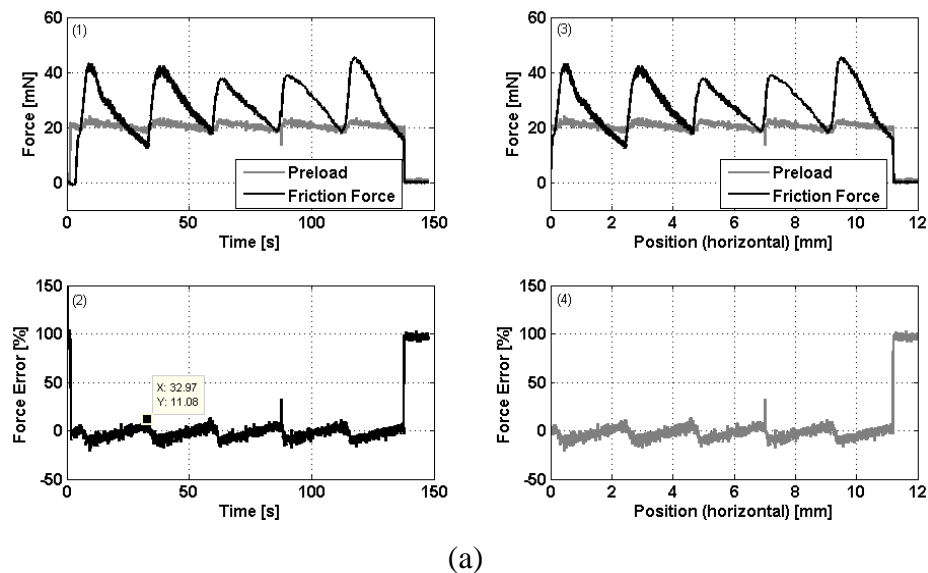
Figure 8.18 : Velocity effect on pattern detection using 10 mm diameter glass tip under 20 mN preload at 0.09 mm/s (a), 0.15 mm/s (b), 0.26 mm/s (c), 0.34 mm/s (d), and 0.49 mm/s (e) sliding velocity by using force vs time graph (1), force error vs time graph (2), force vs displacement graph (3), force error vs displacement graph (4).

(b)

(c)

(d)

Figure 8.18 (continued): Velocity effect on pattern detection using 10 mm diameter glass tip under 20 mN preload at 0.09 mm/s (a), 0.15 mm/s (b), 0.26 mm/s (c), 0.34 mm/s (d), and 0.49 mm/s (e) sliding velocity by using force vs time graph (1), force error vs time graph (2), force vs displacement graph (3), force error vs displacement graph (4).
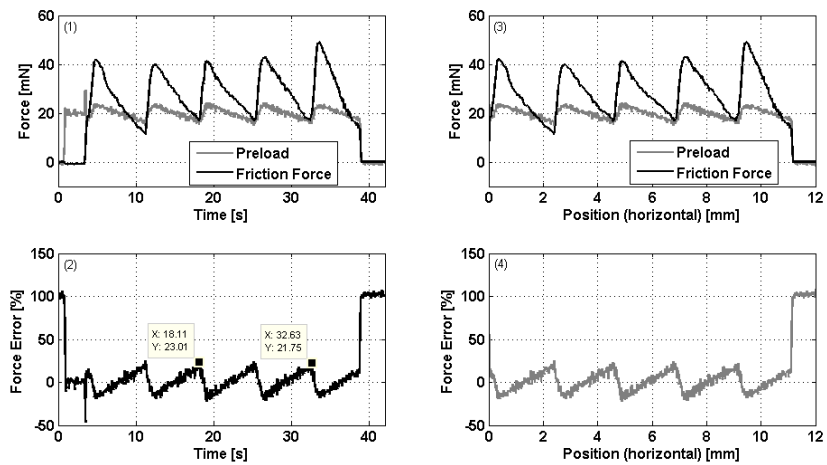
(e)

Figure 8.18 (continued): Velocity effect on pattern detection using 10 mm diameter glass tip under 20 mN preload at 0.09 mm/s (a), 0.15 mm/s (b), 0.26 mm/s (c), 0.34 mm/s (d), and 0.49 mm/s (e) sliding velocity by using force vs time graph (1), force error vs time graph (2), force vs displacement graph (3), force error vs displacement graph (4).
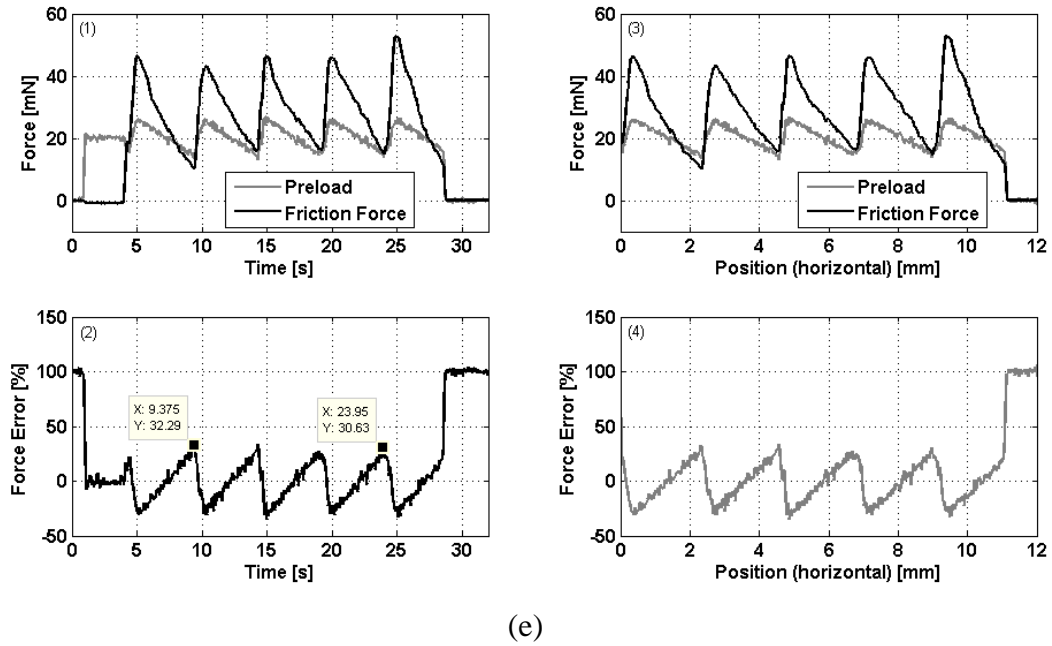
Table 8.4 : Preload error during surface scanning with 10 mm diameter glass tip at different sliding velocities under 20 mN preload.

Sliding Velocity (mm/s)	Preload Error (%)
0.09	~ 11
0.15	~ 15
0.26	~ 17
0.34	~ 22
0.49	~ 32

In addition, the tip-position graphs show that using a glass tip with 10 mm diameter results in obtaining the information only about the wavelength of the ridges because the tip slides on the ridges of the sample instead of travelling between the ridges (Figure 8.19).

To observe the dominant frequency values carrying the information of the pattern, FFT is used to analyze the friction force data. By using the Eq. 8.1, the results demonstrate that the observed frequencies are relatively same with the expected frequency values. As the velocity increases in the range of 0.09-0.49 mm/s, the dominant frequency shifts towards right. Moreover, the force amplitude of the frequencies increase as well when the velocities increase. Although the tip slid on the

ridges of the sample, the harmonics of the signal are also observed as shown in the Figures 8.20-8.24.
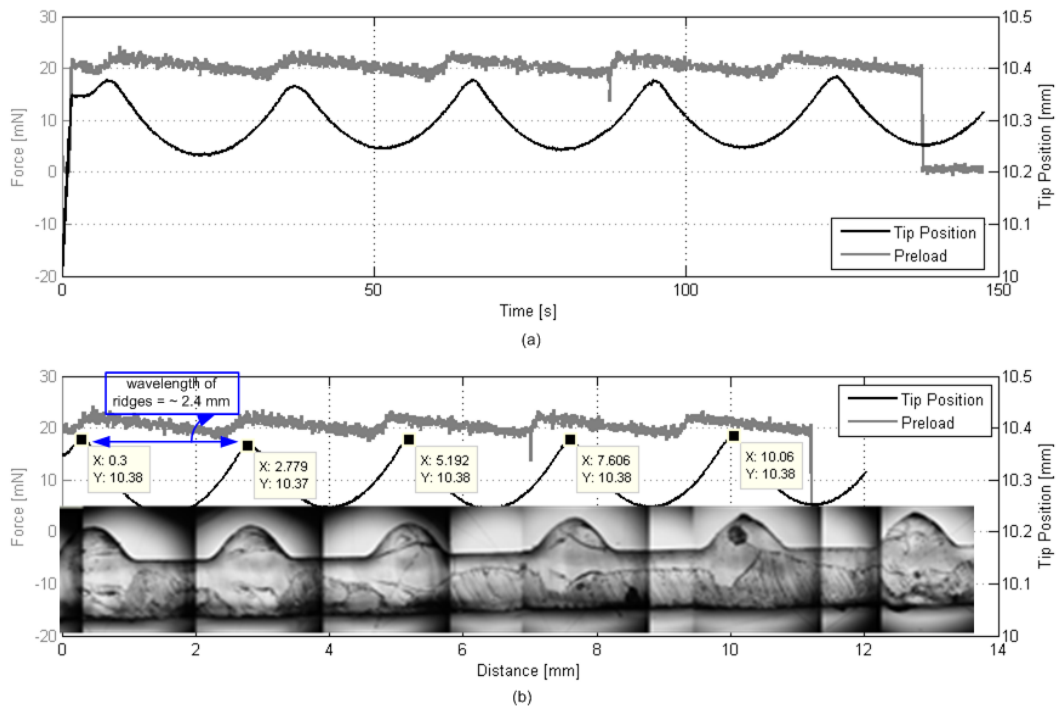
Figure 8.19 : The information of the sample scanned with 10 mm diameter glass tip and obtained in terms of the wavelength of the ridges for 20 mN preload at 0.09 mm/s sliding velocity; tip position and force vs. time graph (a), and tip position and force vs. distance graph (b).

Frequency results are obtained as follows;

- For V = 0.09 mm/s;

  f(expected) = V/λ = 0.09/2.4 = 0.03750 Hz → f(observed) = 0.03774 Hz
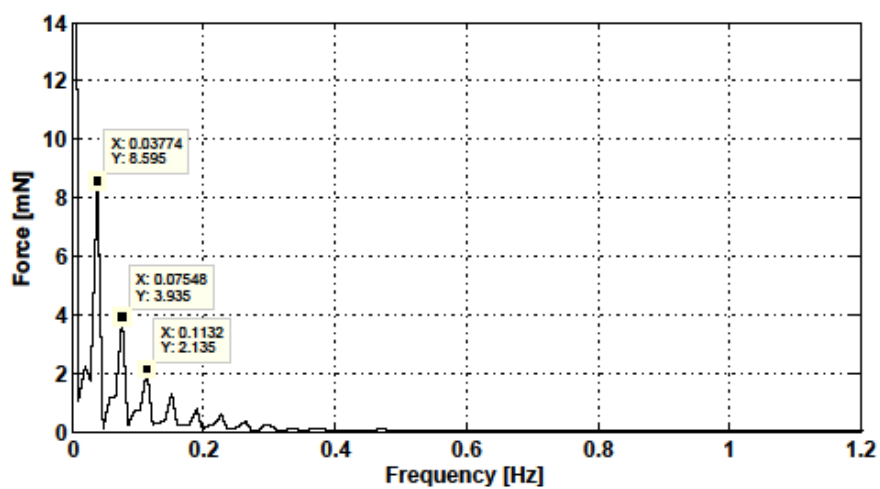
Figure 8.20 : Frequency result for 0.09 mm/s sliding velocity.

- For V = 0.15 mm/s;

  f(expected) = V/λ = 0.15/2.4 = 0.06250 Hz

  f(observed) = 0.06198 Hz
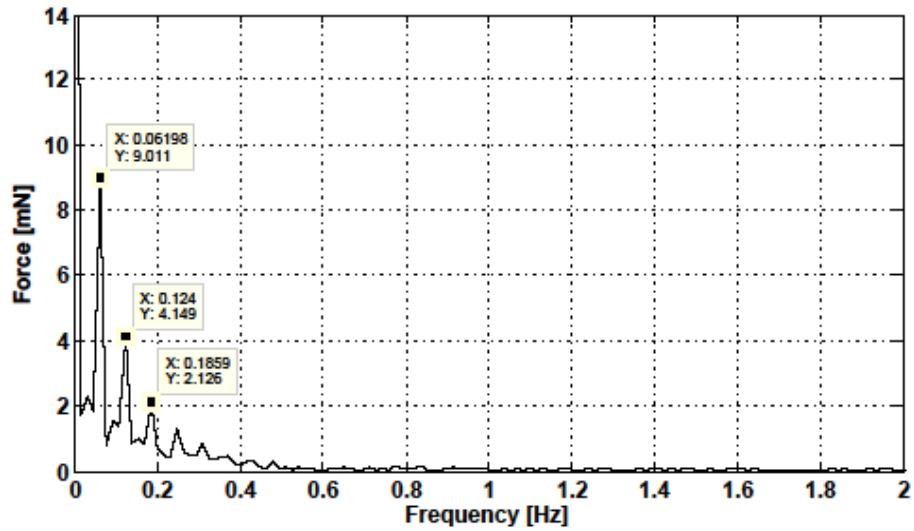
Figure 8.21 : Frequency result for 0.15 mm/s sliding velocity.

- For V = 0.26 mm/s;

  f(expected) = V/λ = 0.26/2.4 = 0.1083 Hz

  f(observed) = 0.1081 Hz
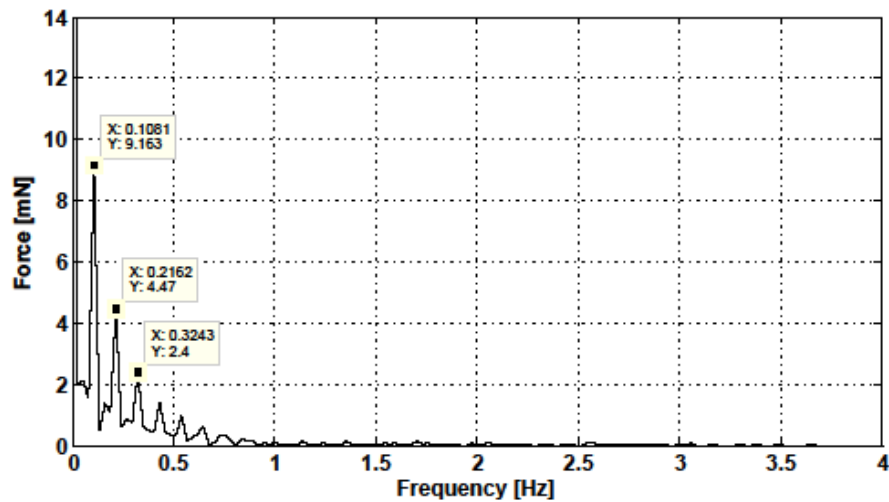
Figure 8.22 : Frequency result for 0.26 mm/s sliding velocity.

- For V = 0.34 mm/s;

  f(expected) = V/λ = 0.34/2.4 = 0.1417 Hz

  f(observed) = 0.1416 Hz
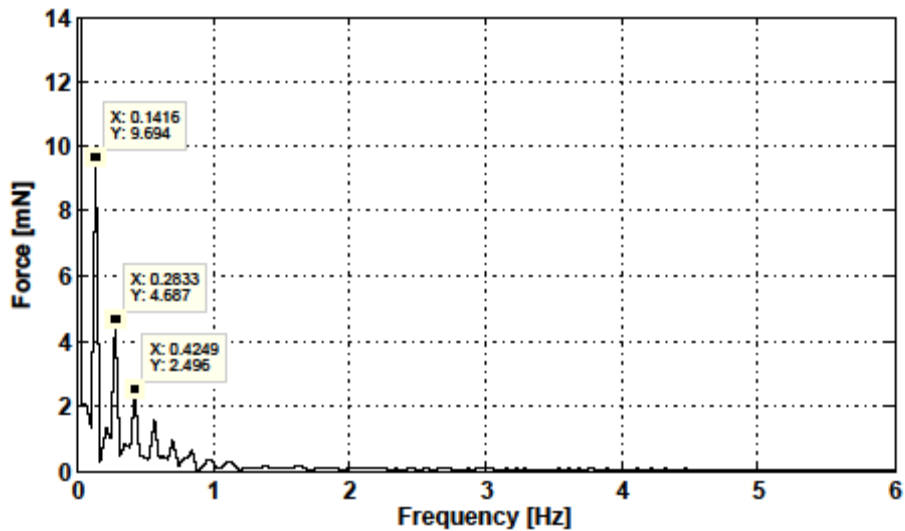
Figure 8.23 : Frequency result for 0.34 mm/s sliding velocity.

- For V = 0.49 mm/s;

  f(expected) = V/λ = 0.49/2.4 = 0.2042 Hz → f(observed) = 0.2049 Hz
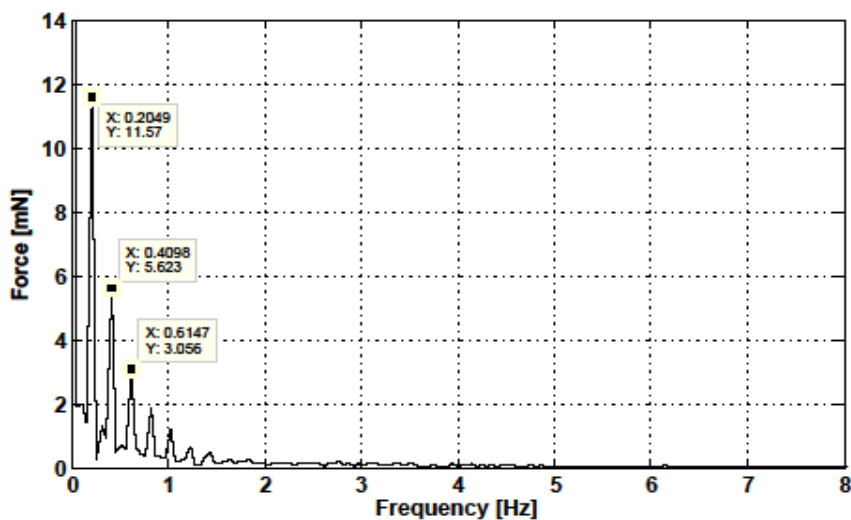
Figure 8.24 : Frequency result for 0.49 mm/s sliding velocity.

8.2.2 Effect of preload

Different preload values ranging from 5 mN to 35 mN are applied to the sample surface at a constant sliding velocity of 0.09 mm/s. As the preload increases, the values of preload errors decrease shown in Figure 8.25 and Table 8.5. In other words, the preload values are inversely proportional to the preload errors as the same effect is obtained on the previous case study. On the other hand, when the results shown in Table 8.2 are compared with the results shown in Table 8.5, it is clear that using a glass tip with larger diameter brings an advantage of reducing the preload error.
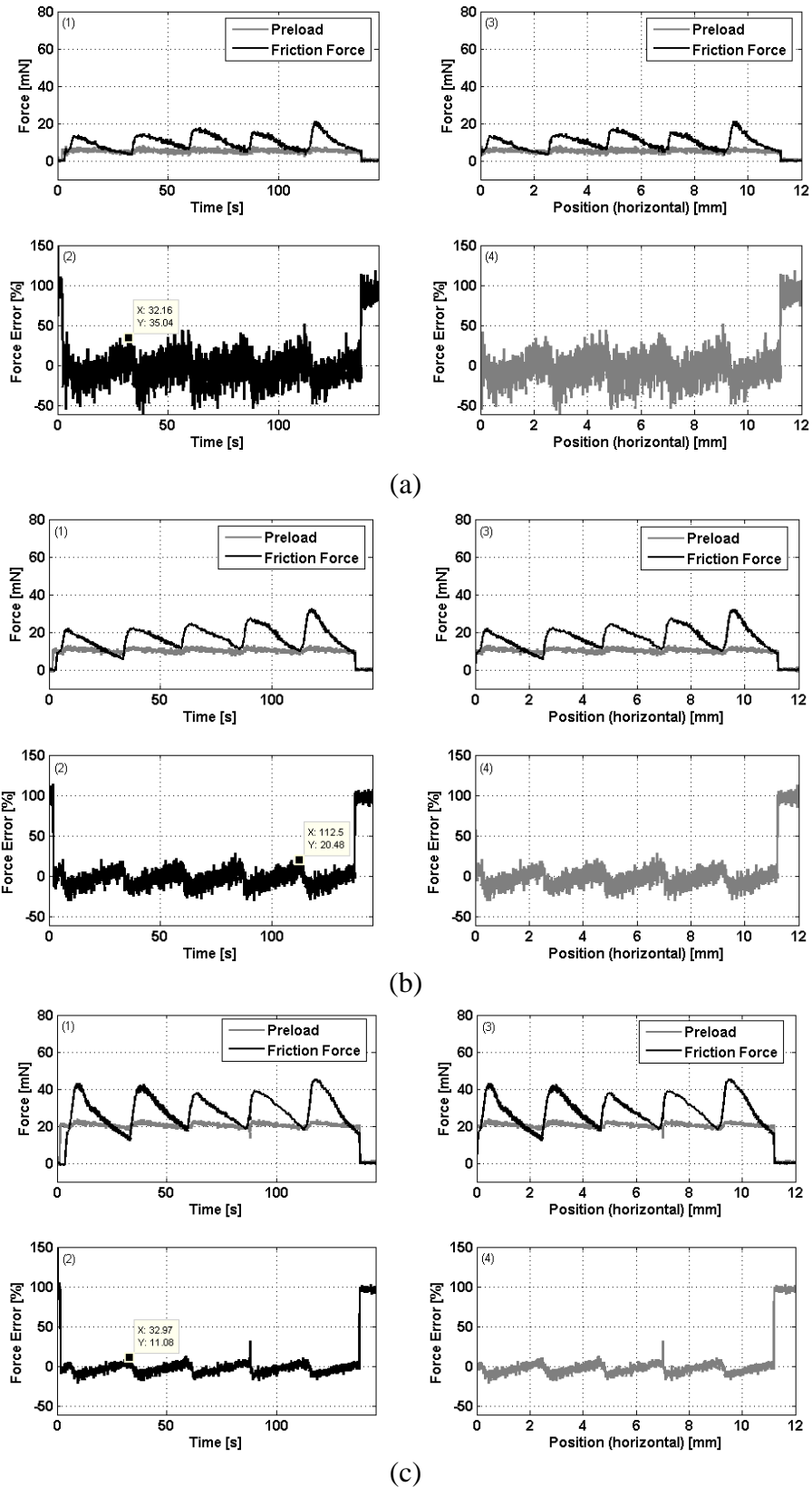
Figure 8.25 : Preload effect on pattern detection using 10 mm diameter glass tip at 0.09 mm/s sliding velocity under 5 mN (a), 10 mN (b), 20 mN (c), 25 mN (d), 30 mN (e), and 35 mN (f) preload by using force vs time graph (1), force error vs time graph (2), force vs displacement graph (3), force error vs displacement graph (4).

Figure 8.25 (continued): Preload effect on pattern detection using 10 mm diameter glass tip at 0.09 mm/s sliding velocity under 5 mN (a), 10 mN (b), 20 mN (c), 25 mN (d), 30 mN (e), and 35 mN (f) preload by using force vs time graph (1), force error vs time graph (2), force vs displacement graph (3), force error vs displacement graph (4).

82
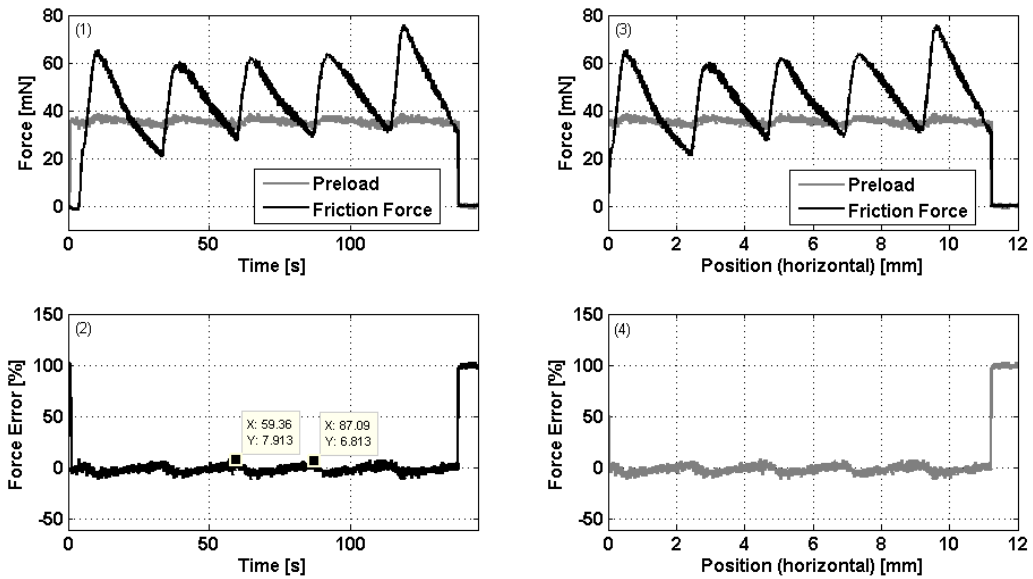
(f)

Figure 8.25 (continued): Preload effect on pattern detection using 10 mm diameter glass tip at 0.09 mm/s sliding velocity under 5 mN (a), 10 mN (b), 20 mN (c),   25 mN (d), 30 mN (e), and 35 mN (f) preload by using force vs time graph (1), force error vs time graph (2), force vs displacement graph (3), force error vs displacement graph (4).

The details about preload errors for the related preload values can be seen on the following Table 8.5.

Table 8.5 : Preload error during surface scanning with 10 mm diameter glass tip under different preload values at 0.09 mm/s sliding velocity.

Preload (mN)	Preload Error (%)
5	~ 35
10	~ 21
20	~ 11
25	~ 9
30	~ 9
35	~ 7

The results about frequency analysis of friction force data are exhibited by applying FFT. Since the tests about preload effects are realized at constant sliding velocity, 0.09 mm/s, the expected frequency value remains unchanged under different preload values. Nevertheless, when the graphs containing the FFT results are considered (Figure 8.26-31), the dominant frequencies with their harmonics belonging to the pattern are observed as they are expected. Meanwhile, the force amplitude of the frequencies increases with increasing the preload values.

Frequency results are obtained as follows;

- For P = 5 mN;

  f(expected) = V/λ = 0.09/2.4 = 0.03750 Hz

  f(observed) = 0.03745 Hz
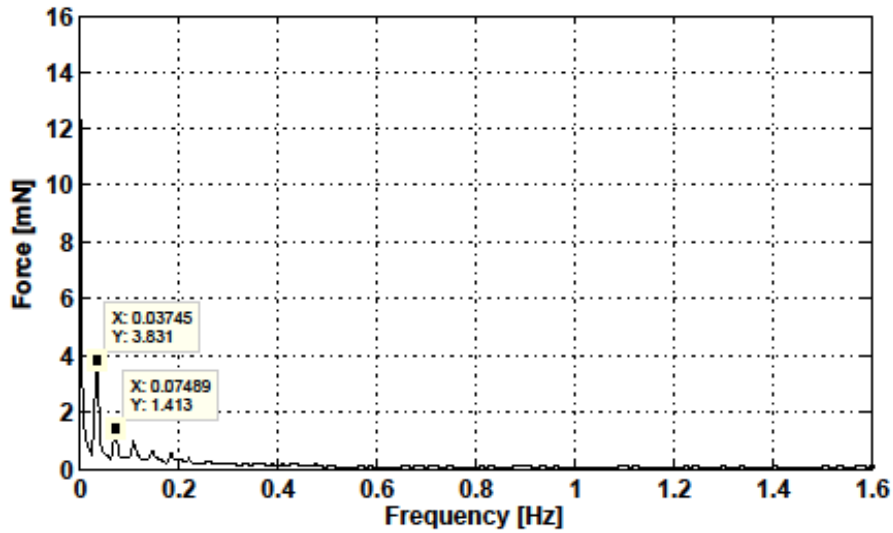
Figure 8.26 : Frequency result for 5 mN preload.

- For P = 10 mN;

  f(expected) = V/λ = 0.09/2.4 = 0.03750 Hz

  f(observed) = 0.03760 Hz
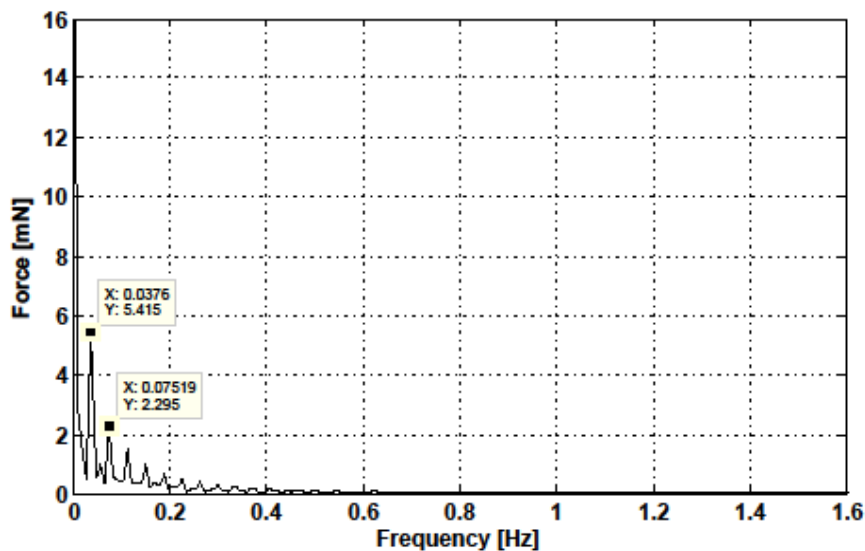
Figure 8.27 : Frequency result for 10 mN preload.

- For P = 20 mN;

  f(expected) = V/λ = 0.09/2.4 = 0.03750 Hz → f(observed) = 0.03774 Hz
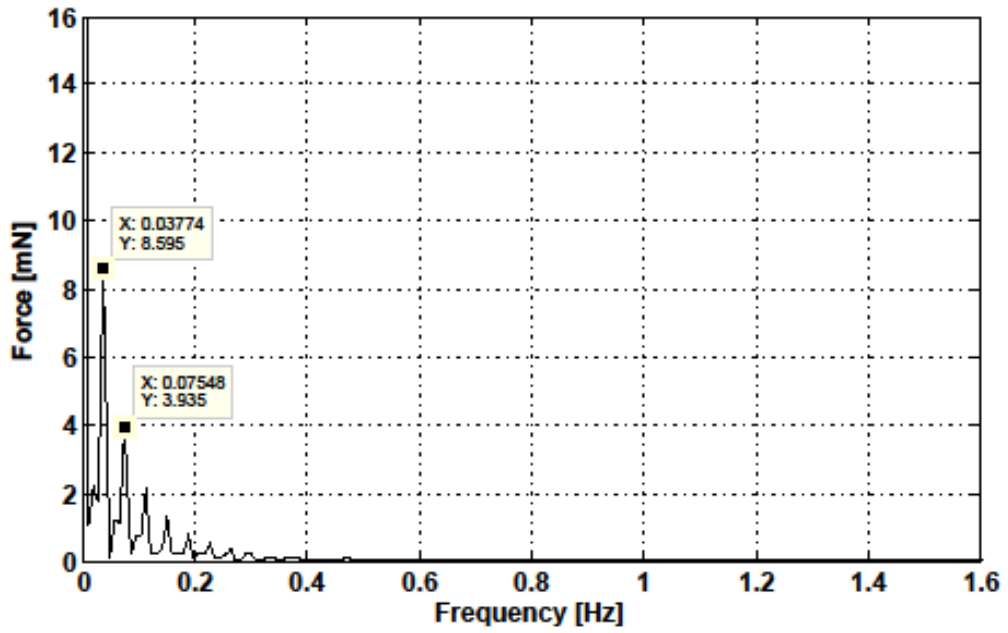
Figure 8.28 : Frequency result for 20 mN preload.

- For P = 25 mN;

  f(expected) = V/λ = 0.09/2.4 = 0.03750 Hz

  f(observed) = 0.03719 Hz
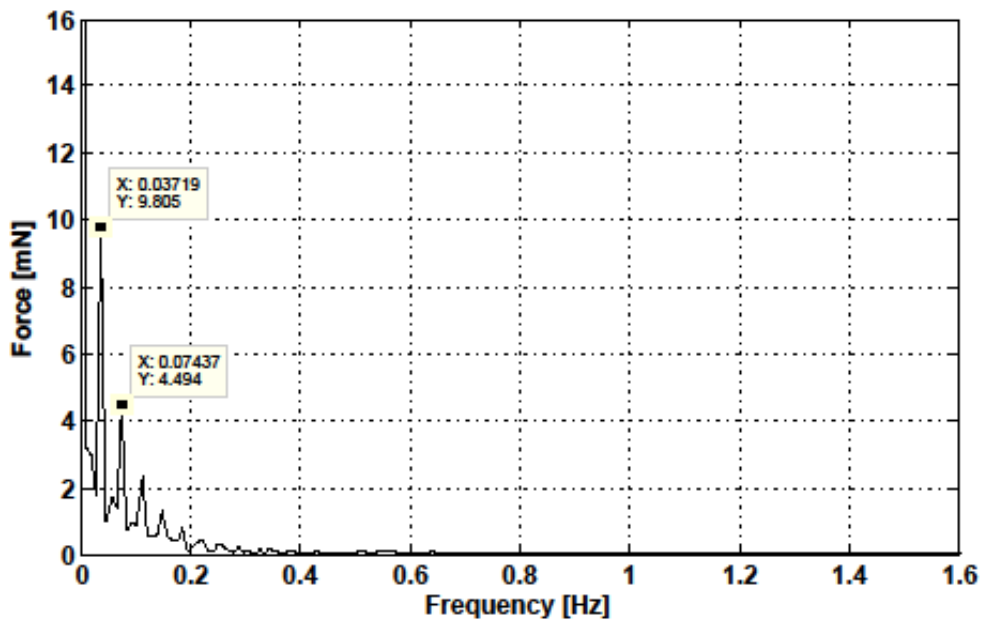
Figure 8.29 : Frequency result for 25 mN preload.

- For P = 30 mN;

  f(expected) = V/λ = 0.09/2.4 = 0.03750 Hz

  f(observed) = 0.03743 Hz
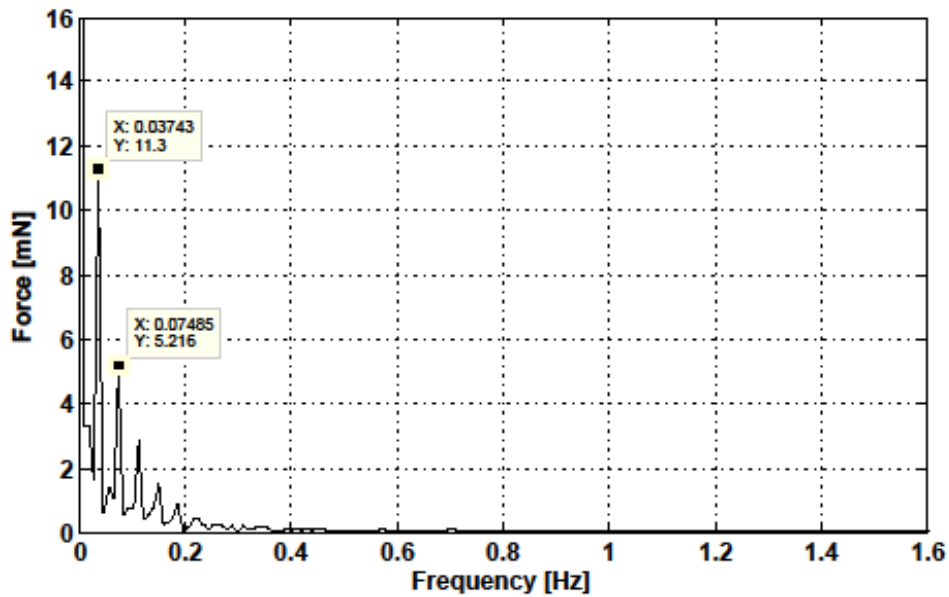
Figure 8.30 : Frequency result for 30 mN preload.

- For P = 35 mN;

  f(expected) = V/λ = 0.09/2.4 = 0.03750 Hz → f(observed) = 0.03739 Hz
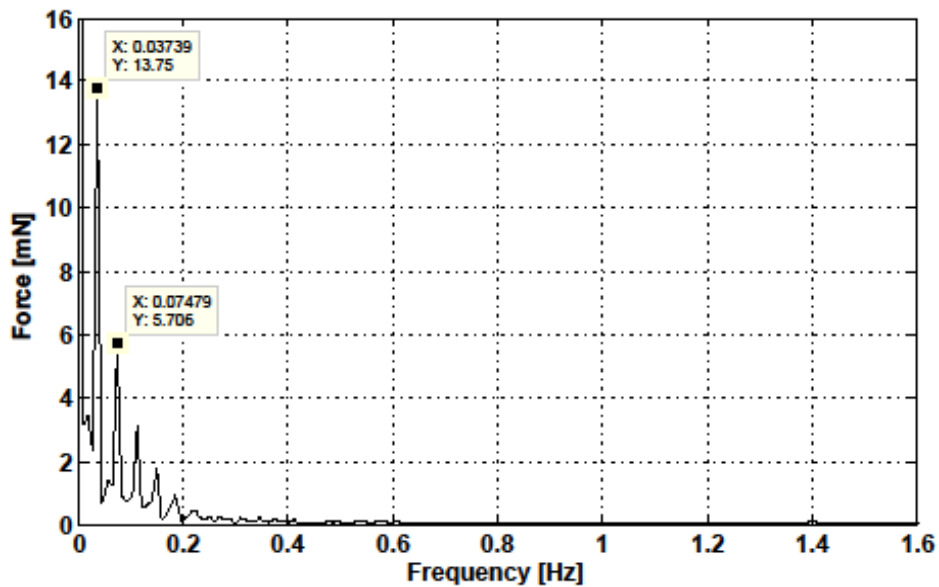
Figure 8.31 : Frequency result for 35 mN preload.

To summarize the results of the tests on this section of 8.2, the following statements are considered. As the sliding velocity increases in the range of 0.09-0.49 mm/s,

- preload errors increase from ~ 11 % to ~ 32 %,
- dominant frequency belonging to the pattern of the artificial skin shifts towards right,
- force amplitude of the dominant frequency increases.

86

As the preload applied to the sample surface increases in the range of 5-35 mN,

- preload errors reduce from ~ 35 % to ~ 7 %,
- expected frequencies with their relatively unchanged values are obtained,
- force amplitude of the dominant frequency increases.

Using a glass tip with a diameter of 10 mm allows

- reducing the preload errors for both sliding velocity and preload effects compared with the same results on the previous section,
- the tip to slide on the ridges of the artificial sample instead of travelling between them,
- obtaining the information about the wavelength of the ridges,
- the observed frequencies to be relatively same with the expected frequency values,
- observing harmonics of the signal although the tip slid on the ridges.

8.3 Frictional Results & Frequency Analysis Using Tip Diameter of 34.74 mm

In order to investigate the pattern detection and the frictional results of the artificial skin, the glass tip with a diameter of 34.74 mm is brought into contact with the sample as shown in Figure 8.32. Furthermore, using such a glass tip also allows to observe the tip diameter effect on pattern detection. The gathered friction force data is analyzed in both time domain and frequency domain. In addition, the related results are compared to the results obtained by using the glass tip with 10 mm diameter.

8.3.1 Effect of sliding velocity

The tests for sliding velocity effect on the pattern detection are realized by scanning the artificial surface with the 34.74 mm glass tip at 0.09 mm/s and 0.15 mm/s sliding velocity under 20 mN constant preload for a travel length of 12 mm amounts to five ridges. When the following frictional results shown in Figure 8.33 are compared with the previous case studies' results in sections 8.1 and 8.2, the tip diameter effect on reducing the preload error can be obviously seen. The values of these errors can be found on Table 8.6. In addition, it is also clear that sliding velocity has the same effect on the preload error. As the velocity increases, the preload errors increase as well.
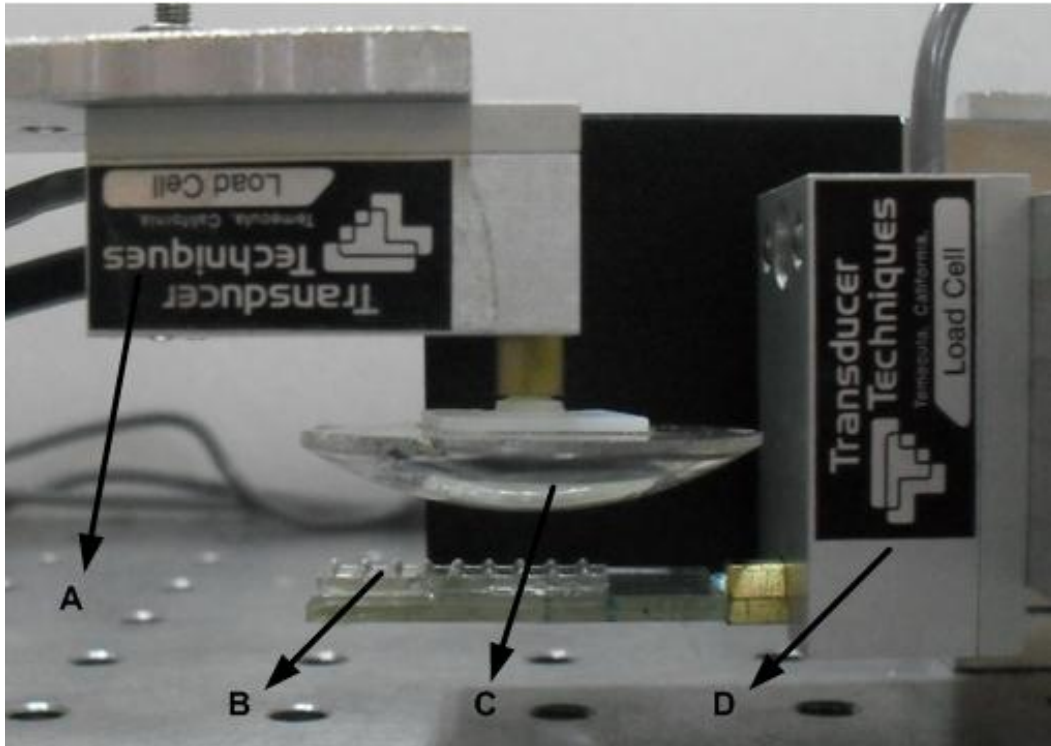
Figure 8.32 : A close-up picture of the experimental set-up; A: Loadcell 1 with 250 g capacity, B: Artificial skin with evenly distributed ridges, C: Glass tip with 34.74 mm diameter, D: Loadcell 2 with 100 g capacity.

(a)
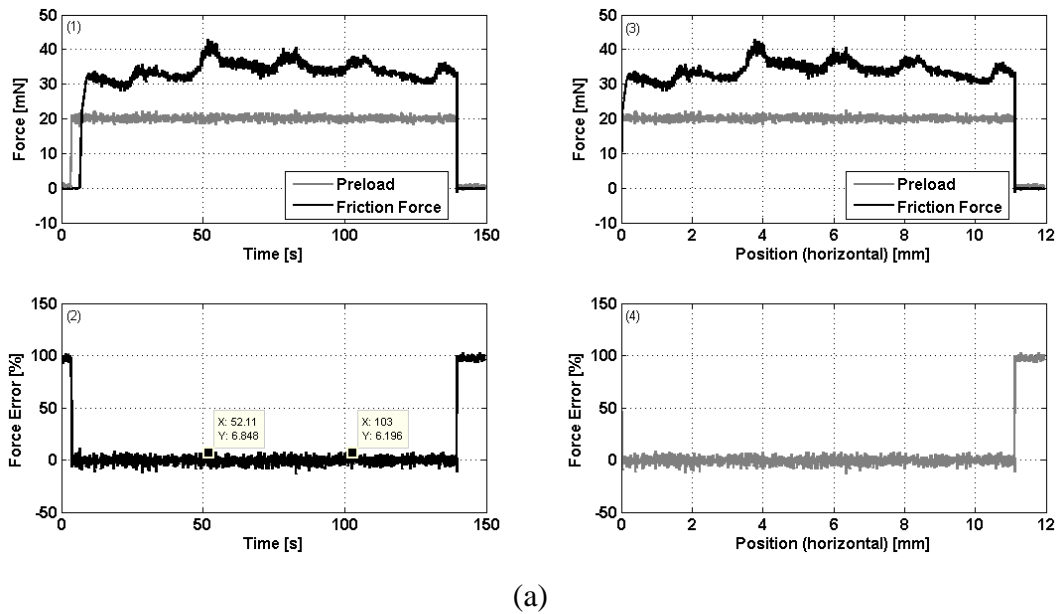
Figure 8.33 : Velocity effect on pattern detection using 34.74 mm diameter glass tip under 20 mN preload at 0.09 mm/s (a), and 0.15 mm/s (b) sliding velocity by using force vs time graph (1), force error vs time graph (2), force vs displacement graph (3), force error vs displacement graph (4).

(b)
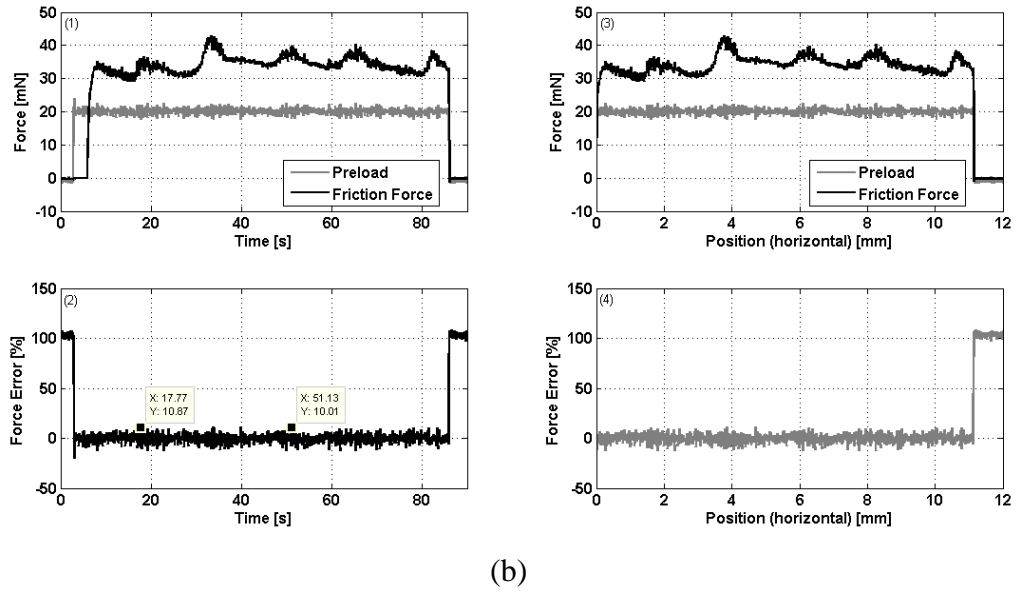
Figure 8.33 (continued): Velocity effect on pattern detection using 34.74 mm diameter glass tip under 20 mN preload at 0.09 mm/s (a), and 0.15 mm/s (b) sliding velocity by using force vs time graph (1), force error vs time graph (2), force vs displacement graph (3), force error vs displacement graph (4).

Table 8.6 : Preload error during surface scanning with 34.74 mm diameter glass tip at different sliding velocities under 20 mN preload.

Sliding Velocity (mm/s)	Preload Error (%)
0.09	~ 6-7
0.15	~ 10-11

Furthermore, when the artificial sample is rubbed against a 34.74 mm glass tip, the information about the wavelength of the ridges is obtained approximately as shown in Figure 8.34.

Friction force data is analyzed in frequency domain as well to obtain the frequency values belonging to the pattern. FFT results can be found in the Figures 8.35 and 8.36. The observed frequencies are close to the expected ones. As the velocity increases, the dominant frequency shifts towards right based on the relation of the Eq. 8.1. Furthermore, scanning the artificial skin with a larger diameter glass tip allows to obtain an important approach for filtering the harmonics of the signal. In other words, using a glass tip with larger diameter such as 34.74 mm results to observe a filter effect on the harmonics of the signal as shown in the following Figures 8.35-8.38.
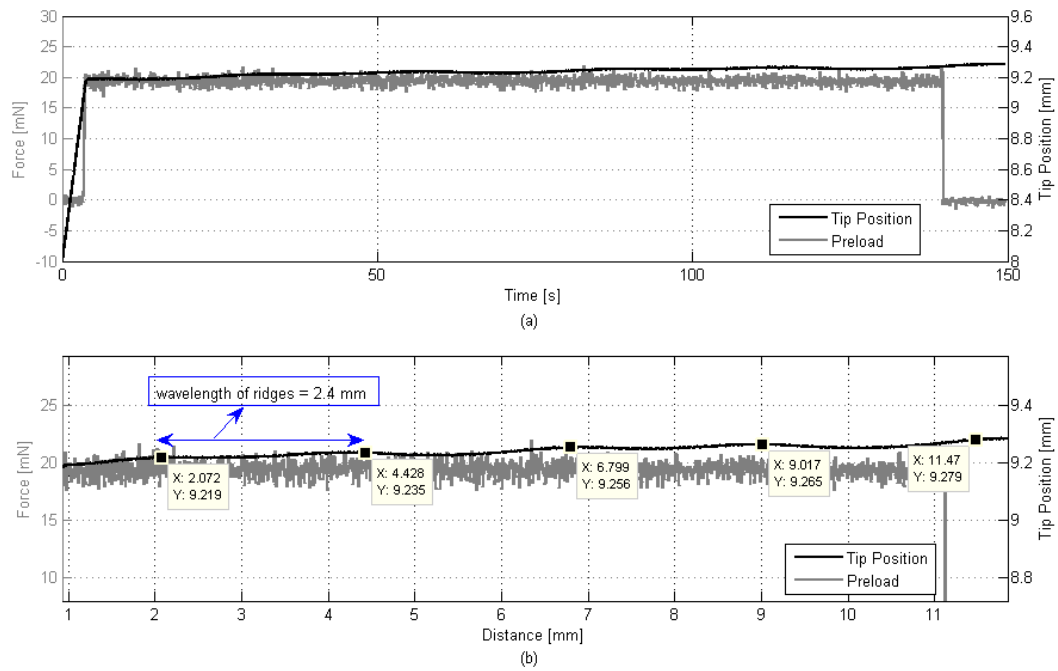
Figure 8.34 : The information of the sample scanned with 34.74 mm diameter glass tip and obtained in terms of the wavelength of the ridges for 20 mN preload at 0.09 mm/s sliding velocity; tip position and force vs. time graph (a), and tip position and force vs. distance graph (b).

Frequency results are obtained as follows;

- For V = 0.09 mm/s;

  f(expected) = V/λ = 0.09/2.4 = 0.03750 Hz

  f(observed) = 0.03942 Hz
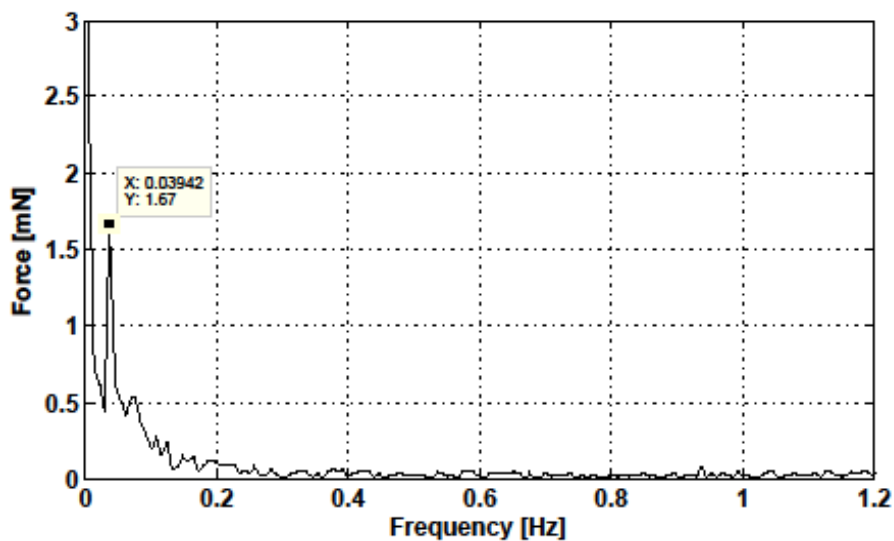
Figure 8.35 : Frequency result for 0.09 mm/s sliding velocity.

- For V = 0.15 mm/s;

  f(expected) = V/λ = 0.15/2.4 = 0.06250 Hz

  f(observed) = 0.06565 Hz
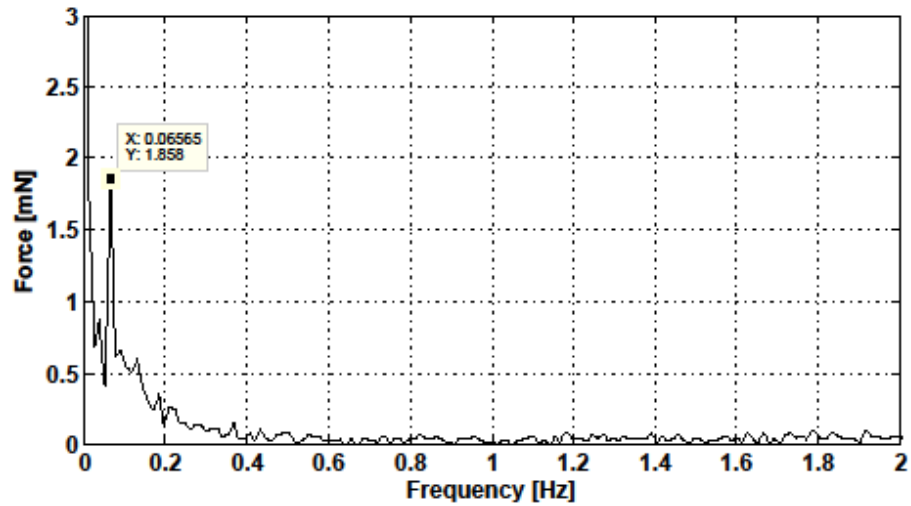
Figure 8.36 : Frequency result for 0.15 mm/s sliding velocity.

In order to emphasize the mentioned filter effect clearly, some tests' results are compared with each other. The comparison is realized under the same working conditions such that 20 mN constant preload is applied on the sample at different sliding velocities, 0.09 mm/s and 0.15 mm/s, during a 12 mm travel length. The comparative frequency results contain the results obtained by using a 34.74 mm and 10 mm diameter glass tip as shown in Figures 8.37 and 8.38. It is clear that using a glass tip with larger diameter allows to filter the harmonics of the signal.
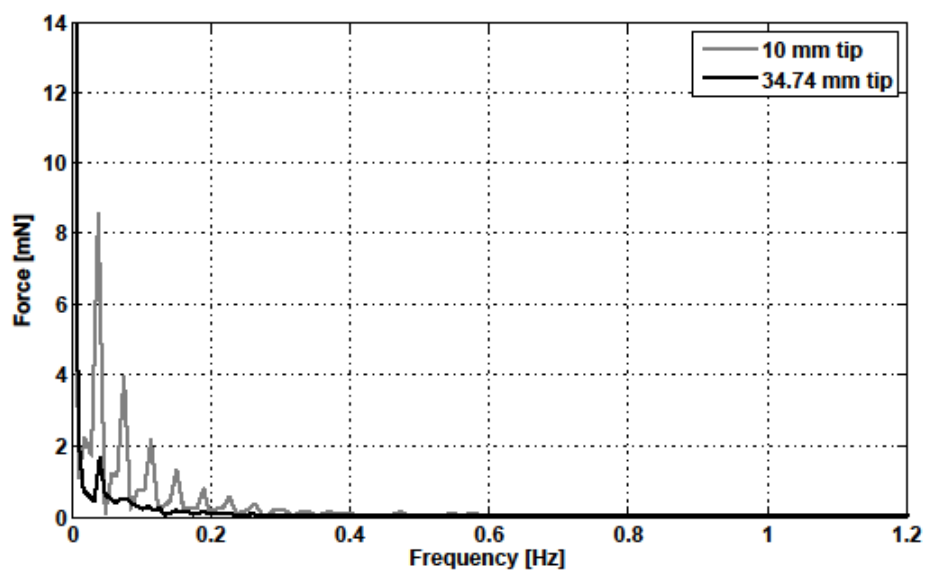
Figure 8.37 : Frequency results at 0.09 mm/s sliding velocity
under 20 mN preload for two different glass tips.
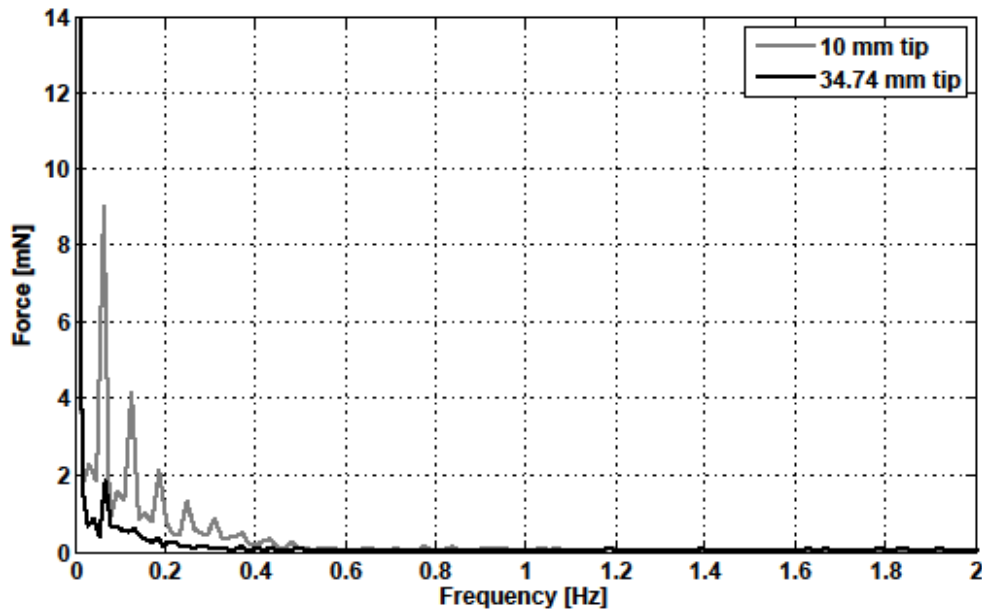
Figure 8.38 : Frequency results at 0.15 mm/s sliding velocity
under 20 mN preload for two different glass tips.

To summarize the results of the tests on this section of 8.3, the following statements
are considered. As the sliding velocity increases,

- preload errors increase from ~ 6-7 % to ~ 10-11 %,
- dominant frequency belonging to the pattern of the artificial skin shifts towards right,
- force amplitude of the dominant frequency increases.

Using a glass tip with a diameter of 34.74 mm allows

- reducing the preload errors compared with the same results on the previous sections,
- the observed frequencies to be relatively same with the expected frequency values,
- filtering harmonics of the signal,
- the tip to slide on the ridges of the artificial sample instead of travelling between them,
- obtaining the information about the wavelength of the ridges.

9. CONCLUSIONS AND RECOMMENDATIONS

Tactile properties of human skin attract researchers' attention, and become an inspiration source to emulate the human sense of touch by producing artificial surfaces. Studies related on the artifacts also allow scientists to comprehend how the process works to acquire tactile sensation, and to improve applications in the fields of robotics with an autonomously surface detection task or surgical task, medicine, fabrics, and cosmetics.

This study exhibits an approach of pattern detection on the artificially made surface based on friction induced vibrations under different design parameters such as sliding velocity, preload, and tip diameter. First of all, custom built semi-autonomous friction-adhesion set-up is designed. Then, artificial surfaces are produced by using soft polymer PDMS. One of them is fabricated as flat sample. The other one is a human-inspired artificial surface with evenly spaced parallel ridges. The dimensions of the designed artifact are such that the diameter of the ridges and the space between the ridges are 1 mm and 1.4 mm, respectively. Peak-to-peak value of two ridges called wavelength is 2.4 mm. The validation of the experimental system is realized using flat PDMS as a control sample, rubbed against a rigid glass tip.

Meanwhile, for constant preload during surface scanning three different force-feedback controllers, PID, Adaptive PID, and SMC, are designed and examined by using both flat PDMS and artificially made sample with evenly distributed ridges. In the first case study, tests are realized under 23 mN constant preload applied to flat PDMS sample which is rubbed against a 6 mm diameter rigid glass tip at 0.15 mm/s sliding velocity. The travel length is approximately 8 mm. During surface sliding, preload remains constant on flat PDMS with approximately 2 %, and 1.5-2 % error values by using PID, and Adaptive PID Controllers, respectively. On the other hand, the preload error is reduced by SMC on approximately 1-1.5 % levels. In the second case study, tests are realized under 20 mN constant preload applied to artificial sample which is rubbed against a 1 mm diameter rigid glass tip at 0.09 mm/s sliding velocity. The travel length is approximately 12 mm amounts to five ridges. Although

appropriate coefficients of PID controller are chosen to give the system fast responses, and deal with the steady-state error, the results showed that the preload does not remain constant. The force error is approximately 80 %. By using adaptive PID, and SMC, the preload is kept constant with ~ 40 %, and 16 % error, respectively. The comparative outcomes indicated that using SMC allowed performing the experiments under constant preload with a minimum percentage of error.

Then, to obtain appropriate working conditions such as travel interval, sliding velocity and preload, some tests are realized. Thus, the occurrence circumstances of stick-slip oscillations and steady sliding between soft polymer and rigid surface are analyzed. As it mentioned before that in contrast to hard materials, stick-slip occurs under high sliding velocity and high contact load, or under low sliding velocity and low contact load in soft materials. Steady sliding is observed under low sliding velocity and high contact load. The tests for stick-slip topic are carried out using flat PDMS as a control sample which is rubbed against a hemispherical glass tip with 6 mm diameter. The experiments show that the stick-slip oscillations are observed under 10 mN preload at 0.02 mm/s sliding velocity. The period of these oscillations is approximately 2.3 s which results in expecting a dominant frequency at 0.43 Hz. In addition, the preload effect on the stick-slip is examined by using various preload values ranging from 10 mN to 110 mN at 0.02 mm/s sliding velocity. Increasing the preload results in obtaining steady-sliding. In other words, transition from stick-slip to steady-sliding is obtained by increasing the preload. The tests for sliding velocity effect on the stick-slip are realized by increasing the velocity values from 0.02 mm/s to 0.5 mm/s under 10 mN constant preload for a duration of 15 s. According to the tests, increasing the sliding velocity results in decreasing the amplitude of the stick-slip effects while they oscillate in the same range of friction force. In addition, increasing the velocity causes to decrease the time spent for transition from the static friction to the kinetic friction which can be observed by the increase of the graphs' slopes. As a result, all of the tests about pattern detection are realized outside of these working conditions about stick-slip effects. In other words, the tests are realized on the steady-sliding region.

Therefore, effects of different design parameters such as sliding velocity, preload and tip diameter on pattern detection and friction are investigated by using the artificial

skin. The tests for sliding velocity effect on the pattern detection are realized by increasing the velocity values from 0.09 mm/s to 0.49 mm/s under 20 mN constant preload for a travel length of 12 mm. During the dynamic contact between the artificial surface and the rigid glass tip, different preload values in the range of 5-35 mN are also applied on the surface at 0.09 mm/s constant sliding velocity to observe the preload effect on pattern detection. To observe the tip diameter effect on pattern detection, three glass tips with different diameter sizes such as 1 mm, 10 mm, and 34.74 mm are used. According to the results of the tests, the preload remains consistent with a minimum percentage of error at low sliding velocity and under high preload value as explained below.

Using a glass tip with a diameter of 1 mm allowed the tip to travel between the ridges of the artificial skin. Therefore, the information of this sample about the height and wavelength of the ridges is obtained. In other words, the profile of the sample is obtained. As the preload applied to the sample surface increases in the range of 5-35 mN, preload errors decrease from ~ 70 % to ~ 8 %. As the sliding velocity increases in the range of 0.09-0.49 mm/s, preload errors increase from ~ 16 % to ~ 55 %, and the dominant frequency belonging to the pattern of the artificial skin shifts towards right. Meanwhile, the observed frequencies are relatively same with the expected frequency values. Due to the fact that the tip travels between the ridges, harmonics of the signal are also observed.

When the artificial sample is detected by the glass tip with a 10 mm diameter, the values of preload errors are reduced for both sliding velocity and preload effects compared with the same results on the previous case study. As the preload applied to the sample surface increases in the range of 5-35 mN, preload errors diminish from ~ 35 % to ~ 7 %. According to the tests for sliding velocity effect, the preload errors increase in the range of ~ 11-32 % with increasing the velocity. Dominant frequency, which is relatively same with the expected frequency values and belonging to the pattern of the artificial skin, shifts towards right as the velocity increases. Because of the fact that the tip slides on the ridges of the artificial sample instead of travelling between them, only the information about the wavelength of the ridges is obtained, and harmonics of the signal are observed as well. Consequently, the results indicate that using large diameter of tip allows decreasing the preload errors.

Furthermore, to observe the tip diameter effect on pattern detection more closely, the artificial skin is rubbed against a 34.74 mm diameter glass tip at 0.09 mm/s and 0.15 mm/s sliding velocity under 20 mN constant preload for a travel length of 12 mm. As the sliding velocity increases, preload errors increase from ~ 6-7 % to ~ 10-11 %. If the values of the errors are compared with the errors gathered by using the 1 mm, and 10 mm diameter glass tips, the errors diminish. In addition, according to the frequency analysis of the friction force data, the dominant frequency belonging to the pattern is obtained, and the harmonics of the signal are filtered. Thus, the tip diameter effect on reducing the preload error and filtering the harmonics of the signal is observed clearly.

In consequence of this study, it is obtained that the investigations of the friction induced vibrations occurred during the dynamic contact of surface scanning between the artificial surface and the rigid glass tip allowed to detect the frequency belonging to the pattern of the artificial skin, and carrying the information of the scanned surface like height and wavelength of ridges while the preload applied to the surface is kept constant during sliding by the force-feedback controller.

It is stated before that tactile properties of human skin are an inspiration source to mimic the human sense of touch by producing various artificial surfaces. Working with such artifacts rubbed against a glass tip allows scientists to understand the steps from contacting the surfaces to detecting their pattern more closely. In this study, some parameters related to sample are kept constant such as the dimensions of the artificial skin, the shape of the ridges, and the type of the polymer. Meanwhile, different glass tips in various diameter sizes are examined. Thus, in order to observe the effect of the sample dimension and the shape of the ridges on pattern detection, the artifact could be designed on various size and shape.

In addition, the artificial skin could be fabricated by using various type of polymer different from the silicone elastomer called PDMS. This effect might be investigated on both pattern detection and frictional properties between the sample and tip.

On the other hand, not only the artifacts but also fabrics might be used. Therefore, as a next case study, the pattern detection on fabrics scanned with such a glass tip that the radius of tip curvature is close to that of the human fingertip could be carried out. If the approach of pattern detection based on friction induced vibrations is applied to

the friction force data, it can be examined that by using this kind of glass tip the pattern of the fabric will be detected or not. This application will carry the clues about surface discriminate mechanism of humans.

REFERENCES

[1] **Prevost, A., Scheibert, J., and Debrgeas, G.** (2009). Effect of fingerprints orientation on skin vibrations during tactile exploration of textured surfaces, *Commun Integr. Biol 2*, No. 5, pp 422-424.

[2] **Mascaro, S., and Asada, H. H.** (2001). Finger posture and shear force measurement using fingernail sensors: initial experimentation,. *Proc.2001 ICRA IEEE Int. Conference on Robotics and Automation,* May 21-26, Seoul, Korea.

[3] **Lederman, S. J., & Jones, L. A.** (2006). *Human Hand Function,* Oxford University Press, New York.

[4] **Scheibert, J., Leurent, S., and Prevost, A.** (2009). The Role of Fingerprint in the Coding of Tactile Information Probed with a Biomimetic Sensor, *Science,* Vol.**23**, pp. 1503-1506.

[5] **Dargahi, J., and Najarian, S.** (2004). Human tactile perception as a standard for artificial tactile sensing-a review, *Int.J.Medical Robotics and Computer Assisted Surgery*, Vol. **1**, pp. 23-35.

[6] **Mukaibo, Y., Shirado, H., Konyo, M., and Maeno, T.** (2005). Development of a texture sensor emulating the tissue structure and perceptual mechanism of human fingers, *International Conf. on Robotics and Automation,* April, Barcelona, Spain.

[7] **Horiuchi, K., & Nakano, K.** (2007). Sliding Test by Using an Apparatus Imitating a Human Finger for Estimating the Tactile Sensation of Cosmetic Foundation. *Journal of Advanced Mechanical Design, Systems, and Manufacturing*, Vol.**1**, No.5, pp. 726-736.

[8] **Shao, F., Childs, T., and Henson, B.** (2009). Developing an artificial fingertip with human friction properties, *Tribology International,* Vol.**42**, No.11-12, pp 1575-1581.

[9] **Wandersman, E., Candelier, R., Debrégeas, G., and Prevost, A.** (2011). Texture-Induced Modulations of Friction Force: The Fingerprint Effect. *Physical Review Letters*, Vol.**107**, No.16, pp. 1-5.

[10] **Candelier, R., Prevost, A., and Debrgeas, G.** (2011). The Role of Exploratory Conditions in Bio-Inspired Tactile Sensing of Single Topogical Features. *Sensors (Peterborough, NH)*, pp. 7934-7953.

[11] **Ramkumar, S. S., Wood D. J., Fox K., and Harlock S.** (2003). Developing a polymeric human finger sensor to study the frictional properties of textiles: Part I: Artificial finger development. *Textile Research Journal*, Vol.**73**, No.6, pp. 469-473.

[12] **Ramkumar, S. S., Wood D. J., Fox K., and Harlock S.** (2003). Developing a polymeric human finger sensor to study the frictional properties of

textiles: Part I: Experimental results. *Textile Research Journal*, Vol.**73**, pp. 606-610.

[13] **Oddo, C. M., Beccai, L., Felder, M., Giovacchini, F., and Carrozza, M. C.** (2009). Artificial Roughness Encoding with a Bio-inspired MEMS-based Tactile Sensor Array. *Sensors*, Vol.**9**, No.5.

[14] **Zhang, Y., & Miki.** (2010). Sensitivity enhancement of a micro-scale biomimetic tactile sensor with epidermal ridges. *Journal of Micromechanics and Microengineering*, Vol.**20**, No. 129801, pp. 1-7.

[15] **Hidaka, Y., Shiokawa, Y., Tashiro, K., Maeno, T., Konyo, M., and Yamauchi, T.** (2009). Development of an elastic tactile sensor emulating human fingers for tele-presentation systems, *IEEE,* pp. 1919-1922.

[16] **Fagiani, R., Massi, F., Chatelet, E., Berthier, Y., Sesieri, A., and Akay, A.** (2011). Tactile perception by friction induced vibrations, *Tribology International,* Vol.**44**, pp 1100-1110.

[17] **Fagiani, R., Massi, F., Chatelet, E., Berthier, Y., and Sesieri, A.** (2010). Experimental analysis of friction-induced vibrations at the finger contact surface*, Proc. IMechE PartJ: J. Engineering Tribology,* Vol.**224**, No.722, pp 1-9.

[18] **Johansson, R.S., & Flanagan, J. R.** (2009). Coding and use of tactile signals from the fingertips in object manipulation tasks. *Nature Reviews Neuroscience*, Vol.**10**, No.5, pp.345–359.

[19] **Blake, D. T., Hsiao, S. S., and Johnson, K. O.** (1997). Neural coding mechanisms in tactile pattern recognition: the relative contributions of slowly and rapidly adapting mechanoreceptors to perceived roughness. *The Journal of neuroscience: the official journal of the Society for Neuroscience*, Vol.**17**, No.19, pp.7480-9.

[20] **Lederman, S., Loomis, J., and Williams, D.** (1982). The role of vibration in the tactual perception of roughness. *Psychonomic Society, Perception & Psychophysics*, Vol.**32**, No.2, pp. 109-116.

[21] **Derler, S., Gerhardt, L. C., Lenz, A., Bertaux, E., and Hadad, M.** (2009). Friction of human skin against smooth and rough glass as a function of the contact pressure. *Tribology International*, Vol.**42**, pp. 1565-1574.

[22] **Johnson, K. O.** (2001). The roles and functions of cutaneous mechanoreceptors. *Current opinion in neurobiology*, Vol.**11**, No.4, pp. 455-61.

[23] **Maegawa, S., & Nakano, K.** (2008). Occurrence of Stick-Slip and Schallamach Waves in Sliding between Hard and Soft Surfaces, *2nd Int. Conference on Advanced Tribology,*, December, Singapore.

[24] **Mate, C. M., & Carpick, R. W.** (2011). A sense for touch. *Materials Science*, Vol.**480**, pp.189-190.

[25] **Dahiya, R. S, & Gori, M.** (2010). Probing With and Into Fingerprints. *Journal of Neurophysiology*, Vol.**104**, pp.1-3.

[26] **Wettels, N., Popovic, D., Santos, V. J., and Loeb, G. E.** (2007). Biomimetic Tactile Sensor for Control of Grip. *2007 IEEE 10th International Conference on Rehabilitation Robotics*, Vol. **c**, pp. 923-932.

[27] **Wettels, N., Santos, V. J., Johansson, R. S., and Loeb, G. E.** (2008). Biomimetic Tactile Sensor Array. *Advanced Robotics*, Vol.**22**, No.8, pp 829-849.

[28] **Nakano, K.** (2007). A sense for touch. *Nature*.

[29] **Westling, G., and Johannson, R. S.** (1984). Factors influencing the force control during precision grip, *Exp. Brain Res.,* Vol.**53**, p-p.277-284.

[30] **Dahiya, R.S., Metta, G., Valle, M., and Sandini, G.** (2010). Tactile Sensing - From Humans to Humanoids. *Robotics, IEEE Transactions on*, Vol.**26**, No.1, pp. 1–20.

[31] **Maheshwari, V., and Saraf, R.** (2008). Tactile devices to sense touch on a par with a human finger. *Angewandte Chemie (International ed. in English)*, Vol.**47**, No.41, pp. 7808-26.

[32] **Shirado, H., and Maeno, T.** (2004). The Relationship between texture and the tactile sense. *Proc. JSME Robotics and Mechatronics Conference,* 1A1-H-33.

[33] **Kandel, E.R., Schwartz, J.H., and Jessell T.M.** (2000). Principles of Science, McGraw-Hill Companies, Inc. 4th edition.

[34] **Akay, A.** (2002). Acoustics of friction. *The Journal of the Acoustical Society of America,* Vol.**111**, No.4, pp. 1525-1548.

[35] **Bae, J. H., Arimoto, S., Yoshida, M., and Ozawa, R.** (2005). Generation of fingering motions by robotic fingers using morphological characteristics of human thumb. *2005 IEEE/RSJ Int. Conf. on Intelligent Robots and Systems,* pp. 1677-1683.

[36] **Xydas, N.** (1999). Modelling of Contact Mechanics and Friction Limit Surfaces for Soft Fingers in Robotics with Experimental Results. *The Int. Journal of Robotics Research,* Vol.**18**, pp. 941-950.

[37] **Cabibihan, J. J., Pattofatto, S., Jomaa, M., Benallal, A., and Carrozza, M. C.** (2008). Towards Human-like Social Touch for Sociable Robotics and Prosthetics: Comparisons on the Compliance, Conformance and Hysteresis of Synthetic and Human Fingertip Skins. *Int. Journal of Social Robotics,* Vol.**1**, pp. 29-40.

[38] **Buehler, B.** (2006). Molecular Adhesion and Friction at Elastomer/Polymer Interfaces. *PhD Thesis*, pp. 1-256.

[39] **Amontons, G.** (1699). De la resistance casu'eke danes logomachines, *Memories de l'Academie Royale*, Vol.**5**, pp.257-282.

[40] **Bowden, F., and Tabor, D.** (1964). The friction and lubrication of solids. *Int. series of monographs on physics*, No.2.

[41] **Galliano, A., Bistac, S., and Schultz, J.** (2003). Adhesion and friction of PDMS networks: molecular weight effects. *Journal of Colloid and Interface Science*, Vol.**265**, pp. 372-379.

[42] **Tabor, D.** (1977). Surface forces and surface interactions. *Journal of Colloid and Interface Science*, Vol.**58**, pp. 2-13.

[43] **Ebenstein, D. M., and Wahl, K. J.** (2006). A comparison of JKR-based methods to analyze quasi-static and dynamic indentation force curves. *Journal of Colloid and Interface Science*, Vol. **298**, pp. 652-662.

[44] **Achanta, S., Liskiewicz, T., Drees, D., and Celis, J. –P.** (2009). Friction mechanisms at the micro-scale, *Tribology Int.*, Vol. **42**, pp. 1792-1799.

[45] **Vaenkatesan, V., Li, Z., Vellinga, W. P., Jeu, W. H.** (2006). Adhesion and friction behaviours of polydimethylsiloxane − A fresh perspective on JKR measurements. *Polymer*, Vol. **47**, pp. 8317-8325.

[46] **Maegawa, S., and Nakano, K.** (2007). Dynamic Behaviours of Contact Surfaces in the Sliding Friction of a Soft Material. *Journal of Advanced Mechanical Design, Systems, and Manufacturing*, Vol. **1**, No. 4, pp. 553-561.

[47] **Maegawa, S., and Nakano, K.** (2010). Mechanism of stick-slip associated with Schallamach Waves, *Elsevire Wear*, Vol. **268**, pp. 924-930.

[48] **Rand, C.** (2008). The frictional response of patterned soft polymer surfaces, PhD Thesis, pp.1-111.

[49] **Tang, W., Ge, S.-rong, Zhu, H., Cao, X.-chuan, and Li, N.** (2008). The influence of normal load and sliding speed on frictional properties of skin. *Journal of Bionic Engineering*, Vol.**5**, No.1, pp. 33–38.

[50] **Url-1** <*http://www.newport.com/MFA-Series-Miniature-Steel-Linear-Stages/300762/1033/info.aspx*>, date retrieved 21.08.2009

[51] **Sümer, B., Onal, C., Aksak, B., and Sitti, M.** (2010). An experimental analysis of elliptical adhesive contact. *Journal of Applied Physics*, Vol.**107**, No.11, pp. 113512-1-113512-7.

[52] **Ogata, K.** (1997). Modern Control Engineering, Prentice-Hall, Inc. 3rd edition.

[53] **Tomizuka, M., and Isaka, S.** (1993). Fuzzy gain scheduling of PID controllers. *IEEE Transactions on Systems, Man, and Cybernetics,* Vol.**23**, No.5, pp. 1392-1398.

[54] **Slotine, J.-J., and Li, W.** (1991). Applied Nonlinear Control, Prentice-Hall, Inc.

[55] **Url-2** <*http://en.wikipedia.org/wiki/Adaptive_control*>, date retrieved 24.07.2012

[56] **Kayacan, E., Member, S., Cigdem, O., and Kaynak, O.** (2012). Sliding Mode Control Approach for Online Learning as Applied to Type-2 Fuzzy Neural Networks and Its Experimental Evaluation. *IEEE*, Vol.**59**, No.9, pp. 3510-3520.

[57] **Vecchio, C.** (2008). Sliding Mode Control: theoretical developments and applications to uncertain mechanical systems. *PhD Thesis*, pp. 1-250.

[58] **Utkin, V.** (2004). Sliding Mode Control. *Control Systems, Robotics and Automation*, Vol.**XIII**.

CURRICULUM VITAE

Name Surname:	Ayşegül GÜVENÇ
Place and Date of Birth:	Ankara, 23.08.1980
E-Mail:	aguvenc@gmail.com
B.Sc.:	Yeditepe University, System Engineering / Control & Automation Engineering Option (Undergraduate 2000-2005)
Professional Experience and Rewards:	Istanbul Technical University, Mechatronics Education & Research Center (2009-2012)

List of Publications and Patents:

PUBLICATIONS/PRESENTATIONS ON THE THESIS

▪ **Guvenc, A.,** Sumer, B., Koc, İ. M., Nikbin, K., 2011: Pattern Detection On An Artificial Skin By Preload Control. *38th Leeds-Lyon Symposium on Tribology – Energy and Health*, September 6-9, 2011 Lyon, France.

▪ **Guvenc, A.,** Sumer, B., Koc, İ. M., Nikbin, K., 2011: Friction Induced Vibration Based Pattern Detection On An Artificial Skin. *International Congress – Innovative Textiles*, October 20-22, 2011 İstanbul, Turkey. (presentation and publication)